# REGULATION OF MACROPHAGE INNATE IMMUNITY DURING INTRACELLULAR BACTERIAL INFECTION

A Dissertation

by

KRYSTAL J VAIL

Submitted to the Office of Graduate and Professional Studies of
Texas A&M University
in partial fulfillment of the requirements for the degree of

DOCTOR OF PHILOSOPHY

| | |
|---|---|
| Co-Chairs of Committee, | Robert O Watson |
| | Sara Lawhon |
| Committee Members, | Albert Mulenga |
| | Angela Arenas |
| Head of Department, | Ramesh Vemulapali |

May 2021

Major Subject: Biomedical Sciences

ABSTRACT

The innate immune system is a rapid response system that functions to prevent, recognize and limit infection by responding to danger signals such as those associated with bacterial pathogens. Macrophages, a type of innate immune cell, possess numerous means of detecting pathogens at multiple points, including at the cell surface and within the macrophage cytosol. For a pathogenic bacterial species to survive, it must evolve ways to escape host detection and elimination. Successful intracellular bacterial pathogens are unique in that they are not only capable of overcoming host immune surveillance but have evolved mechanisms to survive and replicate within the very cells meant to neutralize them. The ability of innate immune cells such as macrophages to overcome these bacterial survival mechanisms and respond efficaciously to infection are dependent on an elegant system of checks and balances between sensors and regulators. Understanding how bacteria are sensed by the host and how host immunity is regulated is imperative for developing ways to promote positive patient outcomes. Here we use three intracellular bacterial pathogens to interrogate this system. First, we explore how macrophages recognize intracellular bacteria and how bacteria can manipulate and exploit the immune system. To begin, we show that *Rhodococcus equi* is recognized by cytosolic DNA sensors. Upon triggering this cytosolic DNA sensing pathway, *R. equi* elicits an antiviral type I interferon (IFN) immune response. We next interrogate innate immune regulation and show that loss of a novel innate immune regulator, leucine rich repeat kinase 2 (LRRK2) results in dysregulation of innate immunity in uninfected

macrophages. This immune defect is associated with an elevated baseline type I IFN signature and impaired response to infection *ex vivo*. Furthermore, we use a *Lrrk2*$^{-/-}$ mouse model to demonstrate an abnormal host response during infection by either *Mycobacterium tuberculosis* or *Listeria monocytogenes*. Finally, we show that the Parkinson's disease (PD) associated *Lrrk2*$^{G2019S}$ mutation contributes to *M. tuberculosis* pathogenesis *in vivo* whereby mice harboring the *Lrrk2*$^{G2019S}$ mutation exhibit overwhelmingly severe lung pathology.

# DEDICATION

This work is dedicated to my son, Nathaniel. You are my motivation, my heart, my everything. I would not be who I am without you.

# ACKNOWLEDGEMENTS

I would like to thank my committee chair, Dr. Watson, my co-chair, Dr. Lawhon, and my committee members, Dr. Mulenga and Dr. Arenas, for their incredible support and guidance throughout the course of this research. I thank my ad hoc committee member, Dr. Kier, for her support. I thank my research mentors, Dr. Watson and Dr. Patrick for their phenomenal mentorship. The two of you have been far greater mentors than I could have ever asked for or imagined. I thank my mentor Dr. Rodrigues-Hoffman for her invaluable guidance, support and mentorship.

Thanks also go to my resident mates and lab mates for making my time at Texas A&M University a great experience. I thank Dr. Bryan, Dr. Weindel and Dr. Bell for their advice and instruction. I thank Ms. Kathie Smith and Ms. Dee Cooper for their assistance and compassion throughout my time at TAMU.

I also extend my gratitude to Texas A&M OGAPS and the National Institutes of Health (NIH) institutional T32 training program grant to Texas A&M Agrilife each for funding three years of PhD graduate studies. Thanks to Texas A&M University College of Veterinary Medicine and Biomedical Sciences for funding three trainee pilot research grants over the course of my training.

Finally, thanks to my son, Nathaniel, for his years of love, support, patience and sacrifice, to my parents and siblings for their encouragement.

CONTRIBUTORS AND FUNDING SOURCES

## Contributors

This work was supervised by a dissertation committee consisting of Assistant Professor Dr. Robert O. Watson [advisor] of the Department of Microbial Pathogenesis and Immunology (MPIM), Associate Professor Dr. Sara Lawhon [co-advisor] of the Department of Veterinary Pathobiology (VTPB), Professor Dr. Albert Mulenga of the Department of Veterinary Pathobiology (VTPB) and Assistant Professor Dr. Angela Arenas-Gamboa of the Department of Veterinary Pathobiology (VTPB).

The analyses depicted in chapter 4 were conducted in part by Dr. Chi Weindel and Dr. Samantha Bell of the Department of Microbial Pathogenesis and Immunology, and were published in 2020, and by Ms. Taylor Huntington of the Department of Neuroscience and Experimental Therapeutics. All other work for the dissertation was conducted by Dr. Krystal Vail independently.

## Funding Sources

The studies outlined in Chapter III were supported by a Texas A&M Triads for Transformation (T3) pilot grant. The studies outlined in Chapter IV were supported by a grant awarded from the Michael J Fox Foundation for Parkinson's Research (grant number 12185), National Institutes of Health (grants 1R01AI125512 and R35GM133720), Texas A&M Clinical Science and Translational Research (CSTR) Pilot Grant Program, and Texas A&M College of Veterinary Medicine and Biomedical Sciences Postdoctoral Trainee Grant.

Three years (2015-2018) of graduate study and salary were funded by a fellowship from Texas A&M University Office of Graduate and Professional Studies (OGAPS). Three years (2018-2021) of graduate study and salary were funded by the National Institutes of Health (NIH) institutional T32 training program grant awarded to Texas A&M Agrilife, grant number 5T32OD011083 (budget years 9-11). Its contents are solely the responsibility of the authors and do not necessarily represent the official views of the NIH or Texas A&M University.

# NOMENCLATURE

| | |
|---|---|
| AIM2 | Absent in melanoma 2 |
| ASC | Apoptosis-associated speck-like protein containing a CARD |
| BAC | Bacterial artificial chromosomes |
| BHI | Brain heart infusion |
| CARD | Caspase activation and recruitment domain |
| cGAMP | cyclic GMP-AMP |
| cGAS | cyclic GMP-AMP synthase |
| DAMP | Damage associated molecular pattern |
| DLS | Dorsal lateral striatum |
| GFAP | Glial fibrillary acidic protein |
| GFP | Green fluorescent protein |
| GTP | Guanosine triphosphate |
| LRRK2 | Leucine rich repeat kinase 2 |
| IBD | Inflammatory bowel disease |
| IFIT | IFN-induced protein with tetratricopeptide repeats |
| IFN | Interferon |
| IL | Interleukin |
| IRF | Interferon regulatory factor |
| ISG | Interferon stimulated gene |
| KO | Knock out |

| | |
|---|---|
| LB | Luria broth |
| LGP | Laboratory of genetics and physiology |
| LPS | Lipopolysaccharide |
| MAVS | Mitochondrial antiviral signaling protein |
| MDA | Melanoma differentiation associated protein |
| MOI | Multiplicity of infection |
| Mtb | *Mycobacterium tuberculosis* |
| MX1 | MX dynamin-like GTPase 1 |
| MyD88 | Myeloid differentiation factor 88 |
| Neun | Neuronal nuclear protein |
| NF | Nuclear factor |
| OASL | 2'-5'-oligoadenylate synthetase-like |
| PAMP | Pathogen associated molecular pattern |
| PBS | Phosphate buffered saline |
| PD | Parkinson's disease |
| PRR | Pattern recognition receptors |
| RIG-I | Retinoic acid-inducible gene I |
| RSAD2 | Radical SAM-domain-containing protein 2 |
| SNc | Substantia nigra pars compacta |
| SNP | Single-nucleotide polymorphism |
| STAT | Signal transducer and activator of transcription |
| STING | Stimulator of interferon genes |

| | |
|---|---|
| ROC | Ras of complex proteins |
| TANK | TRAF family member associated NF-kappa-B activator |
| TBK1 | TANK binding kinase 1 |
| Th | T helper |
| TH | Tyrosine hydroxylase |
| TIRAP | TIR domain-containing adapter protein |
| TLR | Toll-like receptor |
| TNF | Tumor necrosis factor |
| TRAM | Trif-related adapter molecule |
| TRIF | TIR domain-containing adaptor inducing IFNβ |
| TRIM | Tripartite-motif |
| VTA | Ventral tegmental area |
| WT | Wild type |

TABLE OF CONTENTS

Page

LIST OF FIGURES

Page

# CHAPTER I

# INTRODUCTION

## Overview of Innate Immune Sensing

Vertebrates are exposed to an astounding plethora of microbes each day, making the ability to survive and thrive a carefully regulated balance between host and microbe. While the vast majority of these microbes are non-pathogenic, the mammalian host must still detect and guard against microscopic invaders. The immune system functions to identify pathogenic microbes and danger signals and mount an appropriate defense. Effective recognition of such signals requires the host to differentiate normal, functional self from damaged tissues and from pathogenic invaders such as viruses, bacteria and fungi.[1] Likewise, an effective response is dependent upon the ability of the immune system to distinguish the level of threat generated by these signals and react accordingly. Failure to mount a sufficient defense against pathogenic microbes can result in inadequate control of the pathogen while an unregulated overreaction in the form of excessive inflammation can be more detrimental to the host than the infection.

The immune system is broadly classified into nonspecific, rapid response innate immunity and the more targeted, long term adaptive immunity, to which T- and B-lymphocytes belong.[2] Adaptive immunity is critical in the late phases of infection and in developing targeted immunological memory.[2] I am primarily interested in the immune response during the acute stages of infection and thus this work chiefly focuses on innate immunity. Defined as the first line of defense, innate immunity encompasses two main

roles: sensor and effector functions.[3] Each of these functions are realized through cellular and humoral mechanisms.[4] The cellular component of innate immunity includes hematopoietic cells such as monocytes/macrophages, neutrophils, basophils, eosinophils, and NK and dendritic cells.[4] Humoral innate immunity is comprised of lysozyme, antimicrobial peptides, acute phase proteins, complement, cytokines, and natural antibodies.[4]

Innate immune cells such as macrophages and neutrophils use 3 key strategies to recognize microbial invaders. One strategy is to detect molecules expressed by healthy cells but that are absent in infected cells, such as MHC class I proteins in natural killer cells.[2] A second approach is to recognize danger signals from damaged organelles known as damage associated molecular patterns (DAMPs), often generated as a result of inflammation or microbial manipulation.[2] In the third approach, germline encoded sensors known as pattern recognition receptors (PRRS) located in various subcellular niches sense microbial pathogen-associated molecular patterns (PAMPs).[5] These PRRS include Toll-like receptors (TLRs), NOD-like receptors, C-type lectin receptors, and others. Various PRRs recognize specific classes of PAMPs, demonstrate diverse expression patterns, engage specific immune signaling pathways, and elicit distinct antimicrobial responses.[6] Notably, PRRs are not exclusive to immune cells, but are expressed on all cell types.[2] Microbial pathogens have evolved to survive within various extracellular and intracellular niches, and innate immune cells have in turn evolved sensors at each level of the cell, including the cell membrane, intracellular endosomal compartments and within the cytosol.[7] Because microbial pathogens capable of

breaching the cell represent a high level of threat, numerous sensors exist to detect intracellular pathogens. A wide range of highly conserved PAMPS are detected by innate immune cells, including microbial components such as bacterial peptidoglycans, glycolipids, profilin and lipopolysaccharides (LPS).

*TLR Sensing*

The evolutionarily conserved TLR family consists of 13 members in mammals, and are expressed throughout multiple subcellular compartments, including on the cell surface, and intracellularly within endosomal compartments.[3,8] Both immune cells such as macrophages and dendritic cells, as well as nonimmune cells such as fibroblasts and epithelial cells express TLRs, with the degree of expression often dependent upon immune signals.[2] Structurally, TLRs contain a leucine-rich repeat ectodomain that recognizes PAMPs, a transmembrane domain, and a cytosolic Toll-IL-1 (TIR) domain important for activation of downstream signaling.[9]

Generally speaking, TLRs recognize several major categories of ligands: lipid PAMPs, nucleic acids, and LPS.[2] More specifically, TLR1, 2 and 6 recognize lipoproteins, TLR3 recognizes double-stranded RNA, TLR4 recognizes LPS among other ligands, TLR5 recognizes flagellin, TLR7 and 8 recognize single-stranded RNA, and TLR9 recognizes DNA.[9] TLRs 1, 2, 4, 5, and 6 are cell surface receptors, while TLRs 3, 7, 8, and 9 are endosomal.[9] Among bacteria, LPS is a major PAMP of gram-negative bacteria, while gram positive bacterial cell walls contain lipoteichoic acid and lipoproteins. TLR2 in particular, in concert with TLR1 or 6, is a cell surface TLR capable of detecting gram positive lipoteichoic acid, lipoproteins, and lipopeptides.[8]

Intracellularly, TLR9 detects bacterial genomic DNA, specifically unmethylated CpG-dinucleotides, which are distinct from highly methylated mammalian CpG DNA.[2]

Upon activation, TLRs initiate a common signaling pathway through the recruitment of adaptor proteins and activation of nuclear factor (NF)-κB and activating protein-1 (AP-1). A number of adaptor proteins mediate TLR signaling and include: myeloid differentiation factor 88 (MyD88), TIR domain-containing adapter inducing IFNβ (TRIF), TIR domain-containing adapter protein (TIRAP), and Trif-related adapter molecule (TRAM).[8] Of these adapter proteins, MyD88 is used by all TLRs except TLR3.[9] Activation of this signaling pathway culminates in production of pro-inflammatory cytokines and chemokines, including the canonical pro-inflammatory cytokines tumor necrosis factor (TNF), IL-1β, IL-6, and IL-12. Additionally, TLRs 3, 4, 7, 8, and 9 can induce type I interferons.[8]

*Cytosolic Immune Sensing*

Macrophage cytosolic surveillance encompasses a number of pathways capable of specifically detecting RNA or DNA, including endosomal Toll-like receptors (TLR), cytosolic RNA sensors and cytosolic DNA sensors.[7] Cytosolic RNA sensors include retinoic acid-inducible gene I (RIG-I)-like receptors (RLRs), MDA5 (melanoma differentiation associated protein 5), and LGP2 (laboratory of genetics and physiology 2; aka DHX58) which detect RNA viruses and act through the signaling adapter MAVS (mitochondrial antiviral signaling protein), as well as NOD2, which can detect bacterial peptidoglycans in addition to viral RNA.[10] RIG-I activates NF-κB signaling through IKK, leading to the production of pro-inflammatory cytokines, while MDA5 signals

through TANK-binding kinase 1 (TBK1), leading to downstream activation of the nuclear transcription factor IRF3 (interferon regulatory factor 3) and type I IFN signaling.[10] Although this work is centered on macrophages, it should be noted that while TLRs are primarily limited to immune cells, most cell types possess cytosolic RNA and DNA sensors.[6]

Under normal circumstances DNA is restricted to the nucleus and mitochondria such that DNA detected within the cytosolic compartment acts as a potent danger signal.[1] Cytosolic DNA from DNA viruses, retroviruses, bacteria and damaged mitochondria are sensed through the cytosolic DNA sensors cyclic GMP-AMP (cGAMP) synthase (cGAS) or absent in melanoma 2 (AIM2), which signal through stimulator of interferon genes (STING) and ASC (apoptosis-associated speck-like protein containing a caspase activation and recruitment domain), respectively.[11] Detection of cytosolic bacterial DNA in the cytosol results in one of two major effector outcomes: production of type I interferons through cGAS/STING or proinflammatory cytokines through AIM2.[12]

AIM2/ASC activation leads to the formation of the inflammasome, a multiprotein complex involved in regulating caspase-1 activation and inflammatory cell death (pyroptosis).[5] The inflammasome complex consists of a sensor (NLR, ALR, Pyrin), the adaptor protein ASC, and caspase-1.[5] Following activation by PAMPs or DAMPs, inflammasome sensors engage and promote oligomerization and nucleation of ASC.[5] Nucleated ASC recruit nascent caspase-1, cleaving it into active subunits p10 and p20.[13] Activated caspase-1 mediated inflammasome signaling leads to maturation and

release of proinflammatory cytokines such as interleukin (IL)-1β and IL-18.[11] The canonical pro-inflammatory cytokines are instrumental in magnifying and promoting inflammation, and in reducing bacterial burden.[5] IL-1β is a particularly potent cytokine important for neutrophil recruitment, vasodilation, and modulating adaptive immunity, and is tightly regulated.[5,13] Nascent IL-1β is synthesized in an inactive form following activation of NFκB, and must be processed into a biologically active form by the pro-inflammatory protease caspase-1, which is also produced as an inactive zymogen.[10] IL-18 plays an important role in IFN-ɣ production.[5]

Chen and colleagues originally identified the second major cytosolic DNA sensor, cGAS and its second messenger cGAMP, in 2013.[14,15] Upon binding cytosolic DNA, cGAS undergoes conformational rearrangement and generates the second messenger cGAMP, a type of cyclic dinucleotide, which is then recognized by the adaptor protein STING.[14,15] Localized to the endoplasmic reticulum, STING is a 379 amino acid protein with several transmembrane regions.[1] STING responds to cytosolic DNA through activation by second messengers such as host synthesized cGAMP, or by bacterial produced cyclic dinucleotides, such as cyclic di-GMP and c-di-AMP.[16-18] Additionally, STING can be activated by IKKs-NF-κB signaling.[1] Upon binding a second messenger such as cGAMP, STING undergoes oligomerization and translocates from the endoplasmic reticulum to the perinuclear-Golgi compartment where it recruits and forms a signaling complex with the kinase TBK1.[1] TBK1 phosphorylates neighboring STING, creating an IRF3-binding motif capable of recruiting the nuclear transcription factor IRF3.[19] Phosphorylated STING can simultaneously engage both

TBK1 and IRF3, which delivers IRF3 to TBK1 for phosphorylation.[19] Unstimulated IRF3 resides within the cytoplasm, but upon activation by serine/threonine phosphorylation, translocates from the cytosol to the nucleus and promotes transcription of type I IFNs such as IFN-β and IFN-α.[20,21]

While initial studies on the function of cGAS centered on recognition of viral DNA, over the past decade a growing number of reports have demonstrated a role for cGAS in detecting several intracellular bacteria including *M. tuberculosis*,[22-24] *Francisella novicida*[25] and *Chlamydia trachomaris*.[26] Importantly, cGAS does not distinguish host mitochondrial DNA from microbial DNA, however host DNA is sequestered into nuclear and mitochondrial compartments.[1]

*Type I Interferons*

Humoral immunity encompasses a number of sensor (i.e., galectins, mannose binding proteins) and effector proteins. Well described effector proteins within humoral innate immunity include complement, acute phase proteins and cytokines. Among the critical cytokines produced in the host immune response against viral and bacterial pathogens are interferons. Interferons are classified into three types based on sequence homology, receptor, and functional activity.[27] Type I IFNs include IFN-α (13 subtypes in humans, 14 subtypes in mice), IFN-β, IFN-κ, IFN-ω, and IFN-ε.[27] A number of immune cells (macrophages, dendritic cells, lymphocytes, fibroblasts, endothelial cells) secrete type I IFN. The sole type II interferon is IFN-ɣ, and has pro-inflammatory and immunomodulatory functions distinct from the other types of IFN.[27] Type III IFNs

include IFN-λ1, IFN-λ2 and IFN-λ3 and have antiviral and antifungal activity primarily in epithelial cells.[28]

Type I IFNs can be stimulated through several mechanisms, including microbial activation of TLRs that signal through TRIF, or through the activation of cytosolic sensors like cGAS, STING, RNA polymerase III, Ifi204, and others.[25] All members of the type I IFN family signal in an autocrine or paracrine manner through the IFNAR receptor, which consists of two subunits, IFNAR1 and IFNAR2, associated with two Janus family protein tyrosine kinases, Tyk2 and Jak1, respectively.[11,29] IFNAR activation leads to the formation of a transcription factor complex ISGF3, comprised of phosphorylated STAT1, STAT2 and IRF9.[27,30] Upon activation, the ISGF3 complex translocates to the nucleus and engages IFN-stimulated response elements (ISREs) located in promoter regions of members of a large class known as interferon stimulated genes (ISGs) in both immune and non-immune cells.[11,31]

The prevailing paradigm for decades has been that type I and III interferons are antiviral and that type II IFN is antibacterial. However, studies in recent years have uncovered a role for type I IFN signaling in bacterial pathogenesis as well, particularly in conferring pro-bacterial effects. As an example, mice lacking the IFNAR1 subunit of the type I IFN receptor IFNAR (*Ifnar1*$^{-/-}$) are incredibly susceptible to viral infection,[32,33] but they are resistant to infection with Mtb such that they mirror WT mouse death curves up to 80 days post-infection.[34,35] This phenotype is also reflected during infection with *L. monocytogenes*, where *Ifnar1*$^{-/-}$ mice are also resistant to infection.[36] Furthermore, mice lacking IRF3 (*Irf3*$^{-/-}$) are even more resistant to Mtb infection, outlive even WT controls

at 200 days post-infection, have reduced bacterial burdens, and have higher pro-inflammatory cytokine levels.[24] Again, *Irf3*$^{-/-}$ mice are similarly resistant to infection with *L. monocytogenes.*[37] On the other hand, mice pre-treated with exogenous IFN-α/β[38] or in which endogenous type I IFN has been induced (by administration of poly I:C (RNA agonist)),[39] and infected with either Mtb or *L. monocytogenes* exhibit increased bacterial burdens and more severe disease.[37]

There are a number of reasons why type I IFN contributes to a pro-bacterial immune environment, most related to the functions of ISGs. The type I IFN response is not limited to IFN-α, IFN-β or the other members of the type I IFN class, but also includes hundreds of ISGs.[29,31] These ISGs promote a type I IFN response that is highly effective against viral infection, largely because they target viral components to inhibit infection or replication.[33,40] As an example, the ISG RSAD2 (radical SAM-domain-containing protein 2) binds viral proteins to inhibit viral replication,[41] the IFIT (IFN-induced protein with tetratricopeptide repeats) family of ISGs bind viral nucleic acids to inhibit translation,[40,42] TRIM5α (tripartite-motif protein 5 alpha) targets viral capsid proteins to restrict infection,[43] and MX1 (MX dynamin like GTPase 1) binds viral nucleoprotein and polymerase basic protein 2 to inhibit viral polymerase activity.[44] Other ISGs serve to amplify the type I IFN response, such as IRF7, a member of the IRF family, which contributes to a positive feedback loop by promoting continued production of type I IFN.[20] Eliciting a host immune response maladapted to bacteria offers bacterial pathogens a selective advantage by allowing them to establish a replicative niche. This is further illustrated by the fact that many ISGs also function to

inhibit pro-inflammatory cytokines known to restrict bacteria. As an example, work from the Vance lab showed that the ISG IL-1Ra (IL-1 receptor antagonist) blocks activity of the pro-inflammatory cytokine IL-1.[45] In another study, macrophages deficient in IFIT1 had increased expression of TNF-α following stimulation with LPS.[46] Finally, type I and type II interferon responses tend to be polarized, where one or the other immune profile predominates. Teles and colleagues showed that the anti-inflammatory cytokine IL-10, which is associated with a type I IFN response, inhibits IFN-ɣ induced antibacterial response.[47]

## Intracellular Bacterial Pathogens

Bacterial pathogens have derived numerous means to escape host detection and elimination.[48] Successful intracellular bacterial pathogens overcome the host immune response and reside and replicate within the very cells meant to neutralize them. In some cases, such as with *Mycobacterium tuberculosis*, these bacteria are capable not only of thwarting host defenses, but also of manipulating host cell intrinsic immune pathways to the advantage of the pathogen.[11]

### *Rhodococcus equi*

*R. equi,*is a gram-positive, facultative intracellular coccobacillus of the nocardiform acinomycetes.[49] Infection causes severe, potentially fatal respiratory disease in young horses and immunocompromised humans and replicates inside alveolar macrophages in the lung.[50,51]

### *R. equi* Infection

Equine rhodococcal pneumonia is largely restricted to foals less than 6 month of age, and is rare in adult horses where it may occur in immunocompromised horses.[52-54] *R. equi* has a major detrimental impact on the equine breeding industry for several reasons. First, as a saprophytic bacterium, *R. equi* is nearly ubiquitous in the soil of many facilities and nearly all foals are exposed to *R. equi*.[55] Secondly, an efficacious vaccine is not yet available in the United States, although development is an ongoing area of research.[56,57] The occurrence of pneumonia varies widely among farms, with some farms experiencing rare or sporadic disease, and on other farms disease is endemic.[58] Incidence of disease ranges from 10-20% of foals, with some farms reporting higher incidence.[58] There is some debate about the contribution of potential risk factors to the development of disease. While it might seem plausible that soil concentrations of *R. equi*, the degree of maternal shedding of virulent *R. equi*, and management practices might predict the likelihood of foals developing pneumonia, this has not been supported by the literature.[55] Finally, early diagnosis and screening are challenging due to cost and manual labor of tracheobronchial aspiration (the current gold standard), and high false positive rates associated with ultrasonographic screening.[58] Foals with pulmonary lesions may never exhibit clinical signs, and some foals present with extensive pulmonary lesions before they develop clinical signs.[59] In other cases, foals may develop a subacute form where apparently healthy foals rapidly develop respiratory stress and succumb within 48 hours of presentation.[58]

While *R. equi* infection in horses is primarily associated with pyogranulomatous bronchopneumonia and abscessation, it can manifest as extrapulmonary lesions, such as enteritis, ulcerative colitis, synovitis, uveitis, or lymphadenitis.[60] In addition to being an equine pathogen, *R. equi* also causes disease in pigs,[61] cattle,[49] goats,[62,63] dogs,[64,65] cats,[65,66] and humans.[67-69] Non-equid domestic animals most frequently develop non-pulmonary lesions; pigs, for example, develop submaxillary lymphadenitis.[61] Human infections most frequently present as pulmonary lesions and are most common in immunocompromised hosts, although cases have been reported in immunocompetent individuals.[68] Mortality rates are high, at 11% of immunocompetent patients, 50% among AIDS patients, and 20-25% in non-HIV-infected immunocompromised patients.[68]

### *R. equi* Pathogenesis

The primary route of infection is inhalation, although ingestion is another route of exposure.[59] Upon inhalation of contaminated dust, *R. equi* is phagocytosed by alveolar macrophages in the lung, where it replicates inside a phagosome compartment, which fails to undergo subsequent maturation, resulting in an *R. equi*-containing vacuole.[50] Work by von Bargen and others found that *R. equi* remains confined to the vacuole for 24h post-infection, at which point it escapes the vacuole and leads to necrotic cell death.[50,70]

Previous studies have shown that *R. equi* virulence depends in large part on a 80-90 kb plasmid required for intracellular replication in macrophages.[54] This virulence plasmid contains a 21-kb pathogenicity island (PAI) housing the genes encoding the

virulence-associated protein (Vap) family.[71] This family consists of 6 genes (vapA, C, D, E, G, H) and 3 pseudogenes (vapF, I and X), and individual expression often is associated with some degree of host specificity.[72,73] As an example, vapB is commonly associated with pig isolates.[73] Of the Vap proteins, VapA has emerged as the only Vap required for virulence in horses, although it is not sufficient to cause virulence alone and requires two transcriptional regulators, virR and virS.[72,74] Besides being required for intracellular replication,[75] VapA contributes to inhibition of phagosome maturation,[76] and modulating the pH of the phagosome lumen.[70,77]

Studies of host immunity against *R. equi* have found that pro-inflammatory cytokines are critical in controlling infection, while anti-inflammatory cytokines such as IL-4 are detrimental to clearance.[78,79] TNFα and IFN-ɣ are required for macrophage killing of *R. equi* and induce macrophage production of reactive oxygen and reactive nitrogen intermediates, which combine to form peroxynitrate.[80-82] It was once hypothesized that the immunological immaturity of newborn foals was the primary reason for their susceptibility to infection by *R. equi*, however studies have since shown that foals are able to induce IFN-ɣ to similar levels as adult horses.[83,84]

Importantly, *R. equi* is an emerging model for bacterial pathogenesis, and bears some genomic similarities to Mtb. Both bacteria contain a mycolic acid-containing glycolipid rich outer cell envelope, possess type VII secretions systems, and replicate in alveolar macrophages.[59] Upon phagocytosis, both *R. equi* and mycobacteria activate TLR2 sensing at the cell surface.[2] Because of these similarities, I leveraged existing knowledge of Mtb pathogenesis to inform my approach to investigating *R. equi*.

## Leprosy

An ancient scourge of Biblical times that has persisted to modern day, leprosy is a chronic disease with an incubation period of up to 10 years.[85] With over 200,000 new cases diagnosed annually and insidious progression, leprosy is a major cause of peripheral neuropathy and if left untreated, permanent disfigurement.[85,86] The disease can involve the peripheral nerves, skin and rarely respiratory mucosa, eyes, bones and testes and manifests on a wide clinical spectrum ranging from mild, localized lesions (polar tuberculoid leprosy) to disseminated disease (polar lepromatous leprosy) depending on the host immune response.[87] A number of studies have established host genetic background as a risk factor for leprosy susceptibility, with several genes having been identified as important for either susceptibility to infection or clinical manifestation.[88] Multidrug therapy is highly effective but extensive, consisting of up to 12 months of treatment with a combination of dapsone, rifampicin and clofazimine.[89] Alarmingly, multidrug therapy is associated with drug reactions in a subset of patients that can result in exacerbated nerve damage.[85]

## *M. leprae* Pathogenesis

Also known as Hansen's disease, leprosy is caused by *Mycobacterium leprae*, an acid-fast, intracellular bacillus that replicates in macrophages and Schwann cells.[86,90] *M. leprae* is a very slow growing mycobacteria with a generation time of 12 to 14 days.[89] Infection occurs by aerosol transmission through the nasal mucosa where macrophages are thought to encounter bacilli in the respiratory mucosa and carry them to the

peripheral nerves and cool areas of the body such as the dermis of the extremities and ears.[85] Infection of peripheral nerve Schwann cells offers bacteria unrestricted replication as Schwann cells lack many of the antimicrobial mechanisms of immune cells such as macrophages.[89] *M. leprae* also infects macrophages, where it can replicate in the face of a poor adaptive immune response.[89] Together, infection of these two cells contributes to the clinical lesions of axonal degeneration, demyelination, fibrosis, and granulomatous inflammation leading to nerve and tissue damage and loss of sensation.[89]

Leprosy presents on a range of clinical severity depending on the ability of host to establish an effective innate and adaptive immune response.[47,88] Host genetics contribute to shaping the immune response, with mutations in genes for pattern recognition receptors (*TLR2, NOD2*), autophagy (*PARK2, RIPK2*), immune regulation (*LRRK2*), or cytokines (*TNF, IL12*) having been identified as key determinants.[48,91] Although macrophages and Schwann cells are the primary cells infected, neutrophils, keratinocytes, and dendritic cells also play a role in *M. leprae* pathogenesis, contributing to the local immune response.[88] TLRs and Nod2 are key sensors for the recognition of *M. leprae* infection, with monocytes and dendritic cells from lesions in patients with milder disease strongly expressing TLR2 and TLR1, a feature less apparent in patients with more severe leprosy.[2,88] Once internalized, *M. leprae*, like Mtb, triggers the cytosolic DNA sensing pathway, leading to induction of a type I IFN program.[92] The milder, localized tuberculoid form of leprosy is associated with low bacillary load, upregulation of IFN-ɣ (type II IFN) and a T helper (Th) 1, pro-inflammatory cytokine response.[87] The more extreme lepromatous manifestation of leprosy is characterized by

heavy bacterial loads, and a Th2 cytokine response characterized by induction of type I interferons, $PGE_2$ and IL-10.[47,87] IL-10 in particular contributes to promoting an environment permissive to high bacterial burdens by inducing phagocytic activity and impaired anti-microbial/pro-inflammatory cytokine expression.[93] Furthermore, *M. leprae* killing is diminished by ISGs such as 2'-5'-oligoadenylate synthetase-like (OASL) through inhibition of antibacterial mechanisms.[92]

*Mycobacterium tuberculosis*

**Tuberculosis**

*Mycobacterium tuberculosis* (Mtb), like *M. leprae*, is an acid fast, intracellular bacillus and the causative agent of tuberculosis, the primary infectious cause of death globally.[94,95] Approximately one quarter of the global population is infected with Mtb, with 10 million people developing active tuberculosis and over 1 million deaths due to Mtb each year.[96] While up to 10% of immunocompetent individuals with latent Mtb will experience reactivation, the risk of reactivation of latent Mtb is far greater in those coinfected with HIV or other immunosuppressive conditions.[95] In addition to pulmonary lesions, Mtb can lead to extrapulmonary disease, including pleuritis, meningitis, lymphadenitis, osteitis, arthritis, pericarditis, dermatitis, laryngitis, gastroenteritis, cystitis, and ophthalmitis.[97]

As a chronic infection, tuberculosis is a systemic disease in the sense that the host is exposed to persistent variable levels of antigenic stimulation, with outcomes that may include neurodegenerative disease.[98] Peripheral inflammation may be sensed in the brain by various means, including cytokine and inflammatory mediator interaction with

neural organs lacking a blood-brain barrier such as the circumventricular organs, or interaction with brain endothelium.[97] Such persistent inflammatory states may in turn initiate or exacerbate non-infectious chronic diseases in susceptible individuals. For example, Mtb has been associated with the development of malignancy.[95,98] Additionally, a nationwide study by Shen and colleagues found that patients with Mtb had an increased risk of the neurodegenerative disease Parkinson's disease (PD).[98]

**Mtb Pathogenesis**

Mtb is transmitted via inhalation of aerosolized droplets allowing bacilli to reach the lung where they are phagocytosed by alveolar macrophages.[96] Upon phagocytosis, Mtb engages surface TLR sensors to trigger pro-inflammatory cytokine production, and intracellular mycobacterial PAMPS elicit type I IFNs.[24] An important feature of Mtb pathogenesis is the possession of a number of type VII secretions systems named ESX-1-5.[99] Specifically, the ESX-1 secretion system is critical for modulating host-cell functions and promoting Mtb virulence.[100] A key mechanism for ESX-1 mediated host cell modulation is the secretion of virulence proteins such as ESAT6 which are capable of permeabilizing the Mtb-containing phagosome to allow communication with the host cytosol.[34] It is through this interaction that Mtb releases bacterial DNA into the cytosol to engage the cytosolic DNA sensor, cGAS, activate the cytosolic DNA sensing pathway, and elicit type I IFN production.[22] Recruited inflammatory cells contribute to the development of the hallmark lesion of tuberculosis, the granuloma.[96] In human disease, Mtb-induced pulmonary granulomas develop in a cycle of macrophage recruitment, infection, and death and liberation of bacteria, which allow survival of

bacilli within the necrotic caseous core of granulomas.[95] Granuloma formation in turn contributes to the ability of Mtb to establish a chronic, latent infection.[95,101]

### *Listeria monocytogenes*

*L. monocytogenes* is a gram-positive, facultative anaerobic, facultative intracellular bacillus causing gastrointestinal disease.[102] Its primary public health significance is as a food-borne pathogen resulting in gastroenteritis in immunocompetent individuals.[102] In immunocompromised individuals, listeriosis can result in bacterial sepsis and meningitis.[102] As a food-borne pathogen, the primary route of infection is via ingestion of contaminated food or water.[102] Following ingestion, *L. monocytogenes* enters the gastrointestinal tract, crosses the intestinal epithelium into the lamina propria and uses vasculature to disseminate to the liver and spleen.[102] Unlike the previously mentioned bacterial pathogens, *L. monocytogenes* is capable of entering both phagocytic and nonphagocytic cells, such as epithelial cells.[102] While *L. monocytogenes* does trigger the cytosolic DNA sensing pathway, it does so through the production of a cyclic dinucleotide, di-adenylate cyclase (dacA), which directly activates STING and bypasses cGAS.[17]

## Thesis Goals

The work presented here seeks to identify innate immune regulators and uses three bacterial species to interrogate innate immune sensing and regulation specifically during infection by intracellular bacterial pathogens. These pathogens include *R. equi,* Mtb, *and L. monocyotgenes.* While all three microbes are intracellular, gram positive bacteria, they differ in their chronicity and species specificity, among other factors.

There is also a wide range in the depth of literature on their interactions with host immunity. Thus, we began by seeking to interrogate macrophage cytosolic sensing of *R. equi* as well as downstream outcomes, and end with investigating a potent innate immune regulator, LRRK2, in the pathogenesis of Mtb and *L. monocytogenes*.

# CHAPTER II

# MATERIALS AND METHODS

## Animals

All animals and experimental procedures for this study were reviewed and approved by the Texas A&M University Institutional Animal Care and Use Committee (IACUC).

### *Mice*

Mice were kept on a 12h light/dark cycle and provided food and water ad libitum. Mice were group housed (maximum 5 per cage) by sex on ventilated racks in temperature-controlled rooms. All mice used in experiments were compared to age-matched controls. Mice used to generate BMDMs were between 8-12 weeks old. *Lrrk2* KO mice (C57BL/6-Lrrk2tm1.1Mjff/J) stock #016121, and *Ifnar* KO mice (B6(Cg)-Ifnar1Ifnar1$^{tm1.2Ees}$/J) stock #028288) were purchased from The Jackson Laboratories (Bar Harbor, ME). TBK1 KO mice (*Tnfr1*$^{-/-}$ and *Tbk1*$^{-/-}$/*Tnfr1*$^{-/-}$)[103] were generously provided by the Akira lab. BAC LRRK2-G2019S (B6.Cg-Tg(Lrrk2*G2019S)2Yue/J) stock 012467 were purchased from The Jackson Laboratories (Bar Harbor, ME). These mice express overexpress the mouse LRRK2-G2019S mutant protein at ~6-8 fold greater levels than endogenous mouse LRRK2 directed by the endogenous *Lrrk2* promoter/enhancer regions on the BAC transgene. The *Lrrk2*$^{-/-}$ strain has been maintained with filial breeding on a C57BL6/NJ background for five more generations.

### *Horses*

Foals and their mares were housed individually in stalls and separately from other mare and foal pairs for 1 week following experimental infection. After 1 week, these mare/foal pairs were transferred back to their original pasture.

## Cell Culture

### *Cell Lines*

RAW 264.7 cells (murine macrophage cell line) were purchased from ATCC and the cell line was minimally passaged in our lab to maintain genomic integrity. RAW 264.7 *Lrrk2* KO cells (ATCC SC-6004) generated by the MJFF were obtained from the ATCC and used with wild type control Lrrk2 parental RAW 264.7 (ATCC SC-6003). All new cell lines were generated from these low passage stocks. Cell lines were passaged no more than 10 times and tested negative for mycoplasma contamination. Cells lines were cultured in complete media (DMEM, 10% FBS, 2% HEPES buffer).

### *Murine Primary Macrophages*

Mouse bone marrow derived macrophages (BMDMs) were differentiated from bone marrow cells isolated by washing mouse femurs with 10 ml DMEM. Harvested bone marrow cells were centrifuged 5 min at 1000 rpm and resuspended in BMDM media (DMEM, 20% FBS, 1mM sodium pyruvate, 10% MCSF conditioned media). Cells were counted and plated at 5 x $10^6$ in 15 cm non-TC treated dishes in 30 ml BMDM media and fed with an additional 15 ml of media on Day 3. Bone marrow cells were allowed to mature until 80-95% confluent (6-8 days). Nonadherent cells were

washed away with PBS. Adherent cells were harvested with PBS-EDTA, centrifuged for 5 min at 1000 rpm and resuspended in BMDM media for counting.

*Equine Primary Monocytes*

Thirty ml of heparinized blood was incubated at room temperature for 30 min. The plasma layer containing white blood cells was removed, diluted with the same volume of PBS, and layered over Ficoll-Paque™ Plus (GE Healthcare, Uppsala, Sweden) for density gradient separation of peripheral blood mononuclear cells (PBMCs). PBMCs were washed 3 times with PBS, counted in an automated cell counter (Cellometer Auto T4, NexelomBioscience, Lawrence, MA), and suspended at a concentration of $3 \times 10^6$ cells/mL in RPMI-1640 (BioWhittaker®, Lonza, Walkersville, MD, USA) containing 15% heat-inactivated horse serum, 1% Glutamax™ (Life Technology Corporation, Grand Island, NY, USA), 1% NEAA mixture (BioWhittaker®, Lonza, Walkersville, MD, USA), penicillin G (100 U/mL), and streptomycin (80 μg/mL). PBMCs were incubated at 37 °C and 5% $CO_2$ for 3h in a T75 flask, and then non-adherent cells were removed with warm PBS. Adherent cells were detached from the flask with Accutase® (Innovative Cell Technology) for 10 min at room temperature and PBS. Cells were pelleted, washed with PBS to remove Accutase®, and the adherent cells (monocytes) counted using the automated cell counter, pelleted again, and stored in Trizol® (Invitrogen) at -80 °C until RNA extraction.

*Cell Stimulations*

For cell stimulations, RAW 264.7 cells and BMDMs were plated in 12 well tissue culture treated dishes at $5 \times 10^5$ cells/well and allowed to adhere overnight at

37°C/5% $CO_2$. Cells were stimulated with 100 ng/ml LPS or transfected with 1μg/ml ISD for 4h.

## Bacterial Strains

### *R. equi*

Virulent *R. equi* ATCC 33701+ (VapA +; ATCC reference strain; Rockville, MD) was used as the wild type strain and a plasmid cured (33701-) isogenic strain was used as an avirulent control.[54] GFP expressing *R. equi* ATCC 103 was generously provided by Dr. Mary Hondalus[75,104] in collaboration with Dr. Angela Bordin and Dr. Noah Cohen. *R. equi* strain EIDL 5-331, obtained from a Texas foal confirmed to have *R. equi* pneumonia, was used for the equine experiments.[105]

Frozen stocks of *R. equi* were streaked onto BHI agar plates and allowed to grow at 37° for 48h. Plates were then stored at 4° for no longer than one week. To prepare the inoculum, approximately 5 colonies of *R. equi* were inoculated into 5 ml of brain-heart infusion (BHI) broth and shaken overnight at 37° C, then 0.5 ml of the culture was subcultured into 5 ml of fresh BHI overnight, shaken at 37°C. The bacterial suspension was centrifuged at 1000 rpm for 10 minutes at 25°C. The suspension was discarded and the pellets washed twice with 1 ml of PBS. The supernatant was discarded, the bacteria re-suspended into sterile PBS, and the concentration of bacteria determined spectrophotometrically at an optical density of 600 nm (OD 600) where OD 1.0 represents approximately 2 x $10^8$ CFU/ml. Concentrations were verified by plating the inoculum and counting CFUs. Bacterial suspensions were diluted to the desired

concentration. Strains were confirmed to be virulent (VapA positive) by PCR before infection.

### *M. leprae*

*M. leprae* cultivated in the footpads of nude mice were generously provided by the National Hansen's Disease Program. Bacilli were harvested at the National Hansen's Disease Program on a Tuesday and shipped overnight to arrive at Texas A&M Health Science Center on Wednesday on dry ice. Upon arrival, bacilli were allowed to recover in their original media at 33° C overnight. To prepare the inoculum, bacteria were pipetted to break up clumps and suspended in DMEM with 10% horse serum.

Because *M. leprae* cannot be cultivated in media,[85,106-108] bacterial survival was determined using genomic equivalents by qPCR with DNA extracted from infection samples, primers from a published sequence[106] (sense5_ATTTCTGCCGCTGGTATCGGT 3_, antisense 5_TGCGCTA-GAAGGTTGCCGTAT 3), and Powerup Sybr green reaction mix. Standard curves were determined using bacterial genomic DNA extracted from 5 x $10^6$ *M. leprae*.

### *M. tuberculosis*

The Erdman strain was used for all Mtb infections. Low passage lab stocks were thawed before each experiment to ensure virulence was preserved. Mtb was cultured in roller bottles at 37°C in Middlebrook 7H9 broth (BD Biosciences) supplemented with 10% OADC, 0.5% glycerol, and 0.1% Tween-80 or on 7H11 plates (Hardy Diagnostics). All work with Mtb was performed under Biosafety Level 3 (BSL3) containment using procedures approved by the Texas A&M University Institutional Biosafety Committee.

To prepare the inoculum, bacteria grown to log phase (OD 0.6-0.8) were spun at low speed (500g) to remove clumps and then pelleted and washed with PBS twice. Resuspended bacteria were briefly sonicated and spun at low speed (500g) to further remove clumps.

*L. monocytogenes*

*L. monocytogenes* strain 10304s was streaked on BHI agar plates from lab stocks and incubated at 37° overnight. 5-10 colonies were inoculated into 2.5 ml of BHI and incubated at 30° under static conditions overnight. On the day of infection, overnight cultures were diluted 1:10 into fresh BHI for *in vivo* infections or 1:5 for cell infections. *In vivo* subcultures were incubated at 37° shaking for ~2h until reaching an optical density of 0.5-1.5. Subcultures for cell infections were incubated at 30° under static conditions for ~2h until reaching an OD of 0.5-1.5. Once bacteria reached mid-log phase, 1 ml of subculture was spun down at 5000 rpm for 3 min and washed twice with PBS.

## Macrophage Infections

Macrophages were plated in 12 well dishes at 5 x $10^5$ cells/well and allowed to adhere overnight. Macrophages were infected with virulent *R. equi* or *L. monocytogenes* at an MOI of 5 for gene expression studies, secreted protein levels, and immunofluorescent microscopy studies; an MOI of 1 for CFU experiments; or MOI of 50 for immunoblot analysis. Macrophages were infected with *M. leprae* at an MOI of 50 for gene expression studies. Following infection, macrophages were centrifuged for 10 minutes at 1000 rpm, then incubated for 30 minutes at 37°C. Noninfected macrophage

monolayers were cultured under the same conditions. Media containing *R. equi* or *M. leprae* was removed and each well washed twice with PBS, then replaced with complete media and cultured at 37°C until the appropriate time point. At each time point, supernatants were removed and monolayers washed with PBS.

For CFU studies, hypotonic lysis was achieved by adding 500 µl of sterile water to monolayers after removing PBS wash. Cells were allowed to incubate for at least 10 minutes and then were manually pipetted to ensure complete lysis. 100 µl of 1:10 serial dilutions were plated on LB plates and allowed to incubate at 37°C for 24h *(L. monocytogenes*) or 48h (*R. equi*) before counting colonies.

For gene expression studies, monolayers were harvested using 500 µl of Trizol reagent and stored at -80°C until processing.

For protein studies, after removing PBS wash, monolayers were harvested using 50 µl of RIPA buffer and stored at -80°C until processing.

## ***In Vivo*** **Infections**

### *R. equi Mouse Infections*

Ten 8- to 12-week-old C57Bl/6 mice were transferred to an ABSL-2 holding facility and allowed to acclimate for one week prior to infection. For *R. equi* infections, at the time of infection, mice were injected intra-peritoneally with 100µl of *R. equi* suspension (Figure II-1). Following infection, animals were monitored and weighed daily until the experimental end point 5d post-infection to detect physical signs of disease. Lungs, spleens, mesenteric lymph nodes and peritoneal cells were harvested aseptically.

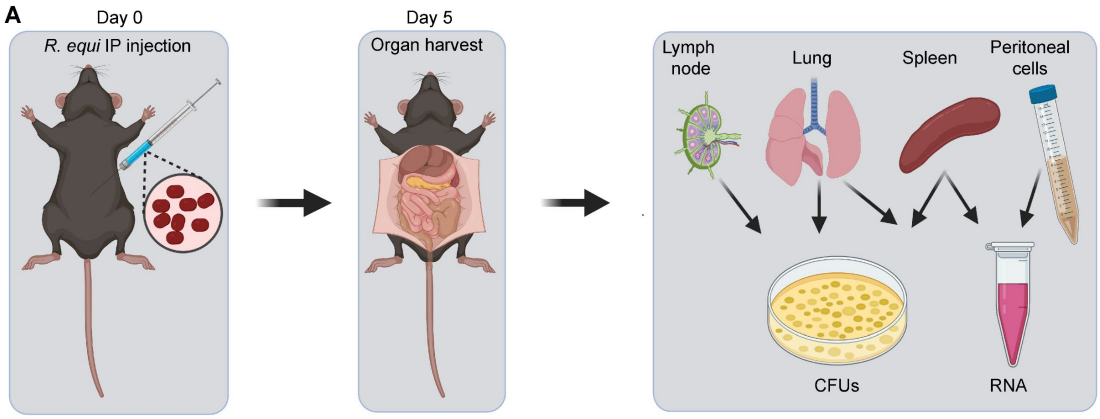


Figure II-1: Mouse *R. equi* infection schematic. Mice were infected with *R. equi* by IP injection on Day 0. On day 5, mice were euthanized and organs harvested for CFU and qRT-PCR. Figure was made using BioRender.com.

Samples for CFU experiments were placed in pre-weighed, 10 ml conical tubes containing 2 ml of PBS. Tubes were then weighed to obtain organ weight, and organs were homogenized. Serial dilutions of the homogenate were placed onto LB agar plates and allowed to grow for 24-48h at 37°C to determine the bacterial concentration per gram of organ.

Samples for gene expression studies were placed in 500 µl of Trizol reagent, homogenized and stored at -80°C until further processing.

### *Mtb Mouse Infections*

The Mtb inoculum was prepared as described above. Age- and sex-matched mice were infected via inhalation exposure using a Madison chamber (Glas-Col) calibrated to introduce 100-200 CFUs per mouse. For each infection, approximately 5 mice were euthanized immediately, and their lungs were homogenized and plated to verify an

accurate inoculum. Infected mice were housed under BSL3 containment and monitored daily by lab members and veterinary staff.

At the indicated time points, mice were euthanized, and tissue samples were collected. Blood was collected in serum collection tubes, allowed to clot for 1-2h at room temperature, and centrifuged to separate serum. Serum cytokine analysis was performed by Eve Technologies (Calgary, Alberta, Canada). Organs were divided to maximize infection readouts. For histological analysis, 2 right lung lobes and ¼ spleen were fixed in 10% neutral buffered foramlin  for 24h. One brain hemisection was fixed in 4% paraformaldehyde for 24h, then stored in 30% sucrose. For CFU enumeration, organs were homogenized in 5 ml PBS + 0.1% Tween-80, and serial dilutions were plated on 7H11 plates. Colonies were counted after plates were incubated at 37° for 3 weeks.

### *L. monocytogenes Mouse Infections*

All work with *L. monocytogenes* was performed in BL2 facilities. Two days prior to infection, mice were treated with 5 mg/ml streptomycin in the drinking water. Mice were fasted approximately 16h prior to infection. The *L. monocytogenes* inoculum was prepared as described above. Washed bacteria were resuspended in PBS so that each 5 µl aliquot consisted of 1 x $10^8$ CFU (1 ml of OD 1 in 50 µl PBS). 2-3 mm aliquots of bread were infused with 3 µl of melted unsalted butter and 5µl of bacteria. Age- and sex-matched mice were separated for infection and fed an aliquot of contaminated bread

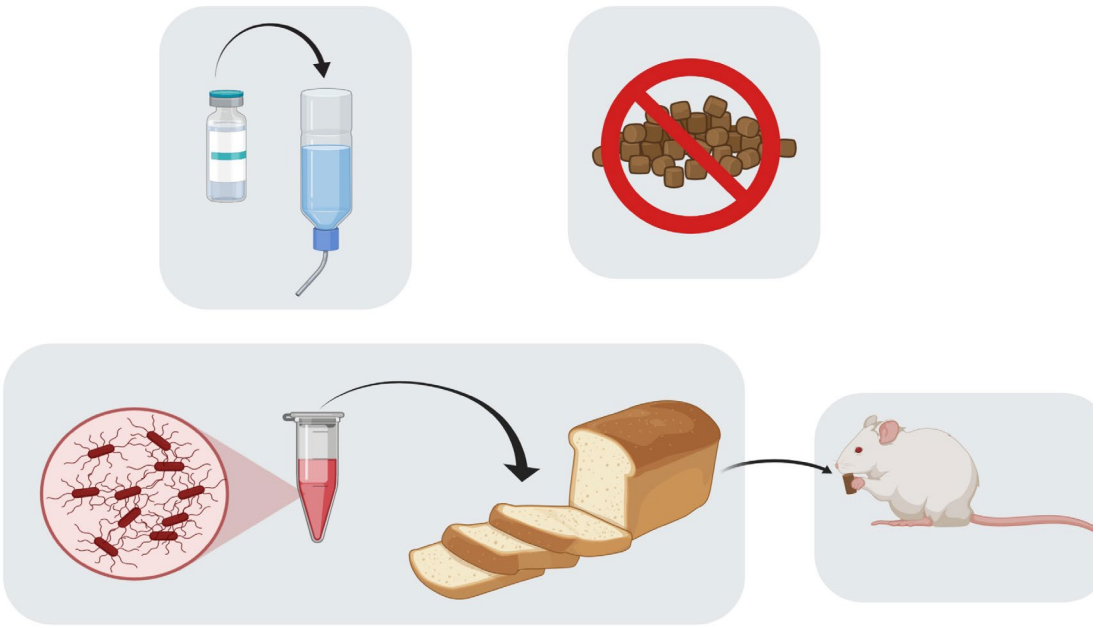

Figure II-2: Mouse *L. monocytogenes* infection schematic**.** Mice were infected with *L. monocytogenes* by ingestion of contaminated bread on Day 0. On day 4, mice were euthanized and organs harvested for CFU. Figure was made using BioRender.com.

(Figure II-2). Mice were observed until the bread was ingested, then returned to their original cage and given fresh food and streptomycin-free water. The challenge dose was determined by vortexing an aliquot of contaminated bread for 5 minutes in 1 ml PBS and plating 100 µl at 1 x $10^5$ dilution on LB agar. Mice were weighed and monitored daily until the experimental end point.

Feces were collected on days 1 and 5 post-infection to determine fecal CFUs. Mice were placed on a paper towel covered with a 1000 ml beaker until they defecated, then were returned to their cage. Feces were weighed, and vortexed with 1 ml of PBS.

Serial 10-fold dilutions were plated on LB agar and incubated overnight at 37°C to determine fecal shedding.

Mice were euthanized at 5d post-infection and tissue samples were collected. Spleens, liver, ileum, colon and cecum were placed in lysis buffer (0.1% NP-40 in water) in pre-weighed tubes, weighed to obtain organ weight and homogenized. Serial 10-fold dilutions were plated on LB agar and incubated overnight to determine CFU.

### *Foal Infections*

For transendoscopic infection,[56,109,110] foals were sedated using intravenous (IV) injection of xylazine hydrochloride (0.5 mg/kg; Vedco, St. Joseph, MO) and IV butorphanol tartrate (0.02 mg/kg; Zoetis, Florham Park, New Jersey). An aseptically-prepared video-endoscope with outer diameter of 9 mm was inserted via the nares into the trachea and passed to the bifurcation of the main-stem bronchus. A 40-ml suspension of virulent *R. equi* strain EIDL 5–331 containing approximately 1 x $10^6$ viable bacteria was administered transendoscopically (Figure II-3), with 20 ml infused into the right mainstem bronchus and 20 ml into the left mainstem bronchus via a sterilized silastic tube inserted into the endoscope channel. The silastic tube was flushed twice with 20 ml of air after each 20-ml bacterial infusion.

## Quantitative PCR

Trizol reagent (Invitrogen) was used for total RNA extraction according to the manufacturer's protocol. RNA was isolated using Direct-zol RNAeasy kits (Zymogen). cDNA was synthesized with BioRad iScript Direct Synthesis kits (BioRad) according to

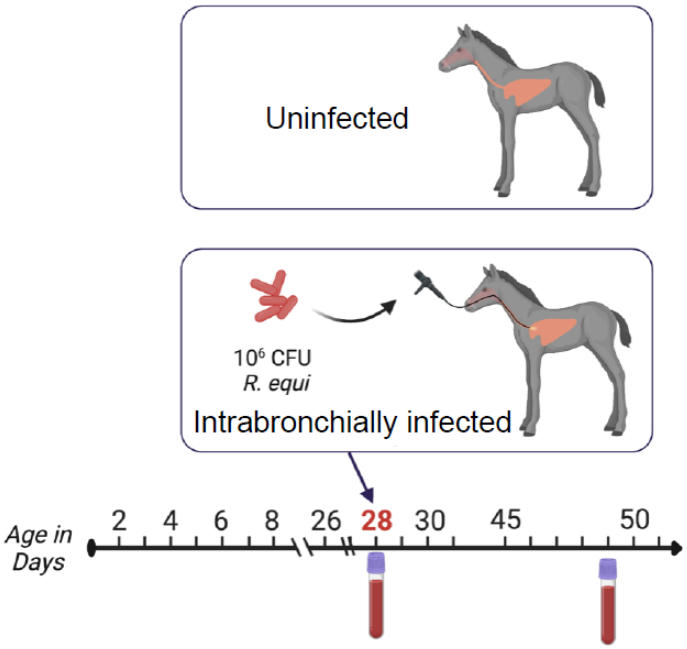


Figure II-3: *In vivo* intrabronchial infection of foals with *R. equi.* Foals were infected with *R. equi* by intrabronchial route on post-natal day 28. At post-natal days 28 (day 0 of infection) and 49 (21 days post-infection), peripheral blood samples were taken, from which monocytes were isolated for RTqPCR.

the manufacturer's protocol. qRT-PCR was performed in triplicate wells using PowerUp SYBR Green Master Mix. Data were analyzed on a QuantStudio 6 Real-Time PCR System (Applied Biosystems).

**RNA-Sequencing**

RNA was isolated from cells in biological triplicate using Trizol reagent (Invitrogen) and Direct-zol RNAeasy miniprep kit (Zymogen) according to the manufacturer's protocol. Agilent Technologies Bioanalyzer 2100 (Agilent Technology, Santa Clara, CA US) was used to verify RNA integrity number (RIN), rRNA ratio and

RNA concentration. RNA-seq and library prep was performed by Texas A&M AgriLife Research Genomics and Bioinformatics Service. Samples were sequenced on NovaSeq 6000 S1 X using 2x 100-bp paired end reads. Raw reads were filtered and trimmed and Fastq data was mapped to the Mus musculus Reference genome (RefSeq) using CLC Genomics Workbench (Qiagen). Differential expression analyses were performed using CLC Genomics Workbench. Relative transcript expression was calculated by counting Reads per Kilobase of exon model per Million mapped reads (RPKM). Canonical pathway analysis was performed using Ingenuity Pathway Analysis (IPA, Qiagen).

**ISRE Reporter Assay**

Macrophage secreted type I IFN levels were determined using an L929 cell line stably expressing a luciferase reporter gene under regulation of the type I IFN signaling pathway (L929 ISRE cells). At the indicated times post-infection, macrophage cell culture media was harvested and stored at -80°C until thawing on the day of the bioassay. On the day prior to the bioassay, 5 x $10^4$ L929 ISRE cells were added to each well of a white 96 well flat-bottomed plate and incubated at 37°C/5%$CO_2$ overnight. On the day of the bioassay, spent ISRE media was discarded and a 1:5 dilution of media from infected macrophages was added to each well of L929 ISRE cells, then incubated for 5h. Cells were washed with 1X PBS, lysed in 30 µl of 1X reporter lysis buffer, then 30 µl of Luciferase Assay System solution (Promega) added and luminescence read immediately using a Cytation5 plate reader.

## ELISA

Macrophage supernatant samples were harvested at 0, 8 and 24h post-infection and stored at -80°C until thawing on the day of the assay. Invitrogen Nunc MaxiSorp 96-well plates were coated with 50µl of capture antibody diluted 1:5000 (Santa Cruz, sc-57201) in 0.1M carbonate buffer and were incubated at 4°C overnight. Wells were then blocked using PBS+10% FBS for 2h at 37°C. 50 µl of undiluted sample was added to each well. IFN-β standard (PBL, 12400-1) was diluted 1:4 for serial dilutions and incubated at room temperature overnight. Samples were washed with PBS+0.05% TWEEN before each step. Detection antibody (RnD Systems, 32400-1) was added at a 1:2000 dilution and incubated at room temperature overnight. After washing, secondary antibody (Cell signaling technology, 7074) was added to each well at a 1:2000 dilution and incubated for 3 h. Following washing, the reaction was visually monitored until the standard was developed, then TMB substrate (SeraCare) was added and the reaction stopped with 2N H2SO4. The ELISA was read immediately at 450 nm.

## Immunoblot Analysis

Cell monolayers were washed with 1X PBS and lysed in 1X RIPA buffer (150 mM NaCl, 1.0% NP-40, 0.5% sodium deoxycholate, 0.1% SDS, 50 mM Tris, pH 8.0) with protease and phosphatase inhibitors (1 tablet per 10 ml; Pierce). DNA was degraded using 250 units benzonase (EMD Milipore). Proteins were separated by SDS-PAGE and transferred to nitrocellulose membranes. Membranes were blocked for 1h at RT in Odessey blocking buffer (Licor) or 4% BSA and incubated overnight at 4°C with the following antibodies: pNF-κB Ser536, 1:1000 (Cell signaling 3033S), STAT1, 1:1000

(Cell Signaling 9172S), pSTAT1 Tyr701, 1:1000 (Cell Signaling 9177S); IRF3, 1:1000 (Cell Signaling 4302), pIRF3 Ser396, 1:1000 (Cell Signaling 4947); ACTIN 1:5000 (Abcam 6276), TUBULIN, 1:5000 (Abcam 179513). Membranes were washed 3x in 1X TBS 0.1% Tween 20, and incubated with appropriate secondary antibody (Licor) for 2h at RT (20°C) prior to imaging on Odessey Fc Dual-Mode Imaging System (Licor).

## Immunofluorescence Microscopy and Histopathology

### *Coverslips*

RAW 264.7 macrophages expressing epitope tagged galectins were seeded at 2 x $10^5$ cells/well on glass coverslips in 24-well dishes. At the indicated time point, cells were fixed in 4% paraformaldehyde for 10 minutes at 37°C, then washed three times with PBS. Coverslips were incubated in primary antibody diluted in TBS+ 0.25% Triton-X + 5% Normal Goat Serum (TBST-NGS) for 3h. Cells were then washed three times in PBS and incubated in secondary antibodies diluted in TBST-NGS for 1h. Coverslips were incubated in DAPI for 5 minutes, then washed twice with PBS and mounted on glass slides using Fluoromount (Diagnostic Biosystems; K024) for imaging. Images were obtained using a FV1200 Olympus inverted confocal microscope equipped with 60X oil immersion objective. Images were analyzed using ImageJ. Maximum intensity projections of z-stacks were obtained and projected images were thresholded such that 3XFLAG-tagged galectin puncta in macrophages were masked and counted. To obtain percent colocalization, GFP-tagged *R. equi* 103 were thresholded until they were masked, and region of interest (ROI) was saved. The *R. equi* ROI was then applied

to the thresholded galectin channel and measured. Results are expressed as percentage of bacteria colocalized with galectin.

### *Histopathology*

Lungs and spleens were fixed in 10% neutral buffered formalin, subjected to routine processing, embedded in paraffin, and 5-µm sections were cut and stained with hematoxylin and eosin (H&E) or acid-fast stain (Diagnostic BioSystems). A boarded veterinary pathologist (KJV) performed a masked evaluation of lung sections for inflammation using a scoring system: score 0, none; score 1, up to 25% of fields; score 2, 26-50% of fields; score 3, 51-75% of fields; score 4, 76-100% of fields. To quantify the percentage of lung fields occupied by inflammatory nodules, scanned images of at least 2 sections of each lung were analyzed using Fiji Image J[111] to determine the total cross-sectional area of inflammatory nodules per total lung cross sectional area. For acid fast staining, one brain hemisphere was fixed with paraformaldehyde for 48h, then transferred to a cryoprotective buffer (30% sucrose in a phosphate buffer), and frozen for coronal slicing into 40-µm sections. At least two sections per mouse were stained with an acid-fast stain (Diagnostic BioSystems) according to the manufacturer's instructions and visualized by an Olympus BH2 light microscope.

### *Brain Immunohistochemistry*

At indicated time points, infected or uninfected mice were anesthetized with isoflurane and quickly decapitated. The brain was gently removed from the skull and postfixed in 4% paraformaldehyde overnight at 4°C. The tissue was cryoprotected in 30% sucrose + PBS solution for 48-72h. Forty µm thick coronal sections were obtained

using a cryostat microtome (Leica) and preserved in 0.01% sodium azide + PBS at 4°C. Immunohistochemistry was performed using previously published techniques.[112,113] Briefly, sections were washed three times for 10 minutes in 1X TBS, then blocked for 1h in 5% normal goat serum (NGS) and 0.25% Triton-X-100 in 1X TBS at room temperature. Sections were incubated overnight at 4°C in primary antibodies diluted in blocking solution. The following primary antibodies were used: rabbit anti-GFAP (1:1000; Abcam ab7260), rabbit anti-Iba1 (1:250; Wako Chemical 019-19741), mouse anti-NeuN (1:500; Abcam ab104224), and chicken anti-TH (1:1000; Abcam ab76442). The following day, sections were washed 3 times for 10 minutes each in 1X TBS and incubated with appropriate secondary antibodies in blocking solution for 2h at room temperature. The following secondary antibodies were used: goat anti-rabbit (1:1000; Abcam ab150077), goat anti-mouse (1:1000; Abcam ab150120), and goat anti-chicken (1:1000; Abcam ab150176). The sections were rinsed 3 times for 10 minutes in 1X TBS and then mounted on microscope slides in Fluoromount (Diagnostic Biosystems; K024) for imaging.

*Brain Imaging and Analysis*

Images were obtained using a FV 1200 Olympus inverted confocal microscope equipped with 20x, 0.85 NA oil immersion objective, 473 nm, and 561 nm laser lines to excite appropriate Alexa Fluor secondary antibodies. Images were obtained at 1x digital zoom. HV, gain, and offset was adjusted so that fluorescent signals from images were just below saturation. Laser power for 473 and 561 excitation lines were maintained between 2-3% of maximum. All images were acquired as z-stacks with a 1 μm step size

and stack sizes ranged between 25-30 μm. Parameters were kept constant for all mice in an experimental group, which was defined based on infection status. Images were collected and processed with mouse genotypes blinded. Images were processed using ImageJ.[111] For image analysis, maximum intensity projections of z-stacks were first obtained. Projected images were thresholded such that GFAP staining in astrocytic cell bodies or Iba-1 staining in microglial cell bodies along with branches (1° and 2°) were masked and ROIs were obtained in this way. In each case, corresponding NeuN labeled or TH labeled sections were processed in a similar manner to astrocytic and microglial staining. Integrated density values were extracted from astrocytic, microglial, and corresponding neuronal components of each slice. Ratios of astrocytic or microglial integrated density to respective neuronal integrated density (NeuN/TH) were obtained and averaged across each brain region and all slices for each mouse. By utilizing ratios of glial signal to neuronal staining intensity, we controlled for differences between individual sections that occur due to variations in the efficiency of antibody binding or tissue quality. Data are presented as averages for each mouse. Mean values ± SEM from the averages are presented.

**Statistical Analysis**

All data are representative of at least 2 independent experiments with n of 3 or greater. qRT-PCR results are reported as the mean ± SD unless otherwise noted. Statistical analysis was performed using GraphPad Prism software (GraphPad, San Diego, CA). Unless otherwise noted, two-tailed unpaired Student's t tests were used for statistical analysis of cell culture studies. CLC Genomics Workbench (Qiagen) was used

for statistical analysis of RNA-seq experiments using the EDGE test. Differentially expressed genes were selected as those with a p-value threshold of $<0.05$.

# CHAPTER III

# THE OPPORTUNISTIC INTRACELLULAR BACTERIAL PATHOGEN *RHODOCOCCUS EQUI* ELICITS TYPE I INTERFERONS BY ENGAGING CYTOSOLIC DNA SENSNG IN MACROPHAGES

## Overview

*Rhodococcus equi* is a major cause of foal pneumonia and an opportunistic pathogen in immunocompromised humans. While alveolar macrophages constitute the primary replicative niche for *R. equi*, little is known about how intracellular *R. equi* is sensed by macrophages. Here, we discovered that that in addition to previously characterized pro-inflammatory cytokines (e.g., Tnfα, Il6, Il1b), macrophages infected with *R. equi* induce a robust type I IFN response, including *Ifnb* and interferon-stimulated genes (ISGs), similar to the evolutionarily related pathogen, *Mycobacterium tuberculosis*. Follow up studies using a combination of mammalian and bacterial genetics, demonstrated that induction of this type I IFN expression program is largely dependent on the cGAS/STING/TBK1 axis of the cytosolic DNA surveillance pathway, suggesting that *R. equi* perturbs the phagosomal membrane and causes DNA release into the cytosol following phagocytosis. Consistent with this we found that a population of ~12% of *R. equi* phagosomes recruited the galectin-3, -8 and -9 danger receptors. Interesting, neither phagosomal damage nor induction of type I IFN required the *R. equi*'s virulence-associated plasmid. Importantly, *R. equi* infection of both mice and foals stimulated ISG expression, in organs (mice) and circulating monocytes (foals).

By demonstrating that *R. equi* activates cytosolic DNA sensing in macrophages and elicits type I IFN responses in animal models, our work provides novel insights into how *R. equi* engages the innate immune system and furthers our understanding how this zoonotic pathogen causes inflammation and disease.

## Introduction

*Rhodococcus equi* is a gram positive, intracellular bacterial pathogen that causes severe, potentially fatal respiratory disease in young horses up to 6 months of age. *R. equi* infection has a major detrimental impact on the equine breeding industry for several reasons: it is nearly ubiquitous in the soil of some facilities, there is not currently an efficacious vaccine, and early diagnosis is challenging.[52] Virtually all foals are exposed by inhalation of contaminated soil. While many develop subclinical infection, 18-50% of foals develop pneumonia but recover with treatment, and 2-5% perish.[51,55,57,114] Those that do not succumb to disease develop lifelong immunity and active infection is rare in adult horses.[58]

*R. equi* is also a pathogen of humans, causing a pneumonia that radiographically and pathologically resembles pulmonary tuberculosis (TB), as well as extrapulmonary infections.[68,69,115] The majority of human cases manifest as pneumonia and occur in immunocompromised individuals, such as those with impaired cell mediated immunity due to HIV infection[116] or immunosuppression therapy related to organ transplantation.[117] However, a growing number of cases have been reported in immunocompetent humans, less than half of which develop pulmonary lesions.[69,115] Over 50% of human infections are derived from porcine- or equine-adapted strains,

indicating that most human *R. equi* infections are zoonotic.[116,118] Upon inhalation, *R. equi* survives and replicates within alveolar macrophages in a phagosomal compartment that fails to mature into a lysosome, resulting in the *R. equi*-containing vacuole. Previous studies have shown that *R. equi* pathogenesis depends in large part on expression of bacterial virulence factors[70,72,76,77] and production of pro-inflammatory cytokines,[79,81,119] but the nature of the innate immune milieu generated by *R. equi* infection remains ill-defined.

The toll-like receptor (TLR) family is a vital component of innate immunity against microbial pathogens. TLR signaling, through adaptor proteins such as MyD88 and TRIF, as well as transcription factors like NF-κB, is central to pro-inflammatory cytokine production.[8] Several lines of evidence demonstrate the importance of host expression of pro-inflammatory cytokines such as IFN-ɣ and TNF-α in *R. equi* pathogenesis. While most laboratory strains of mice are resistant to *R. equi*, treatment with monoclonal antibodies against IFN-ɣ, TNF-α, or both fail to clear *R. equi* infection, develop pulmonary lesions, and succumb to disease.[79,81,82] Likewise, *R. equi* replication is reduced in equine monocyte derived macrophages primed with IFN-γ or TNF-α prior to infection.[78] The requirement for pro-inflammatory cytokine production in clearing *R. equi* was further illustrated by Darrah and colleagues, who showed that IFN-γ deficient (*Ifng*$^{-/-}$) mice infected with low dose *R. equi* were hypersusceptible to infection (died 13 days post-infection), and mice with impaired nitric oxide (*Nos2*$^{-/-}$) or superoxide (*Gp91*$^{phox-/-}$) production were even more susceptible and died by days 7.5 and 9.5 post infection respectively.[80] Together, these studies suggest that IFN-γ activates

macrophages to produce reactive oxygen species that limit intracellular replication and kill *R. equi.*[80]

While signaling via IFN-γ, a type II IFN, is important for macrophage activation and control of bacterial infection, type I IFN can act as a negative regulator of host defenses against intracellular bacterial infection. This paradigm is particularly evident in mycobacterial infection, where a type II IFN signature is associated with mild pathogenesis and increased pathogen clearance during both *Mycobacterium tuberculosis* and *Mycobacterium leprae* infection: a type I IFN response is correlated with diffuse lepromatous leprosy and active tuberculosis in humans.[47,120] Both *M. leprae* and *M. tuberculosis* replicate within a modified phagosome, which they permeabilize via their ESX-1 virulence-associated secretion systems, to interact with the host macrophage. It is increasingly appreciated that numerous intracellular bacterial pathogens, including *M. tuberculosis*, *L. monocytogenes,* and *F. tularensis,* activate cytosolic DNA sensing and induce type I IFN signaling through similar mechanisms.[12,22,25] Like mycobacteria, *R. equi* also possesses an ESX secretion system,[49] but the contribution of cytosolic surveillance to the macrophage response to *R. equi* has not known.

In spite of the detrimental impact this important pathogen has on the equine breeding industry, data on macrophage sensing of *R. equi* is incomplete, and to date, studies of this pathogen have centered on extracellular macrophage receptors. Here, we sought to investigate whether this vacuolar pathogen triggers innate immune responses in the macrophage cytosol. Additionally, we sought to characterize the transcriptional response triggered by *R. equi* during *ex vivo* infection in murine macrophages as well as

*in vivo* in mice and in foals. Using RNA-seq, we found that numerous type I IFN genes were upregulated during *R. equi* infection and that this bacterium induces phagosomal permeabilization in a way that recruits galectin danger sensors. While both galectin recruitment and the type I IFN gene expression profile was not dependent on expression of the *R. equi* virulence-associated protein A (VapA), type I IFN production did require the cGAS/STING/TBK1 signaling axis. Furthermore, we found that a type I IFN program was induced *in vivo* in both a mouse model as well as in an equine model. These data provide evidence that *R. equi* activates the cytosolic DNA sensing pathway during macrophage infection and suggest that type I IFN signaling may be critical for *R. equi* pathogenesis.

## Results

### *Transcriptomics Uncovers Upregulation of Pro-Inflammatory Cytokines and Type I Interferon in R. equi Infected Murine Macrophages*

To begin to define the nature of the macrophage innate immune response to *R. equi*, we turned to RNA-seq as an unbiased approach to assess global gene expression changes following infection. Briefly, RAW 264.7 macrophages were infected with virulent *R. equi* (ATCC 33701+) at a multiplicity of infection (MOI) of 5 and total RNA from uninfected and infected cells was harvested after 4h (previous studies of Mtb infection of RAW 264.7 cells show robust induction of TLR and cytosolic nucleic acid sensing pathways at this time point).[22,24,100] High-throughput RNA sequencing was carried out on 3 biological replicates of uninfected and infected macrophages. After filtering transcripts with a fold change of $> \pm 2$ ($p < 0.05$), we identified 390 genes that

were upregulated and 65 genes that were downregulated in *R. equi*-infected macrophages compared to uninfected controls (Figure III-1A). Interestingly, the expression profile had considerable overlap with that of macrophages infected with Mtb, with 167 *R. equi*-induced genes also upregulated in Mtb-infected macrophages, and 6 genes downregulated in both groups (Figure III-1B). Consistent with previous findings,[119,121,122] we observed significant upregulation of numerous canonical pro-inflammatory cytokines (*Il1a, Il1b,* and *Tnf)*, chemokines (*Cxcl2*, *Ccl4*, *Ccl3*, Cxcl10), inflammasome genes (*Nlrp3*)*,* and prostaglandins (*Ptgs2*) at 4h post-*R. equi* infection (Figure III-1C). We also observed upregulation of several antiviral genes that are induced downstream of the IRF (interferon regulatory factor) family of transcription factors (*Rsad2*, *Ifit1*). To validate RNA-seq gene expression changes during *R. equi* infection, representative upregulated (*Lif, Nlrp3*) and downregulated (*Mafb* and *S1pr1*) transcripts were measured by RT-qPCR (Figure III-1D). Because some innate immune transcripts can peak after 4h, we measured gene expression at both 4h and 8h following infection.

Using Ingenuity Pathway Analysis (IPA, Qiagen), we next asked which pathways were enriched for differentially expressed genes (DEG) in uninfected vs *R. equi*-infected macrophages. Unbiased canonical pathway analysis of the biological processes most enriched during *R. equi* infection showed strong upregulation of genes related to innate immune signaling ("Role of pattern recognition receptors in recognition of bacteria and viruses", "Interferon signaling", "Glucocorticoid receptor signaling"), cell death ("Death receptor signaling"), and tumor pathogenesis ("Tumor

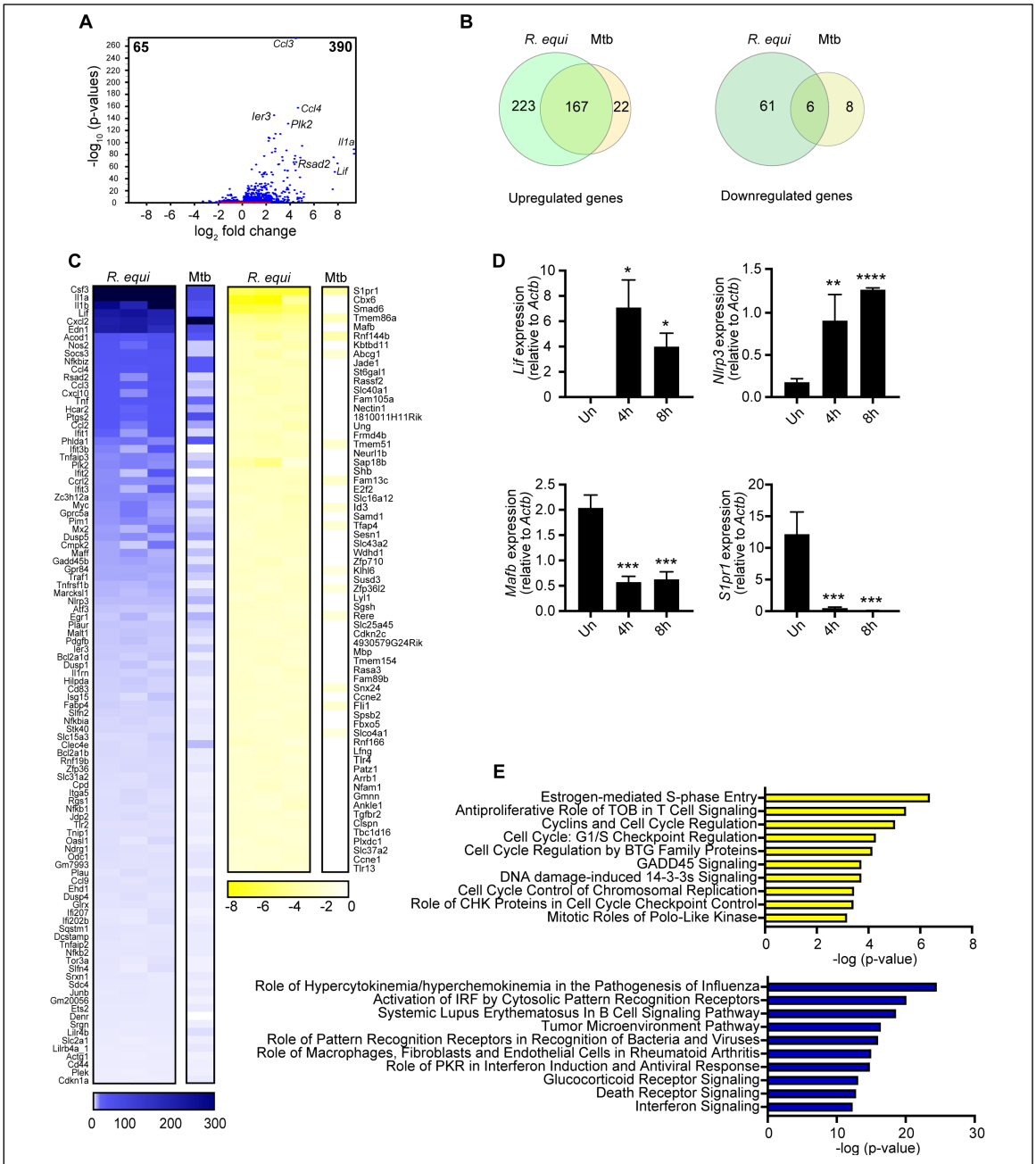


Figure III-1: RNA-seq reveals upregulation of pro-inflammatory cytokines and type I IFN genes in *R. equi*-infected macrophages. (A) Volcano plot of gene expression analysis. X-axis shows fold change of gene expression and y-axis shows statistical significance. (B) Venn diagram of differentially expressed genes in *R. equi*- and Mtb-infected RAW 264.7 macrophages. (C) Heatmap of gene expression of macrophages infected or not for 4h with *R. equi* or Mtb. Each column for *R. equi* represents a biological replicate. Mtb is shown as average of 3 replicates. Genes upregulated in infected cells are shown in blue and downregulated genes in yellow. (D) qRT-PCR validation of upregulated (*Lif*, *Nlrp3*) and downregulated (*Mafb*, *S1pr1*) genes. (E) IPA analysis of *R. equi*-infected RAW 264.7 macrophages infected. Downregulated genes are in yellow and upregulated genes are in blue.

microenvironment pathway") (Figure III-1E). Pathways enriched for downregulated genes were primarily related to cell-cycle regulation ("Estrogen-mediated S phase entry", "Cyclins and cell cycle regulation", "Cell cycle G1/S checkpoint regulation", "Cell cycle regulation by BTG family proteins", "Cell cycle control of chromosomal replication") (Figure III-1E). Intriguingly, viral pathogenesis-related pathways, specifically "Role of hypercytokinemia/hyperchemokinemia in the pathogenesis of Influenza" and "Role of PKR in IFN induction and antiviral response", were among the most enriched pathways in our IPA analysis of upregulated genes. Together, these findings began to suggest that antiviral IFN expression, in addition to pro-inflammatory cytokines and chemokines, may play an important role in *R. equi*.

### *R. equi Induces Both Pro-Inflammatory Cytokine and Type I Interferon Expression During Macrophage Infection*

To more closely examine the macrophage innate immune response to *R. equi* infection, we first measured pro-inflammatory cytokine induction in macrophages infected with *R. equi*. *R. equi*-infected macrophages had robust induction of the pro-inflammatory cytokines *Tnfa, Il1b* and *Il6* at 4h and 8h, consistent with initial sensing events. This was the case both for RAW 264.7 macrophages (Figure III-2A) as well as primary BMDMs (A.1A). To track NF-κB activation, we measured phosphorylation of NF-κB (Ser536) in cell lysates by immunoblot analysis and observed robust NF-κB phosphorylation at 2, 4 and 6h (Figure III-2B). Expression of these cytokines was at least partially dependent on MyD88, as RAW 264.7 macrophages with *Myd88* knocked down by shRNA (*Myd88* KD, 65% efficiency) (A.2B) had reduced levels of *Il1b*, *Il6* and *Tnfa*

after *R. equi* infection compared to Scr controls (Figure III-2C, A.1C). These findings are consistent with an early study by Darrah and colleagues, who reported production of pro-inflammatory mediators in a TLR2- and MyD88-dependent manner.[119]

Our transcriptomics analysis also revealed upregulation of several type I IFN response genes (Figure III-1C), and canonical pathway analysis revealed antiviral signaling as a highly enriched pathway in *R. equi*-infected macrophages (Figure III-1E). To further investigate the type I IFN response induced by *R. equi*, we first assessed the dynamics of *Ifnb* expression over a time-course of *R. equi* macrophage infection, in murine BMDMs and in RAW 264.7 macrophage cells by RT-qPCR. We observed strong induction of *Ifnb* peaking at 4h post-infection in both cell types (Figure III-2D). To determine whether transcriptional upregulation of *Ifnb* led to elevated protein levels in *R. equi* infected cells, we used an IFN-stimulated response element (ISRE) luciferase reporter cell line as a readout for secreted IFN-α/β from *R. equi*-infected RAW 264.7 macrophages (Figure III-2E). Consistent with the transcriptional changes, we observed robust production of IFN-α/β in response to *R. equi* infection. Secreted IFN-β is recognized in an autocrine and paracrine manner through the IFN-α/β receptor (IFNAR1/2) and results in downstream expression of interferon stimulated genes (ISGs). Thus, we next measured expression of several ISGs, including *Isg15*, *Ifit1* and *Mx1,* over the same time course. We observed significant induction of these genes 4h post-infection with peak induction at 8h in both RAW 264.7 cells and BMDMs (Figure III-2F). The kinetics of both *Ifnb* and ISG induction in *R. equi*-infected macrophages closely

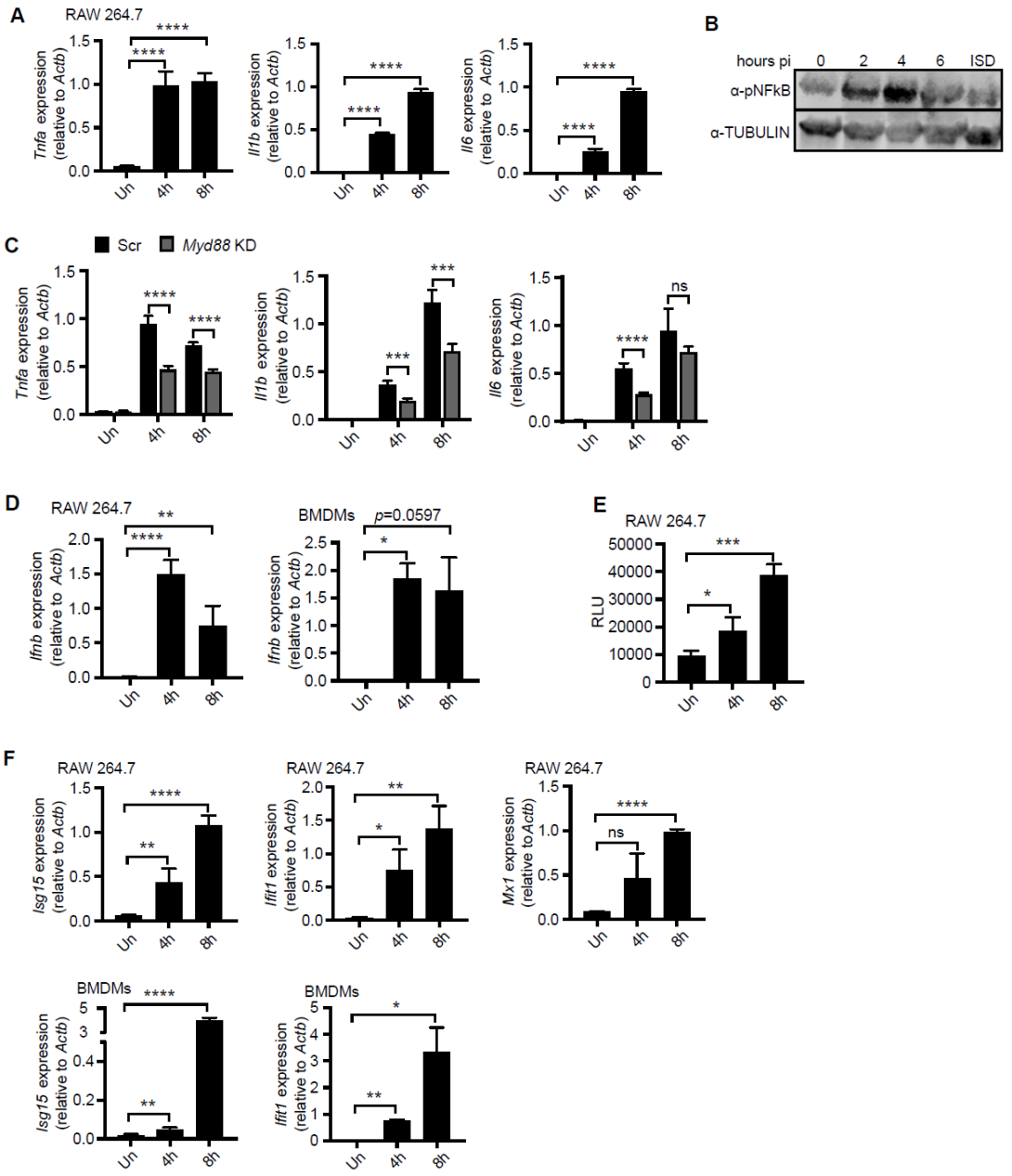


Figure III-2: *R. equi* induces type I IFN expression during macrophage infection (A) qRT-PCR of *Tnfa*, *Il1b* and *Il6* in RAW 264.7 macrophages at 4 and 8 h post infection with *R. equi*. (B) Western blot of pNFκB in RAW 264.7 macrophages infected or not with *R. equi* 33701+ for 2, 4 or 6h, or treated with ISD, with TUBULIN as a loading control. (C) qRT-PCR of *Tnfa, Il1b* or *Il6* in RAW 264.7 in *Myd88* KD macrophages infected with *R. equi*. (D) qRT-PCR of *Ifnb* in RAW 264.7 macrophages and BMDMs infected with *R. equi*. (E) ISRE reporter assay expressing luciferase with relative light units measured as a readout for secreted I IFNα/β from *R. equi* infected macrophages. (F) qRT-PCR of *Isg15*, *Ifit1* and *Mx1* in RAW 264.7 and BMDMs.

resembles what we have previously reported for Mtb-infected macrophages.[22,123] Therefore, we concluded that *R. equi* infection elicits a robust type I IFN response in macrophages.

### *The R. equi Virulence Factor VapA Is Not Required for Induction of Pro-Inflammatory Cytokines or Type I Interferons in Macrophages*

*R. equi*'s ability to survive and replicate within macrophages is largely dependent on a ~ 90 kb virulence plasmid and the virulence associated proteins (Vaps) it encodes. The best characterized, VapA, is required for virulence in foals and promotes bacterial intracellular survival,[70,76] as plasmid-cured strains of *R. equi* fail to replicate inside macrophages and do not cause inflammatory cell death.[72] To investigate if VapA is required for inducing pro-inflammatory cytokines or type I IFNs in response to *R. equi* infection, we infected RAW 264.7 macrophages with isogenic strains of *R. equi* with (33701+) and without (33701-) VapA at a MOI of 5 for 4 and 8h and measured gene expression. Macrophages infected with plasmid-cured *R. equi* (33701-) had reduced expression of *Tnfa* at 8h, and of *Il6* at both 4 and 8h after infection (Figure III-3A). Consistent with a previous study using *R. equi* strain ATCC 103 in mouse peritoneal macrophages,[122] macrophages infected with *R. equi* 33701- lacking VapA had greater *Il1b* expression at 8h post-infection (Figure III-3A). However, *Ifnb* and *Isg15* expression in macrophages infected with *R. equi* 33701- was virtually identical to macrophages infected with virulent *R. equi* 33701+ (Figure III-3B). These findings indicate that while VapA does influence pro-inflammatory cytokine expression, it is not required for induction of type I IFNs during macrophage infections.

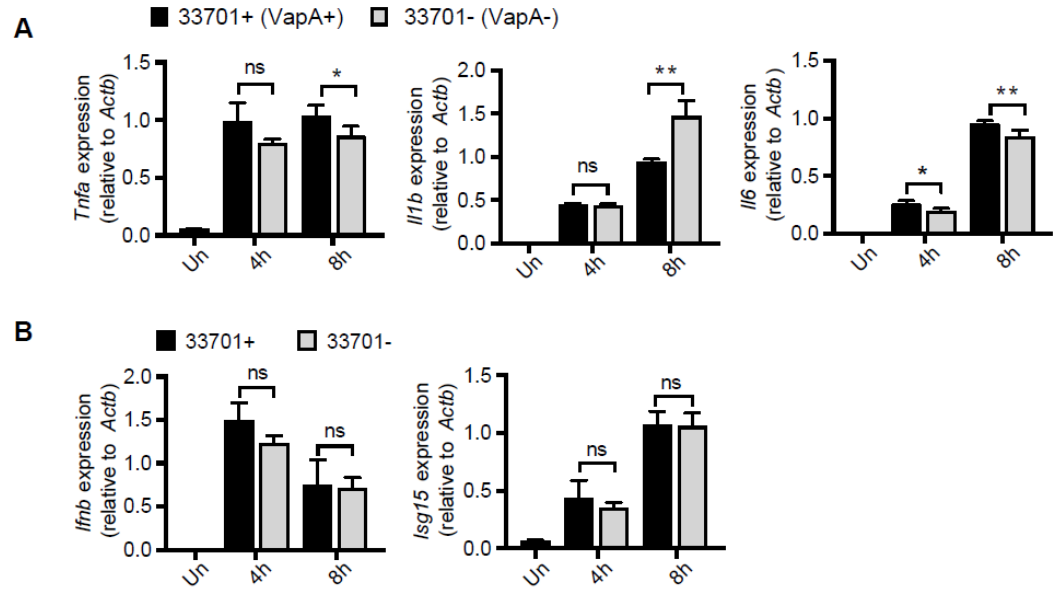


Figure III-3: VapA is not required for induction of pro-inflammatory cytokines or type I IFN in murine macrophages. (A) qRT-PCR of *Tnfa*, *Il1b* and *Il6* in RAW 264.7 macrophages infected with *R. equi* with (33701+) and without (33701+) VapA. (B) As above but measuring *Ifnb* and *Isg15*.All qRT-PCRs represent 3 biological replicates ± SD, n=3. For all experiments in this study, statistical significance was determined using Students' t-test. *p < 0.05, **p < 0.01, ***p < 0.001, ****p < 0.0001, n.s. = not significant.

### *TBK1 Is Required for Type I Interferon Induction in Response to R. equi Infection in Primary Murine Macrophages*

*Ifnb* is induced in a number of ways, including downstream of endosomal (e.g., TLR9 sensing of CpG DNA, TLR3 sensing of double-stranded RNA) or cytosolic (e.g., cGAS sensing of double-stranded DNA) sensing pathways, each of which trigger phosphorylation and activation of the interferon regulatory transcription factor (IRF) family proteins, primarily IRF3 and IRF7. Because IRF7 is expressed at low levels in macrophages until induced downstream of type I IFN, while IRF3 is expressed

ubiquitously and activated downstream of pathogen associated molecular patterns,[124,125] we focused on IRF3. To determine if IRF3 is activated in response to *R. equi* infection, we infected RAW 264.7 cells (MOI of 50) and measured phosphorylated (Ser396) IRF3 by immunoblot. We detected IRF3 phosphorylation at 2-, 4- and 6h post-*R. equi* infection, peaking at 4h (Figure III-4A). We also examined STAT1 activation, which occurs downstream of the IFN α/β receptor IFNAR1/2 and found strong phosphorylation at 4, and 6h post-infection, with peak activity at 4h (Figure III-4A). To implicate specific adapter proteins in type I IFN induction during *R. equi* infection, we measured ISG expression (i.e., *Isg15*, *Ifit1* and *Mx1*) by RT-qPCR in *Myd88*- (Figure III-4B) and *Trif*-knockdown macrophages (*Trif* KD, 70% efficiency) (A.2A). We detected no major difference in ISG expression with the reduction of either of these TLR adapters, with the exception of a modest reduction in *Isg15* expression in *Trif* knockdown *R. equi*-infected RAW 264.7 cells relative to Scr controls (A.2B). These results suggest that neither TLR9 nor TLR3 are required for type I IFN signaling during *R. equi* infection.

Having observed activation of IRF3 in *R. equi*-infected macrophages (Figure III-4A), we hypothesized that the innate immune kinase TBK1 is required for type I IFN production. To test the contribution of TBK1 in type I IFN signaling during *R. equi* infection, we isolated BMDMs from mice lacking the kinase TBK1. Because *Tbk1* deletion in C57BL/6 mice causes a TNF receptor-dependent embryonic lethality, we used $Tbk1^{-/-}/Tnf^{-/-}$ double KO (TBK1 KO) mice to assess the contribution of TBK1 and compared them to $Tbk1^{+/+}/Tnf^{-/-}$ controls.[22,126] As expected, $Tbk1^{-/-}$ macrophages fail to

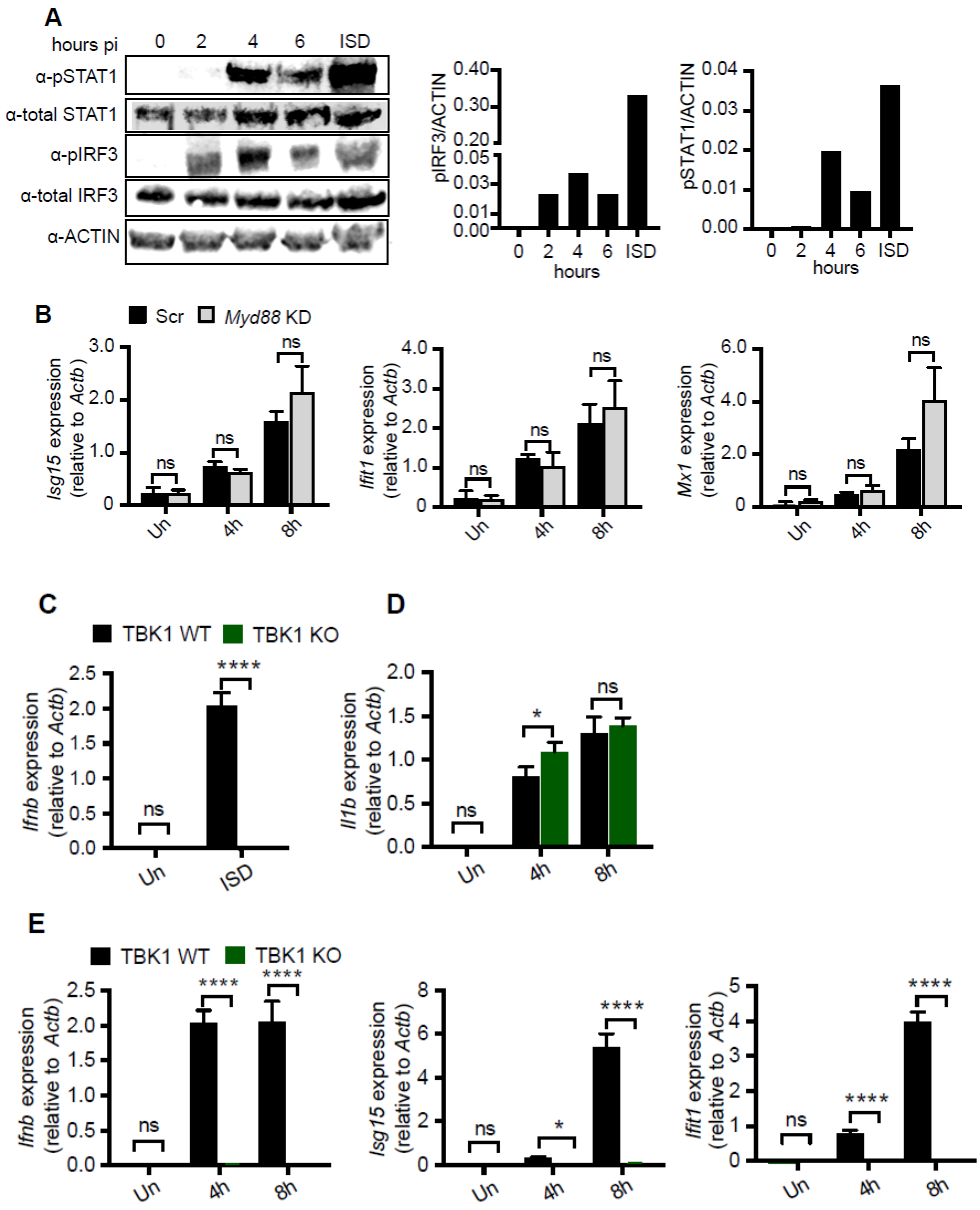


Figure III-4: TBK1 is required for type I IFN induction in response to *R. equi* infection in primary murine macrophages. (A) Immunoblot of pSTAT1, total STAT1, pIRF3 and total IRF3 in RAW 264.7 macrophages uninfected (0) or infected with *R. equi* for 2, 4 or 6h or stimulated with ISD for 4h. ACTIN was used as a loading control. (B) qRT-PCR of *Isg15*, *Ifit1* and *Mx1* in *Myd88* KD macrophages infected with *R. equi* for the indicated times. (C) qRT-PCR of *Ifnb* in TBK1 WT (*Tbk1*$^{+/+}$*Tnfr*$^{-/-}$) and KO (*Tbk1*$^{-/-}$*Tnfr*$^{-/-}$) BMDMs treated with ISD for 4h. (D) qRT-PCR of *Il1b* in TBK1 BMDMs uninfected or infected with *R. equi* for the indicated times. (E) As in D but *Ifnb*, *Isg15* and *Ifit1*. All qRT-PCRs represent 3 biological replicates ± SD, n=3. Statistical significance was determined using Students' t-test. *p < 0.05, **p < 0.01, ***p < 0.001, ****p < 0.0001, n.s. = not significant.

induce *Ifnb* in response to transfection with the double-stranded DNA agonist ISD (Figure III-4C). *R. equi*-infected *Tbk1*$^{-/-}$ BMDMs had no difference in expression of the pro-inflammatory cytokine *Il1b* compared to controls (Figure III-4D). However, *R. equi*-infected *Tbk1*$^{-/-}$ macrophages had almost no induction of *Ifnb, Isg15* and *Ifit1* at 4 and 8h after infection (Figure III-4E), indicating that TBK1 is required for induction of a type I IFN response following infection with *R. equi*.

Because autocrine sensing of IFN-β by IFNAR1/2 elicits ISG expression via STATs, we predicted that loss of IFNAR would abrogate the type I IFN response in *R. equi* infected macrophages. As a positive control, when we transfected *Ifnar1*$^{-/-}$ macrophages with ISD (which stimulates *Ifnb* production), there was no ISG induction (A.2C). Compared to WT controls, *Ifnar1*$^{-/-}$ macrophages had no differences in pro-inflammatory cytokine levels after *R. equi* infection (A.2D). However, *R. equi*-infected *Ifnar1*$^{-/-}$ macrophages displayed a modest reduction in *Ifnb* levels (A.2E), and ISG expression (*Isg15)* was completely abrogated (A.2E). These data indicate that *R. equi* induces type I IFN through TBK1 and IFNAR, but that this occurs by a sensor other than TLR3 or 9.

*The Cytosolic DNA Sensing Axis of Cgas/STING/TBK1 Is Required to Induce Type I IFN During R. equi Infection of Primary Murine Macrophages*

Having ruled out type I IFN induction by several adapter proteins downstream of TLR sensors, we next asked whether *R. equi* infection directly stimulates cytosolic nucleic acid sensing. STING is an adaptor protein in the cytosolic DNA sensing axis that is activated by host cyclic dinucleotides like cGAMP produced by activated cGAS, or

bacterial cyclic dinucleotides like c-di-AMP or c-di-GMP.[11,16,18] To investigate whether STING is required for *R. equi* induction of type I IFNs, we infected CRISPR-Cas9-generated STING knock out (KO) RAW 264.7 macrophages with *R. equi* and measured cytokine expression by RT-qPCR. In response to *R. equi* infection, while STING KO macrophages induced *Tnfa* to comparable levels as control macrophages (expressing a GFP-targeting guide RNA), they failed to induce *Ifnb*, *Isg15,* or *Ifit1* at 4 or 8h post-infection (Figure III-5A). As a positive control we first transfected STING KO RAW 264.7 macrophages with ISD (to stimulate cGAS and thus STING) and found that these cells fail to induce *Ifnb* (A.3A).[127] Using ISRE reporter cells, we also observed a reduction in protein levels of IFN-α/β in the supernatants of STING KO macrophages compared to controls (A.3B). These data indicate that STING is absolutely required for type I IFN expression in response to *R. equi* infection in macrophages.

Some intracellular bacterial pathogens such as *Listeria monocytogenes* activate cytosolic sensing by producing cyclic dinucleotides (c-di-AMP) that bind to and activate the adaptor protein STING, which in turn activates TBK1.[128] To determine if *R. equi* might activate the cytosolic DNA sensing pathway in a similar way, we searched the Kegg database and found that *R. equi* also encodes a cyclic dinucleotide, diadenylate cyclase that could produce c-di-AMP.[71] To test if *R. equi* was stimulating STING directly via production and secretion of c-di-AMP or via activation of cGAS, which produces the cyclic dinucleotide cGAMP in response to binding cytosolic double-stranded DNA,[14,26] we generated cGAS KO RAW 264.7 cells using CRISPR-Cas9. As with loss of STING, cGAS KO macrophages fail to induce *Ifnb* in response to ISD

transfection (A.3C). Upon infection with *R. equi*, cGAS KO macrophages had reduced levels of *Ifnb*, *Isg15* and *Ifit1* transcripts (Figure III-5B), and a significant but less dramatic reduction in *Tnfa* (Figure III-5B). At the protein level, cGAS KO macrophages had defective IFN-α/β production as measured by ISRE reporter cells, but notably, expression was not completely ablated (A.3D). However, when we measured IFN-β protein levels at 0, 8 and 24h post-infection by ELISA, we observed a complete loss of IFN-β in supernatants from both cGAS and STING KO macrophages (Figure III-5C). This loss of type I IFN production was not due to impaired bacterial engulfment or replication as bacterial burden was similar in control, STING KO and cGAS KO macrophages (A.3E). Because there was a slight inconsistency in IFN-β levels measured by ISRE reporter cells (which measure both IFN-α and -β) and by an IFN-β-specific ELISA (Figure III-5C, A.3D), we also measured STAT1 activation in *R. equi*-infected control, STING KO and cGAS KO macrophages by immunoblot probing for phosphorylated (activated) STAT1 (Tyr701). We found that in control macrophages STAT1 was robustly phosphorylated at 4 and 6h post-infection, but phosphorylated STAT1 was not detected in STING KO or cGAS KO macrophages at all time points (Figure III-5D). These results show that *R. equi* infection results in activation of the cGAS/STING/TBK1 axis and further suggests that release of double-stranded DNA into the cytosol is responsible for activation of the cytosolic DNA sensing pathway leading to production of type I IFN.

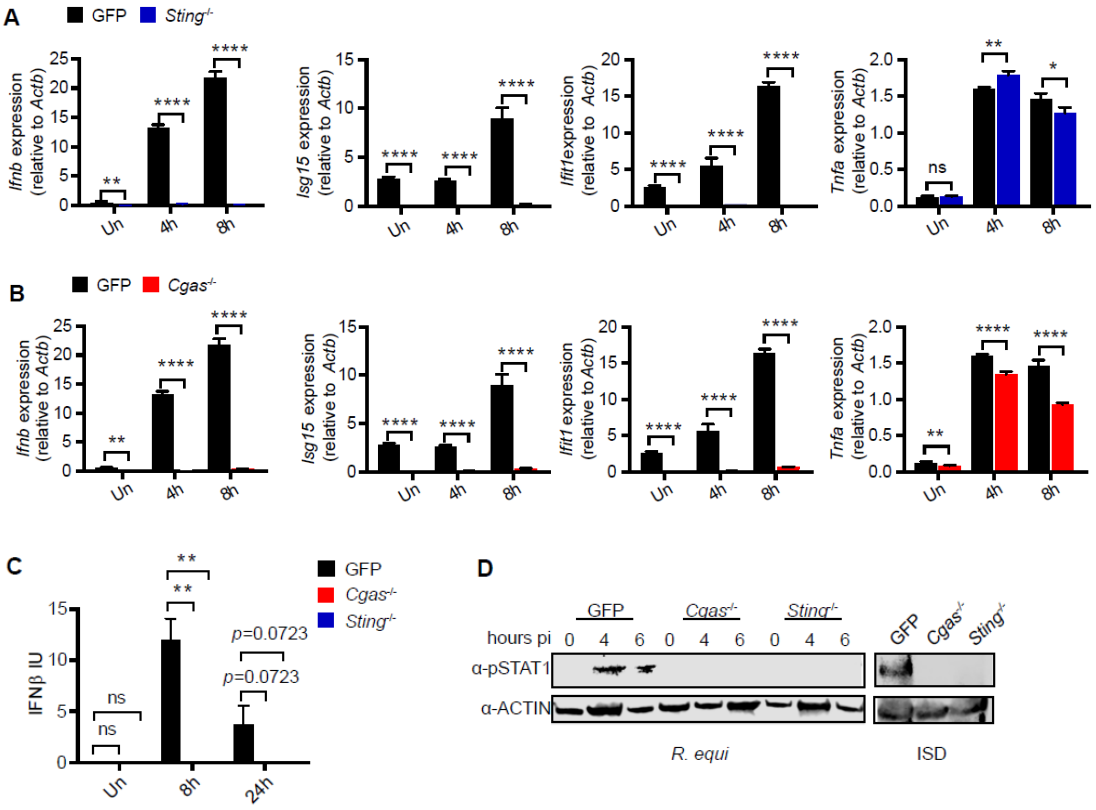


Figure III-5: The cytosolic DNA sensing axis of cGAS/STING/TBK1 is required to induce type I IFN during *R. equi* infection of macrophages. (A) qRT-PCR of *Ifnb*, *Isg15*, *Ifit1* and *Tnfa* in GFP control or STING KO RAW 264.7 macrophages infected with *R. equi* 33701+ for the indicated times. (B) As in A but in GFP control and cGAS KO RAW 264.7 macrophages. (C) IFN-β protein ELISA of cGAS KO, STING KO and GFP control RAW 264.7 macrophages infected with *R. equi* for the indicated times. (D) Immunoblot of pSTAT1 in *R. equi*-infected GFP, cGAS KO and STING KO RAW 264.7 cells for the indicated times or transfected with ISD for 4h. ACTIN was used as a loading control. All qRT-PCRs represent 3 biological replicates ± SD, n=3. For all experiments in this study, statistical significance was determined using Students' t-test. *p < 0.05, **p < 0.01, ***p < 0.001, ****p < 0.0001, n.s. = not significant.

### *Galectin-3, -8, And -9 Are Recruited to R. equi-Containing Vacuoles*

Because *R. equi* is confined by a phagosomal membrane until 24h post-infection in macrophages,[50] it was puzzling to observe activation of the cytosolic DNA sensor

cGAS early during infection. Previous studies discovered that Mtb, another "vacuolar" pathogen, permeabilizes its phagosomal membrane using its ESX-1 secretion system.[24] Therefore, we hypothesized that *R. equi* may also permeabilize its phagosomal membrane to allow for communication with the host cytosol resulting in detection by cytosolic DNA sensors. We recently reported that the cytosolic glycan-binding proteins galectin-3, -8, and -9 access the lumen of damaged Mtb-containing vacuoles following ESX-1-mediated permeabilization.[129] To investigate whether *R. equi* phagosomal membranes are sufficiently damaged during infection to recruit these galectins, we infected RAW 246.7 cells stably expressing 3xFLAG-tagged galectins.[129] Specifically, we used galectins-3, -8, and -9 because they have been shown to colocalize with Mtb*, L. monocytogenes*, *Salmonella enterica* serovar Typhimurium, and *Shigella flexneri;*[129,130] galectin-1 was used as a negative control. Each of these galectin cell lines were infected with virulent GFP-expressing *R. equi* [104] (MOI 5) and over a time course of 4, 8, and 16h, cells were fixed and imaged by immunofluorescence microscopy.[104] Galectin-3, -8, and -9 but not galectin-1 were all recruited to *R. equi* to varying degrees. Recruitment of galectins-8 and -9 peaked at 8h post-infection, with galectin recruited to ~10% and ~6% of *R. equi*, respectively (Figure III-6A, B). Galectin-3 recruitment peaked at 4h post-infection, with recruitment to ~12% of *R. equi* at 4h and declining to ~5% by 16h post-infection. Curiously, by 4h post-infection, galectin-3, -8, and -9 formed puncta in the cytosol of *R. equi* infected cells (Figure III-6C), but the nature of these puncta is unclear. Galectin-1 formed rare puncta but did not associate with *R. equi* (Figure III-6C). A

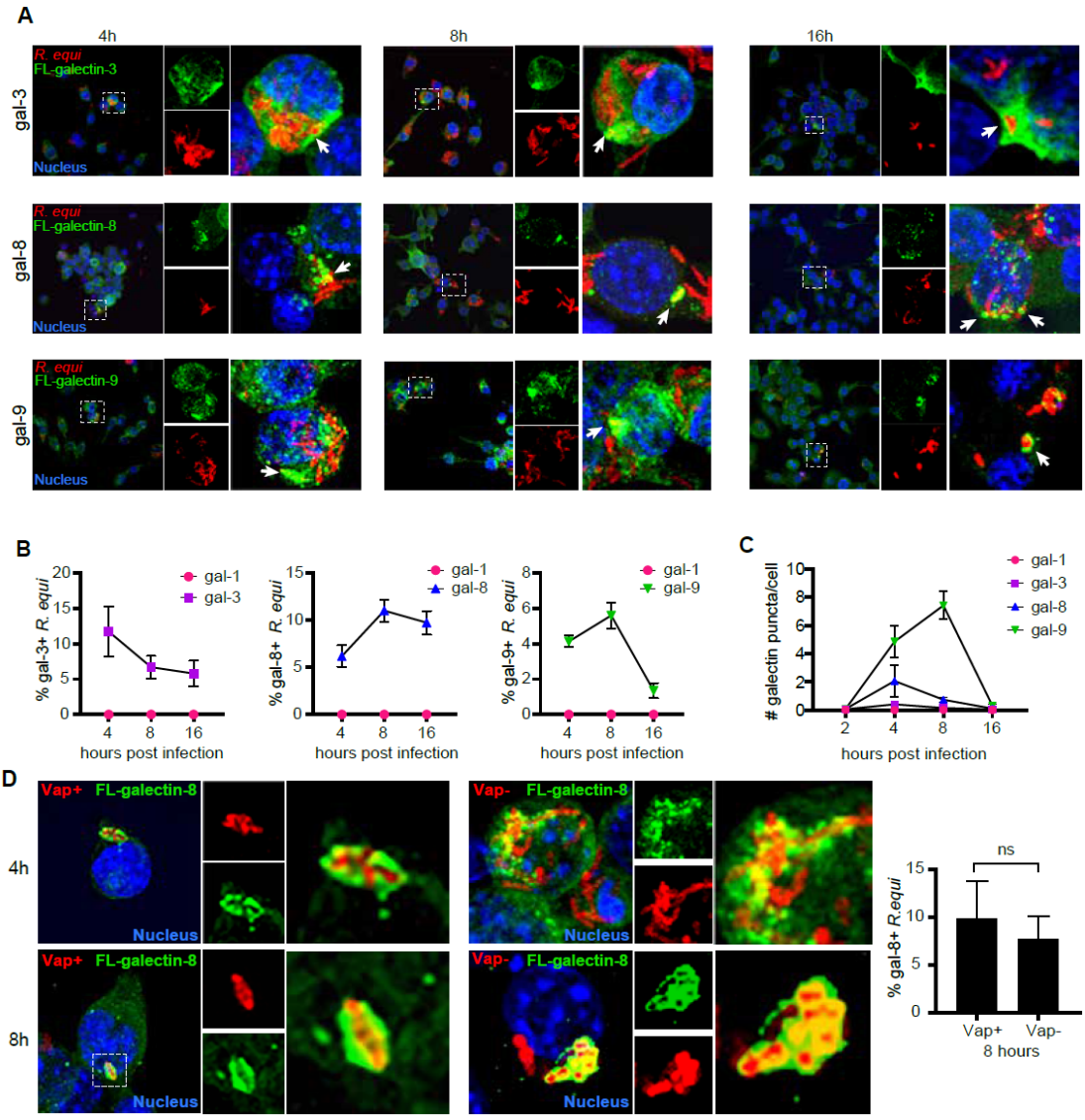


Figure III-6: Galectin-8 is recruited to *R. equi.* (A) Immunofluorescence (IF) of RAW 264.7 cells stably expressing 3XFLAG (FL)-tagged galectin-3, -8, or -9 infected with *R. equi* 103+ for the indicated times. (B) Quantification of galectin-1, -3, -8, or -9 recruitment to *R. equi* at the indicated times. (C) Quantification of galectin-1, -3, -8, or -9 puncta in *R. equi*-infected RAW 264.7 cells at the indicated times. (D) IF of RAW 264.7 cells stably expressing 3X FL-tagged galectin-8 infected with *R. equi* 103+ or 103- for the indicated time and quantification of galectin-8 positive *R. equi* in at 8 hours. IF images are representative of at 3 independent experiments. Quantification is the percent of positive bacteria with at least 100 bacteria quantified per coverslip. Error bars are ±SEM. Statistical significance was determined using Students' t-test. *$p < 0.05$, n.s. = not significant.

galectin-positive population of *R. equi* suggests that phagosomal membrane damage and access to the cytosol occurs as early as 4h following infection. Interestingly, at 16h, many of the galectin-positive *R. equi* had markedly reduced GFP expression compared to galectin-negative bacteria, suggesting they had potentially been killed or lysed.

Given that the *R. equi* virulence factor VapA has been shown to permeabilize lysosomal membranes to modulate lysosome pH[70] and are required for survival and replication within macrophages,[72] we hypothesized that VapA might be required for permeabilizing the phagosomal membrane and permitting galectin recruitment. To test this, we infected 3xFLAG tagged galectin-8 RAW246.7 cells with GFP-expressing, plasmid-cured *R. equi* 103-, which do not express VapA.[75] The plasmid cured strain of *R. equi* had similar recruitment of galectin-8 as VapA expressing *R. equi* (Figure III-6D), indicating that the *R. equi* phagosomal membrane permeabilization does not require VapA and occurs via an alternative mechanism. Taken together, these data indicate that the *R. equi*-containing vacuole is permeable and accessible to the macrophage cytosol, which could enable detection of bacterial-derived ligands by cGAS and other cytosolic sensors.

### *R. equi Induces Both A Pro-Inflammatory and Type I Interferon Expression Program In Vivo*

Having shown that *R. equi* induces type I IFNs in macrophages, we next sought to determine how the type I IFN response contributes to *R. equi* pathogenesis *in vivo*. Because we can exert a greater degree of control over the murine environment, we began by infecting 8-week-old C57BL/6 mice with *R. equi* by intraperitoneal (IP) injection. At

5d post-infection we harvested lungs, mesenteric lymph nodes, spleens and peritoneal cells (Figure II-1). Age-matched mice injected with an equal volume of PBS (Un) served as negative controls. Bacteria were recovered from the spleen, mesenteric lymph nodes and lungs, which indicates the bacteria disseminated from the point of initial infection (Figure III-7A). We measured spleen weights as a readout for inflammatory responses and observed a ~1.5-fold increase in splenic weight in infected mice compared to those injected with PBS (Figure III-7B). We measured pro-inflammatory cytokines and type I IFNs in the spleen and peritoneal cells isolated from *R. equi*-infected mice 5d post-infection by qRT-PCR, and consistent with our observations in macrophages, spleens and peritoneal cells from mice infected with *R. equi* had significantly elevated levels of both pro-inflammatory cytokines and ISGs compared to uninfected controls (Figure III-7C).

Because mice are relatively resistant to *R. equi* infection, and since horses are the primary natural host and most physiologically relevant model, we next turned to an equine model of infection. We collected pre-infection, baseline blood samples from 28-day-old horses and assessed their lungs for pulmonary lesions by thoracic ultrasonography. We next infected foals intrabronchially via endoscopy[56,109,110] with 1 x $10^6$ virulent *R. equi*, and monitored them for 21d; age-matched uninfected foals served as negative controls. At 21d post-infection, we again collected blood and evaluated lungs by thoracic ultrasonography to monitor disease progression or resolution (Figure II-3). To investigate if *R. equi* induces a type I IFN program in horses, we isolated monocytes

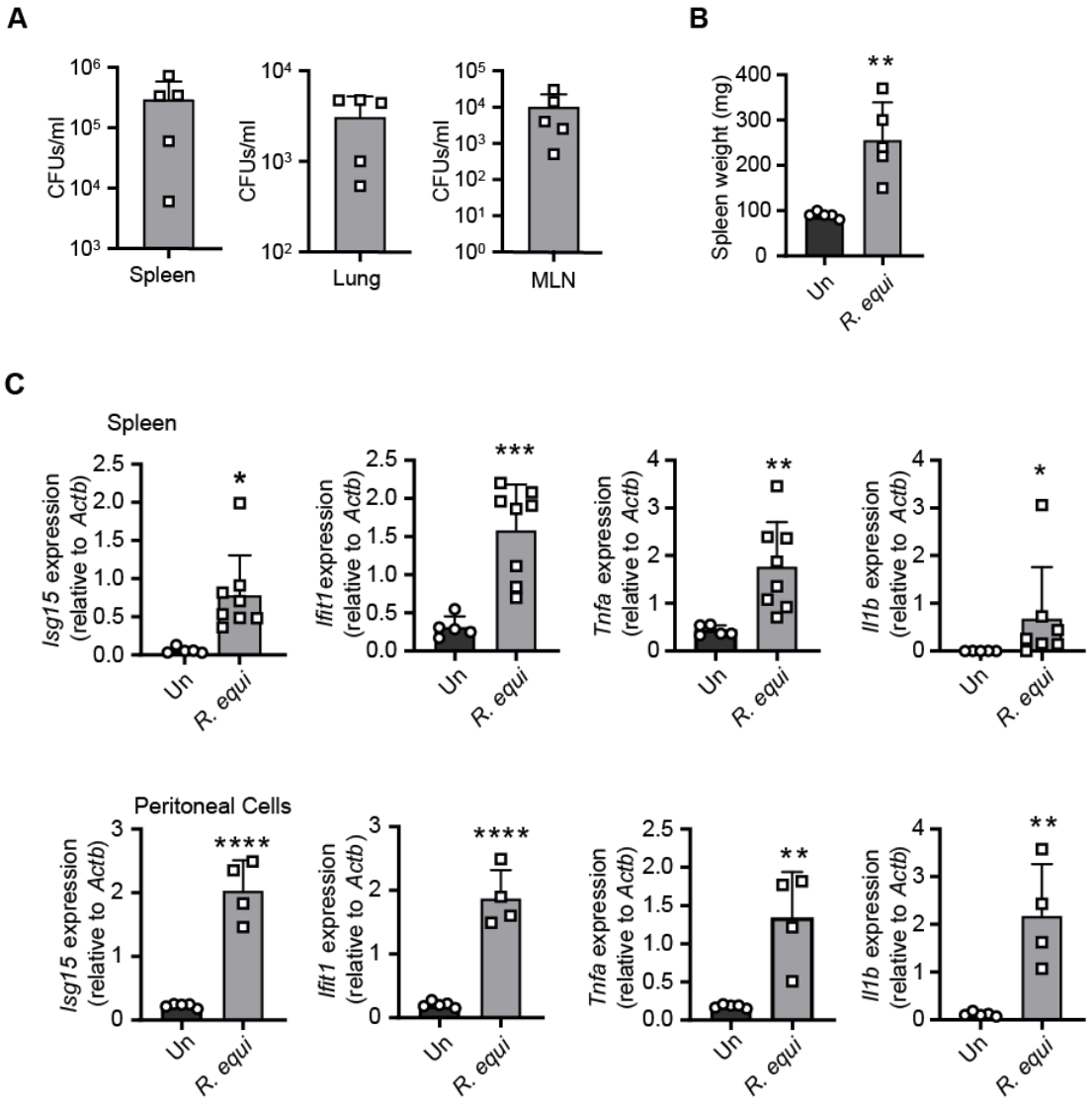


Figure III-7: *R. equi* induces both a pro-inflammatory and type I IFN expression program in a mouse model of infection. (A) CFUs/gram organ weight in the spleen, lung and mesenteric lymph nodes of mice infected with *R. equi* for 5 days. Each square represents an individual mouse. (B) Spleen weight in g of mice 5 days after being infected or not with *R. equi*. (C) qRT-PCR of *Isg15*, *Ifit1*, *Tnfa* and *Il1b* in the spleen or peritoneal cells of mice infected or not with *R. equi*. Mouse qRT-PCRs represent 5 biological replicates ± SD. Statistical significance was determined using Mann-Whitney test. *p < 0.05, **p < 0.01, ***p < 0.001, ****p < 0.0001.

from peripheral blood samples taken at 0- and 21d post-infection and measured ISGs by RT-qPCR. To rule out age-related changes in ISG levels, we first compared uninfected and *R. equi*-infected foals at 21d post-challenge, normalizing individual post-challenge values to baseline levels. Uninfected foals had no significant induction in ISGs between the baseline and 21d post-challenge samples (Figure III-8A). However, we observed a significant induction of *ISG15* in infected foals, with infected foals falling into subgroups with modest induction or high induction. Notably, the sole foal that became clinically ill following experimental challenge fell within the high induction subgroup (denoted by yellow square in (Figure III-8A). Since individual foals varied in their response to infection, and having shown that pre- and post-challenge cytokine levels were similar in uninfected foals, we next focused on infected foals and compared baseline *ISG15* levels with post-infection levels. We observed an upward trend in *ISG15* induction when compared to pre-infection samples, but it did not reach statistical significance (Figure III-8C). We also observed a robust induction of pro-inflammatory cytokines (*IL1b*, *IL6*) in *R. equi*-infected foals (Figure III-8D). Given that *R. equi* is ubiquitous in the environment and likely shed by mares, and given that 2 foals exhibited evidence of pulmonary lesions prior to experimental infection (denoted by red circles in (Figure III-8C-D), it is possible that foals were exposed to environmental *R. equi*, which may have contributed to innate immune activation during the 0d blood collection. Nonetheless, these results indicate that *in vivo R. equi* infection results in type I IFN activation in both mouse and equine models of infection.

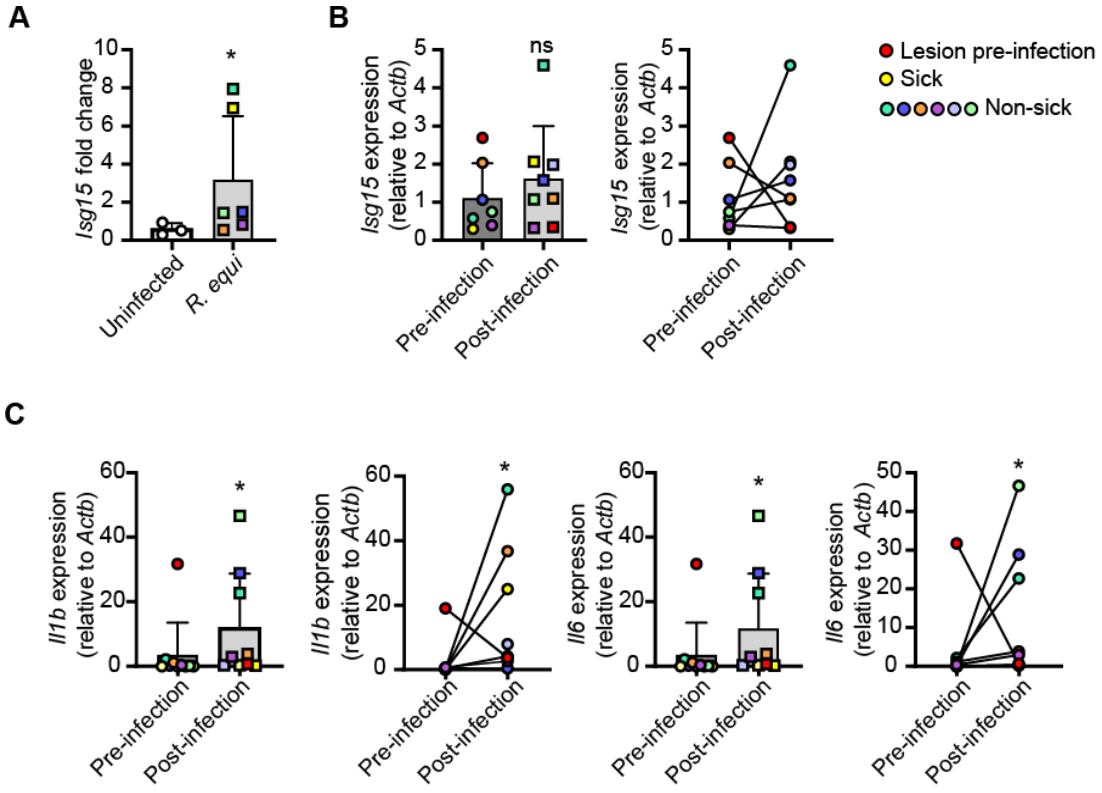


Figure III-8: *R. equi* induces type I IFN response in equine monocytes. (A) qRT-PCR of *Isg15* in uninfected and *R. equi* infected foals at 21d post-infection normalized to baseline *Isg15* levels. Each dot represents an individual foal. (B) As in B, but comparing baseline *Isg15* levels to 21d post-infection in infected foals. Red dot indicates foal with lesions prior to experimental infection and yellow dot indicates foal that became clinically ill after infection. (C) As in C, but for *Il1b* and *Il6*. Horse qRT-PCRs represent >3 biological replicates ± SEM, uninfected n=3, infected n=6. For all experiments in this study, statistical significance was determined using Mann Whitney test. *$p < 0.05$, n.s. = not significant.

## Discussion

The innate immune response is critical as a first line of defense in limiting pathogen replication, but also shapes the adaptive immune response. Because innate immune responses dictate adaptive immune outcomes, defining the innate immune

milieu generated in response to bacterial pathogens like *R. equi* is a crucial step to understanding how it causes disease. Here we show that intracellular *R. equi* triggers the cytosolic DNA sensing pathway in a cGAS- and STING-dependent manner. Activation of the cytosolic DNA sensing pathway following *R. equi* infection led to phosphorylation of IRF3 and initiation of a type I IFN response within 4h of infection, while intracellular bacteria are still replicating within the *R. equi*-containing vacuole.[77,131] Our finding that this type I IFN expression profile is dependent upon the cGAS/STING/TBK1 axis supports a model whereby *R. equi* persists in a modified vacuole capable of interacting with the macrophage cytosol and engaging DNA sensors and other innate immune proteins.

Our observation that vacuolar *R. equi* induces type I IFN expression via activation of the DNA sensing pathway parallels that of Mtb in macrophages. Mtb uses its type VII secretion system, ESX-1, to permeabilize its vacuolar membrane, permitting liberation of extracellular mycobacterial DNA into the macrophage cytoplasm where it triggers cGAS.[22] Genetic evidence indicates that like Mtb, *R. equi* also encodes a type VII secretion system, although the function of this system in *R. equi* remains to be determined.[71,99] Further studies focused on investigating the function of *R. equi*'s ESX secretion systems will be important for uncovering the mechanism of cytosolic DNA sensing during macrophage infection. Mtb ESX-1 effectors ESAT-6 and CFP-10, together with the mycobacterial lipid PDIM, are thought to form pores in the phagosome after their secretion;[132,133] the presence or function of similar effectors in *R. equi* might suggest a similar mechanism, but *R. equi* could have unrelated ways of accessing the

cytosol to communicate with and manipulate the host. Using the readouts and phenotypes we identified here, future screens may serve to elucidate these mechanisms and uncover novel *R. equi* effectors and effector functions.

The recruitment of the glycan binding proteins galectin-3, -8, and -9 to a population of *R. equi* indicates that the *R. equi*-containing vacuole is damaged to the extent that luminal glycans are exposed and recognized by cytosolic danger sensors as early as 4h post-infection. This is consistent with Mtb recruitment of these galectins, which occurs as early as 3h post-infection,[129] while *Salmonella enterica* serovar Typhimurium recruits galectin-3, -8, and -9 to broken vacuoles as early as 1h post-infection.[130] Interestingly, we observed an accumulation of galectin puncta that are unassociated with bacteria. It is possible that virulence factors responsible for permeabilizing *R. equi*'s phagosome are secreted and act in trans to also damage endosomal compartments. Further studies will have to be conducted to understand the nature and fate of the damaged phagosomes and endosomes.

Our finding that cGAS is required for induction of type I IFN signaling during *R. equi* infection indicates that DNA is the major contributor for this activation in macrophages; however, the source of this DNA remains to be determined. Given the data supporting damaged *R. equi* phagosomes, it is likely that bacterial DNA is released into the cytosol, however the possibility of mitochondrial perturbation and cytosolic release of mitochondrial DNA has not been ruled out. Indeed, recent evidence indicates that Mtb infection induces release of host mitochondrial DNA into the cytosol, contributing to the type I IFN response during infection.[134,135] Additionally, the cyclic

dinucleotide produced by *L. monocytogenes* and Mtb, (cyclic diadenosine monophosphate (c-di-AMP)), bypasses cGAS and its second messenger cGAMP to directly activate STING.[17] While some bacteria can directly activate STING, through secretion of c-di-nucleotides, and while *R. equi* does seem to encode deadenylate cyclases, our data suggest that this is not the mechanism of type I IFN induction under the conditions or time points we examined. Because cGAS KO macrophages do not induce type I IFNs, it indicates that without host derived cGAMP, no bacterial cyclic dinucleotides are present to activate STING and induce type I IFNs. It is now clear that intracellular bacterial pathogens have evolved to elicit type I IFN through activating the cytosolic DNA sensing pathway including cGAS (Mtb,[22,23] *Chlamydia* spp.,[26] *F. novicida* [25]) and/or STING (*L. monocytogenes,*[136] Mtb,[137] and *Chlamydia trachomatis*[138]) implicating a selective advantage for at least some bacteria to elicit this response, likely by ISG actions such as blocking IL-1 activity via ILRα,[45] or IL-10 mediated limitation of IFN-ɣ responses.[47]

A key virulence determinant of *R. equi* is the conjugative virulence plasmid which hosts a 21-kb pathogenicity island encoding Vaps. The best characterized of the Vaps is VapA, which is required but not solely sufficient for intracellular growth within macrophages.[72,74] VapA promotes *R. equi* survival in macrophages by inhibiting phagosomal maturation,[75] inducing lysosome biogenesis,[76] and contributing to lysosome membrane permeabilization.[70] Interestingly, disruption of the phagosomal membrane, activation of cytosolic DNA sensing, and production of type I IFNs was not dependent on expression of Vap A. This discrepancy may be explained by the transient nature or

small size of VapA-induced membrane leaks, with VapA-induced membrane lesions ranging from 0.37 nm at pH 6.5 to 1.05 nm at pH 4.5, which are large enough for the passage of ions.[70] Further studies investigating other bacterial mutants may help elucidate additional bacterial factors underlying in the host-pathogen interactions of *R. equi* and macrophages.

It will also be interesting to interrogate downstream outcomes of *R. equi* infection and pathogenesis that result from the activation of cytosolic sensing, especially bacterial survival and replication in macrophages. One potential outcome of TBK1 activation during *R. equi* infection is autophagic targeting.[22,100,139] Autophagy, and selective autophagy in particular, functions as an antimicrobial mechanism that promotes lysosomal degradation of intracellular bacterial pathogens.[140] Future studies will be needed to investigate if *R. equi* also gets targeted to this pathway, but its recruitment of galectins and activation of TBK1 suggests that a population of *R. equi* could potentially be targeted and destroyed by this mechanism. VapA, while seemingly unimportant for type I IFN signaling, is important for evading lysosomal degradation[70] so it may provide a mechanism to counteract the potential drawbacks for bacteria activating this anti-bacterial pathway.

Another outstanding question is how induction of type I IFN signaling influences *R. equi* pathogenesis. It may be interesting to determine the transcriptional signature in foals with severe disease to test the hypothesis that foals that succumb to infection have a robust, or even hyper-induced, type I IFN signature. While we observed induction of type I IFN in response to *R. equi* infection during our equine experiments, we were

unable to draw clear conclusions regarding connections between type I IFN levels and disease outcome largely due to the small study size. All animals in the equine study ultimately cleared infection without treatment, and only one foal became clinically ill following experimental challenge; however, this animal did have highly induced ISGs. Future studies in both mouse and horse models specifically centered on the balance between type I and type II IFN will be key in understanding the clinical implications of a type I IFN-skewed response, and whether such a signature correlates with reduced IFN-ɣ, impaired control of bacterial replication, or detrimental disease outcomes. Identifying factors associated with negative disease outcomes will help determine ways to expedite diagnoses, promote positive disease outcomes, and reduce patient mortality.

# CHAPTER IV

# LRRK2 LOSS OR MUTATION DYSREGULATES INNATE IMMUNITY AND CONTRIBUTES TO MTB PATHOGENESIS[1]

## Overview

The importance of type I IFN in bacterial pathogenesis is becoming increasingly appreciated. In the Mtb field, type I IFN has been identified as a transcriptional signature for active tuberculosis in humans,[120] and humans with a proline deletion in the type I IFN receptor, IFNAR (rendering it nonfunctional) are more resistant to Mtb compared to the general population.[141] While the major players involved in cytosolic DNA sensing and type I IFN signaling have been identified, much remains to be learned about how these immune pathways are regulated. Thus, we turned to the literature to identify candidate regulators of type I IFN active during mycobacterial infection. In addition to its importance in Mtb pathogenesis, type I IFNs are key in determining disease severity during infection with the related pathogen *M. leprae*.[47] Furthermore, our review of the literature uncovered a number of genome wide association studies that implicate LRRK2 single nucleotide polymorphisms (SNPs) in conferring increased or decreased susceptibility to *M. leprae*.[91,142-144] Given the genetic similarities between *M. leprae* and Mtb, we hypothesized that LRRK2 might also be important in Mtb pathogenesis.

---

[1] The data presented in this chapter were published in part in "LRRK2 maintains mitochondrial homeostasis and regulates innate immune responses to *Mycobacterium tuberculosis*" by CG Weindel, SL Bell, KJ Vail, KO West, KL Patrick, and RO Watson, 2020. *eLife* 9:e51071. 

Mutated LRRK2 is the greatest known genetic contributor to Parkinson's disease (PD) and has primarily been studied in the brain. However, the finding that mutations in LRRK2 impact susceptibility to mycobacterial infection supports a role for LRRK2 in peripheral immunity. Here we show that murine macrophages lacking *Lrrk2* exhibit basal elevations in type I IFN and ISGs, and that this IFN response is blunted in *Lrrk2* deficient macrophages in response to mycobacterial infection. Work in our lab has shown that this aberrant innate immune response in *Lrrk2*$^{-/-}$ macrophages is due to a constellation of mitochondrial stress and DRP-1 dependent mitochondrial fragmentation. The culmination of these defects results in mtDNA leakage into the cytosol and chronic engagement of cGAS. We show that while *Lrrk2*$^{-/-}$ mice control Mtb replication, Mtb-induced pulmonary inflammation is exacerbated. We next demonstrate that the *Lrrk2*$^{G2019S}$ mutation contributes to enhanced inflammatory cell death. This phenotype is manifested as exquisite sensitivity to Mtb pathogenesis following aerosol infection in mice overexpressing the *Lrrk2*$^{G2019S}$ mutation and impaired bacterial dissemination following oral infection by *L. monocytogenes* in a mouse model of colitis. Together, these findings further our understanding of *Lrrk2* as a key regulator of innate immunity during intracellular bacterial infection.

## Introduction

### *LRRK2*

LRRK2, also known as Dardarin, is a large, 2527 amino acid, multidomain kinase protein with a wide range of cellular functions. Mutated *LRRK2* is the greatest known genetic contributor to familial and spontaneous PD, a chronic neurodegenerative

disease affecting 7-10 million people.[101] Clinically defined by resting tremor, bradykineseia, posture instability and rigidity, PD is characterized by the hallmark progressive loss of dopaminergic neurons in the midbrain.[145] As a multifunctional protein, LRRK2 is involved in a number of cellular processes including cytoskeletal dynamics, vesicular trafficking, calcium signaling and mitochondrial function.[146] However, the precise mechanism by which LRRK2 contributes to PD is poorly understood.

Eight missense mutations in LRRK2 are considered pathologic, most of which are found in the catalytic core formed by the kinase, ROC-GTPase, and COR domains (Figure IV-1).[147,148] The most common mutation, G2019S, occurs in approximately 5% of cases of familial Parkinson's disease. The G2019S mutation, in which a glutamate at position 2019 of the kinase domain is replaced with a serine, results in increased kinase activity. Increased kinase activity contributes to PD brain pathology, including loss of dopaminergic neurons, impaired dopamine neurotransmission, protein synthesis and degradation defects, mitochondrial oxidative damage, and inflammation.[145] Interestingly, PD also has an inflammatory component involving elevated type I IFN and TNFα expression in the brain as well as increased microglial activation.[149] Chronic


Figure IV-1: Model of LRRK2 protein domains.

systemic inflammation, such as with tuberculosis plausibly prolongs microglial activation, in turn contributing to exacerbation of PD brain pathogenesis.[149]

### *LRRK2 in Innate Immunity*

While LRRK2 has primarily been studied in the context of Parkinson's disease, a growing body of work supports the notion that LRRK2 mutations also contribute to immune outcomes in the peripheral immune system as well as in the brain. SNPs in LRRK2 have been implicated in conferring increased susceptibility to mycobacterial infection,[91,142-144] and have been associated with immune disorders such as IBD[150,151] and Crohn's disease,[152] as well as Alzheimer's disease and certain cancers.[145] In brain immunity, chemical inhibition of LRRK2 has been shown to attenuate proinflammatory cytokine secretion in rat primary microglia.[153] The idea that LRRK2 is important in immunity is further supported by its abundant expression in many immune cells, including macrophages and dendritic cells.[154] Additionally, human macrophages treated IFN-ɣ demonstrate increased expression of LRRK2.[155] LRRK2 deficient macrophages have reduced IL-1β secretion in response to infection with *Salmonella enterica* serovar Typhimurium.[156] While mounting evidence supports a role for LRRK2 in innate immunity, the precise mechanism by which LRRK2 regulates peripheral immune responses is not well understood.

### *Immunity in the Brain*

The brain has historically been considered an immunologically privileged site, protected from the periphery by the blood brain barrier and apparent absence of lymphatics, however this paradigm has been challenged by the discovery of lymphatic

vessels and regulated leukocyte trafficking within the brain.[157] Furthermore, it is becoming more apparent that a balance in innate immune cytokines such as IFNs are important for neural health, with some autoimmune neurodisorders associated with elevated type I IFN, and increased susceptibility to infectious disease associated with inadequate levels of type I IFNs.[158] Neuroinflammation is considered a critical component of neurodegenerative diseases such as PD.[159] CNS inflammation in PD consists of microglial activation, inflammatory cytokine production and infiltration of T lymphocytes.[149] Clinically, PD is characterized by progressive motor impairment due to degeneration and loss of dopaminergic neurons in the substantia nigra pars compacta (SNc) in the midbrain.[149,160] SNc dopaminergic neurons are particularly vulnerable to the effects of neuroinflammation due to a relatively high density of microglia.[149]

The Neurovascular Unit (blood brain barrier), formed by endothelial cells, pericytes, astrocytes and neurons, incorporates cell-cell interactions and signaling involved in neuronal homeostasis, pathogen recognition and innate immune responses.[157,161] Almost all neural cells, including neurons, oligodendrocytes, astrocytes and microglia are able to respond to infection, initiate inflammation, and express cytokine receptors, TLRs, NLRs, RIG-like receptors, MAVS, AIM2-like receptors, and C-type lectin receptors.[157] Two of the major cell types involved in immune surveillance and response within the central nervous system are microglia and astrocytes. Microglia, derived from myeloid cell lineage are established within the brain early during embryogenesis, while astrocytes are derived from neuroepithelial stem cells, as are neurons.[162]

**Microglia**

Microglia function as the resident brain immune cells and initial responders to pathogen and danger signals within the brain, and are cable of clearing debris and infected cells.[157] Their activation elicits a dynamic range of morphological changes and production or upregulation of pro- and anti-inflammatory cytokines.[163] Activation can be by acute injury and neuronal death, infectious stimuli, chronic neurodegeneration and brain tumors.[161] While morphology varies between white and gray matter, quiescent microglia demonstrate a small, round soma with highly ramified processes allowing rapid detection of signals.[161] With activation/priming, microglial processes become shorter, thicker, less branched, more motile and cover a smaller territory.[163] Morphological changes associated with a primed phenotype are accompanied by production of proinflammatory mediators such as TNFα, IL1β and IL6.[163]

**Astrocytes**

Astrocytes are glial cells whose role in maintaining CNS homeostasis was once thought to be restricted to supporting neurons.[157] Now astrocytes are known not only to respond to circulating cytokines but may also have intrinsic immune function.[164] Endfeet "ensheath" brain capillaries and help form the blood brain barrier and modulate endothelial function.[161] During infection or injury, astrocytes proliferate, increase expression of GFAP, and initiate astrogliosis which refers to morphological changes that ultimately result in the formation of glial scars formed from dense networks of astrocytes at sites of damage.[157]

## Results

*Loss of Lrrk2 In Macrophages Results in Elevated Expression of Type I Interferon*

Because SNPs in *LRRK2* have been implicated in conferring susceptibility to *M. leprae*, we sought to investigate how *LRRK2* contributes to the innate immune response during mycobacterial infection. To test the contribution of *Lrrk2* to immunity during infection, we first examined the baseline immune profile. I harvested RNA from uninfected WT (parental) and *Lrrk2* KO RAW 264.7 macrophages and measured gene expression of type I IFNs (*Ifnb*, *Isg15*). *Lrrk2* KO RAW 264.7 macrophages demonstrated higher expression of *Ifnb* and *Isg15* at baseline than WT macrophages (Figure IV-2A). This finding correlated well with a similar experiment done in BMDMs where I observed elevated expression of the ISGs *Isg15* and *Ifit1* (Figure IV-2B).

*Lrrk2 KO Macrophages Have Impaired Immune Response to Mycobacterial Infection*

Having determined that *Lrrk2* KO macrophages have an aberrant immune signature at rest, we next asked how *Lrrk2* deficient macrophages respond to infection

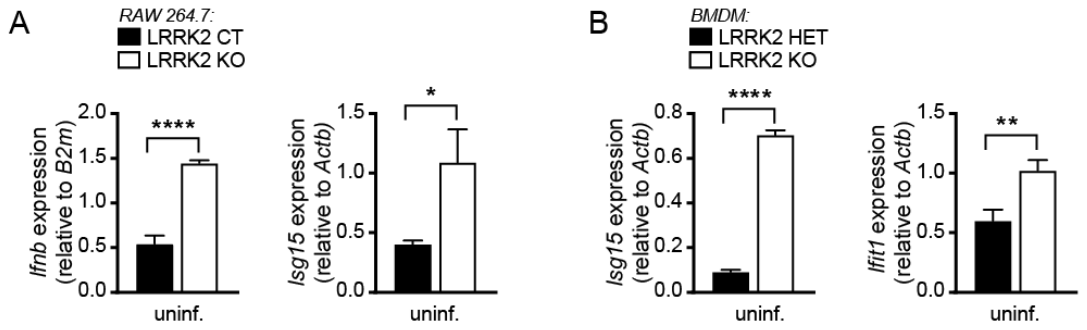


Figure IV-2: *Lrrk2* KO macrophages have elevated baseline type I IFN. (A) RTqPCR of *Ifnb* and *Isg15* expression in uninfected Lrrk2 KO and WT RAW 264.7 cells. (B) RTqPCR of *Isg15* and *Ifit1* in uninfected *Lrrk2*$^{-/-}$ or *Lrrk*$^{+/-}$ BMDMs.

with *M. leprae*. Because *M. leprae* cannot be grown in axenic media, bacilli cultivated in the footpads of nude mice were generously provided for each experiment by the National Hansen's Disease Program. We infected *Lrrk2* KO and WT RAW 264.7 macrophages or *Lrrk2*$^{-/-}$ BMDMs and at 4 or 8h post-infection measured gene expression by RTqPCR. While *Lrrk2*$^{-/-}$ macrophages had basally elevated type I IFN levels, *M. leprae*-infected macrophages had significantly reduced type I IFN levels at 8h post-infection compared to WT or *Lrrk2*$^{+/-}$ controls (Figure IV-3). The finding that *Lrrk2* KO macrophages demonstrate an impaired immune response to mycobacterial infection was further supported by an RNA-sequencing experiment done in our lab which found that Mtb-infected macrophages lacking *Lrrk2* also demonstrated a blunted type I IFN response.[165]

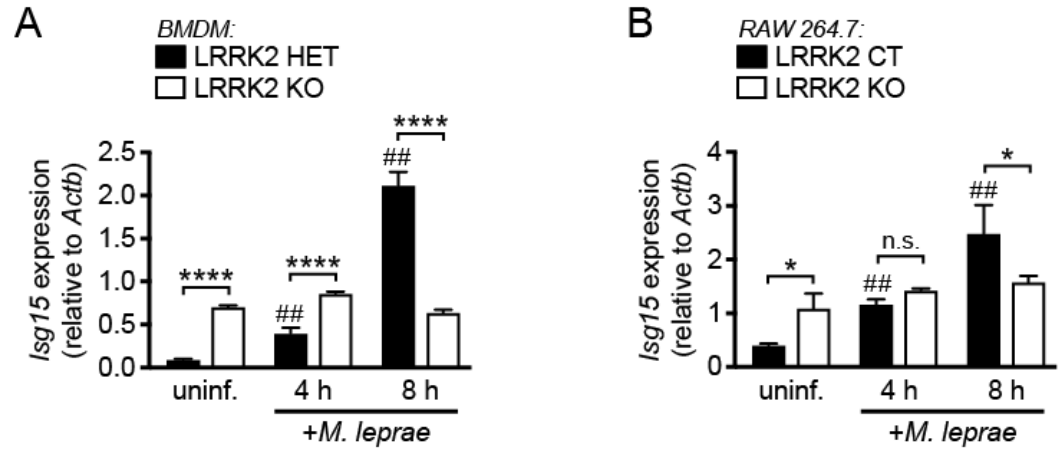


Figure IV-3: RT-qPCR of Isg15 expression after 4 and 8h of infection with *M. leprae* (MOI = 50) in (A) *Lrrk2*$^{-/-}$ BMDMs and *Lrrk2*$^{+/-}$ controls or (B) RAW 264.7 macrophages.[165] Statistical analysis: *p<0.05, **p<0.01, ***p<0.005, ****p<0.001 (comparing indicated data points); ##p<0.001 (comparing stimulated to unstimulated of same genotype). (A–B) two-way ANOVA Tukey post-test.

*Lung Inflammation Is Increased in Lrrk2$^{-/-}$ Mice During Mtb Infection*

Because *LRRK2* SNPs have been linked with susceptibility to human mycobacterial infection, and because studies in our lab indicate a role for *Lrrk2* in macrophage homeostasis, I next wanted to understand how *Lrrk2* deficiency influences innate immunity *in vivo*. We chose *M. tuberculosis* rather than *M. leprae* for these experiments because of the extensive combined experience in the lab working with low-dose aerosol murine models of Mtb and because Mtb can be cultured in axenic media. We used *Lrrk2*$^{+/-}$ (Het) mice as controls for these experiments because preliminary experiments showed no difference in the immune response of *Lrrk2*$^{+/-}$ and *Lrrk2*$^{+/+}$ mice to infection. *Lrrk2*$^{-/-}$ and *Lrrk2*$^{+/-}$ mice were infected with ~150 CFUs of Mtb (Erdman strain) via aerosol chamber delivery.[165] Mice were euthanized at 7-, 21-, 63- and 126d post-infection, and the lungs and spleen were harvested for histology, CFUs, and gene expression. We observed no differences in bacterial burdens in the lungs or spleens of infected mice (Figure IV-4A), or in serum or tissue cytokines. However, when I evaluated histologic sections of lungs, I observed a moderate increase in granulomatous nodules in the lungs (Figure IV-4B-C). Immunohistochemical staining for macrophages (Iba-1), T-lymphocytes (CD3) and B-lymphocytes (CD79-a) demonstrated strong labeling for macrophages and T-lymphocytes (Figure IV-5).

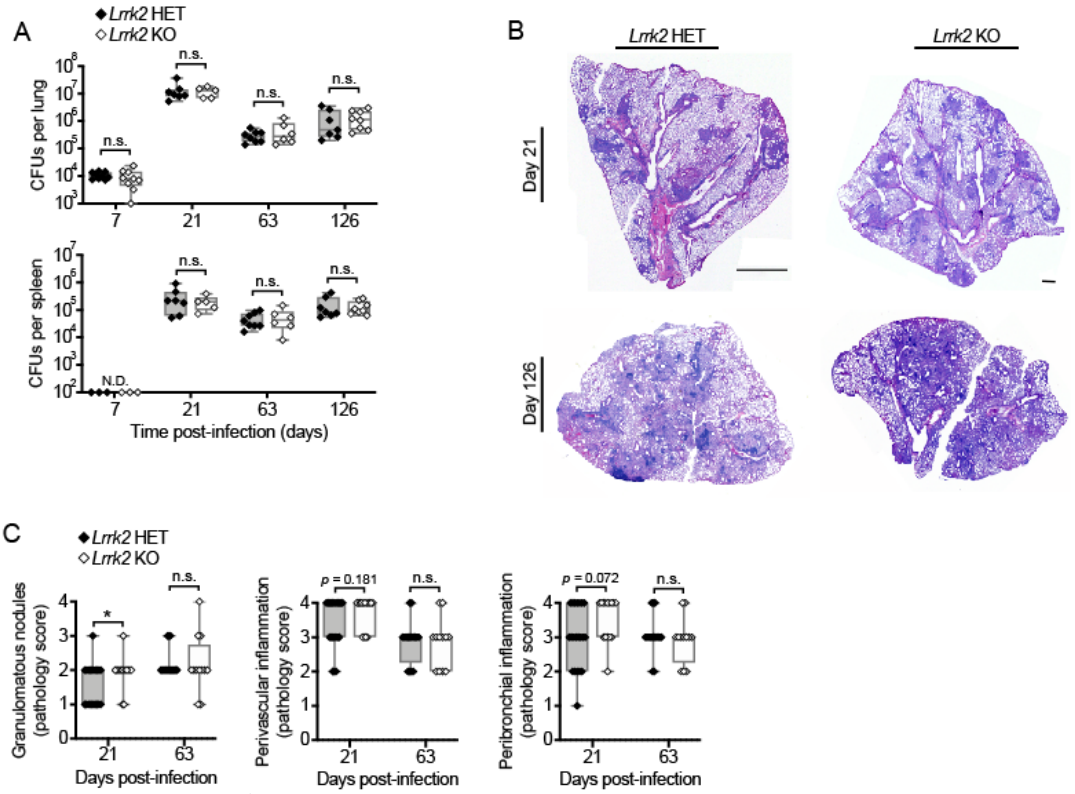


Figure IV-4: *Lrrk2*$^{-/-}$ mice exhibit increased lung inflammation during Mtb infection.[165] (A) (B) Hematoxylin and eosin (H&E) stain of inflammatory nodules in the lungs of *Lrrk2*$^{-/-}$ and *Lrrk2*$^{+/-}$ mice 21d after infection with Mtb. Small scale bar, 500 mm; large scale bar 1 mm. (C) Semi-quantitative score of pulmonary inflammation with a score of 0, 1, 2, 3 or 4 assigned based on granulomatous nodules in none, up to 25%, 26–50%, 51–75% or 76–100% of fields, respectively. Perivascular and peribronchial inflammation was scored using an analogous scale based on percentage of medium-caliber vessels or bronchioles with adjacent inflammatory nodules. Statistical analysis: *p<0.05, **p<0.01, ***p<0.005, Mann-Whitney test.

To further characterize the immune cell populations in the lungs of the *Lrrk2*$^{-/-}$ and *Lrrk2*$^{+/-}$ mice, I scanned histologic slides to create digital images that could be analyzed. I used ImageJ to obtain a semiquantitative measurement of neutrophils in the lungs, and observed significantly more neutrophils in the lungs of *Lrrk2*$^{-/-}$ mouse at 21d

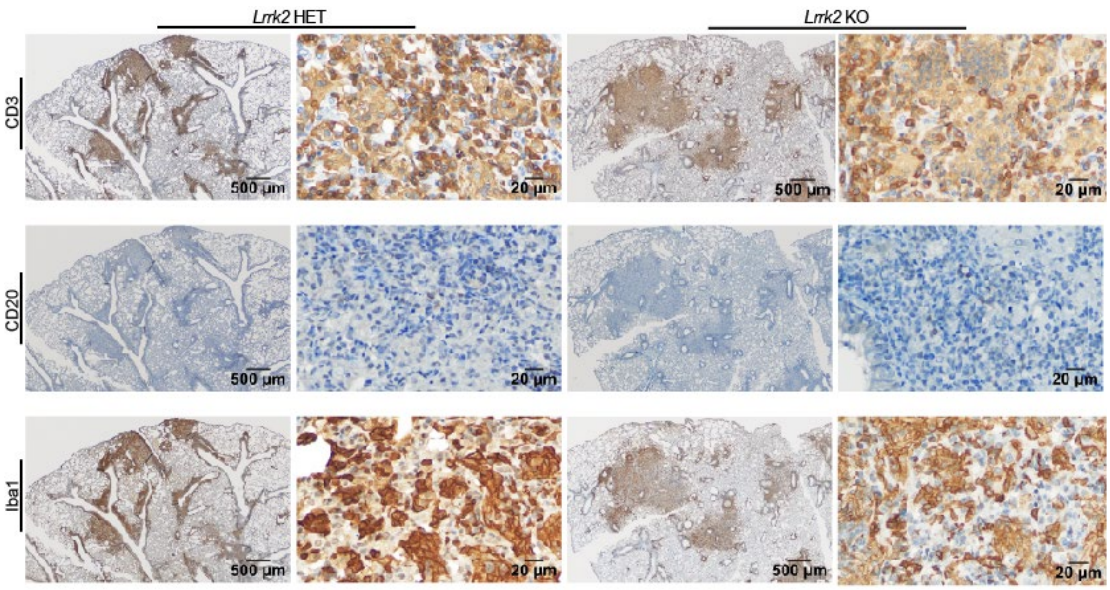


Figure IV-5: Immunohistochemistry of lungs from *Lrrk2*$^{-/-}$ and *Lrrk2*$^{+/-}$ mice infected with Mtb for 21d, with immunolabeling for T lymphocytes (CD3), B lymphocytes (CD20) or macrophages (Iba1).

post-infection (Figure IV-6). When I specifically evaluated degenerate neutrophils, I observed a greater percentage of degenerate neutrophils in the lungs of *Lrrk2*$^{-/-}$ mice. This influx was limited to 21d post-infection, as no inflammatory cells were observed at 7d post-infection, and by 63d, neutrophils were rarely observed. Taken together, these data indicate that while *Lrrk2*$^{-/-}$ and *Lrrk2*$^{+/-}$ mice did not display different bacterial burdens, the *Lrrk2*$^{-/-}$ mice had disproportional innate immune responses, including greater inflammation and enhanced local recruitment of neutrophils during early Mtb infection.

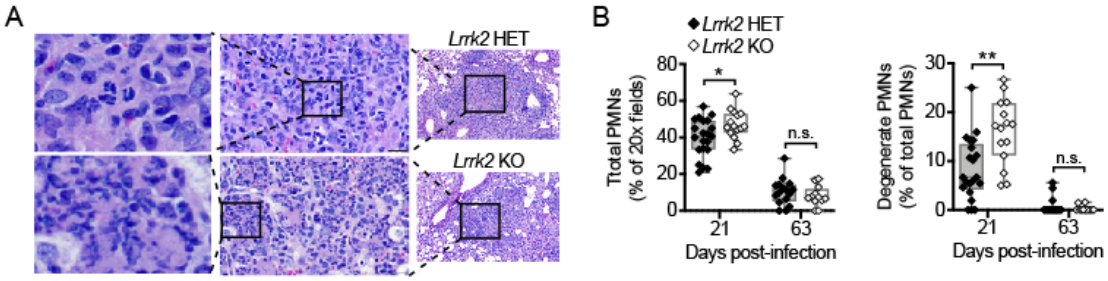


Figure IV-6: *Lrrk2*$^{-/-}$ mice exhibit increased lung inflammation during Mtb infection.[165] (A) H&E stain of neutrophils within an inflammatory nodule in the lung of *Lrrk2*$^{+/-}$ and *Lrrk2*$^{-/-}$ mice 21d after Mtb infection. Middle panel bar is 20 µm. (B) Quantification of neutrophils in the lungs of *Lrrk2*$^{+/-}$ and *Lrrk2*$^{-/-}$ mice infected with Mtb for 21 or 63d. Total neutrophil scores were determined by the percentage of fields of view at 20X magnification containing neutrophils. Degenerate neutrophil scores were determined by the percentage of PMN positive fields containing degenerate neutrophils. Statistical analysis: *p<0.05, **p<0.01, ***p<0.005, Mann-Whitney test.

### *Lrrk2*$^{G2019S}$ *Mutant Mice Have Increased Lung Inflammation During Mtb Infection*

While the aberrant immune response to infection in the absence of *Lrrk2* is informative that *Lrrk2* is important for innate immunity, human disease related to *LRRK2* is associated with *LRRK2* mutations rather than loss. The overwhelming majority of pathogenic *LRRK2* mutations occur in the catalytic kinase domain, and the most common mutation is the G2019S mutation. Thus, we next sought to determine the influence of the *Lrrk2*$^{G2019S}$ mutation on Mtb pathogenesis using our low-dose aerosol model for Mtb mouse infections. To test this, we used a bacterial artificial chromosomes (BAC) transgenic mouse strain overexpressing *Lrrk2*$^{G2019S}$ under the control of an endogenous promoter. Age- and sex-matched *Lrrk2*$^{+/+}$ littermate mice were used as controls. Mice were again infected with ~150 CFUs of Mtb (Erdman strain) via

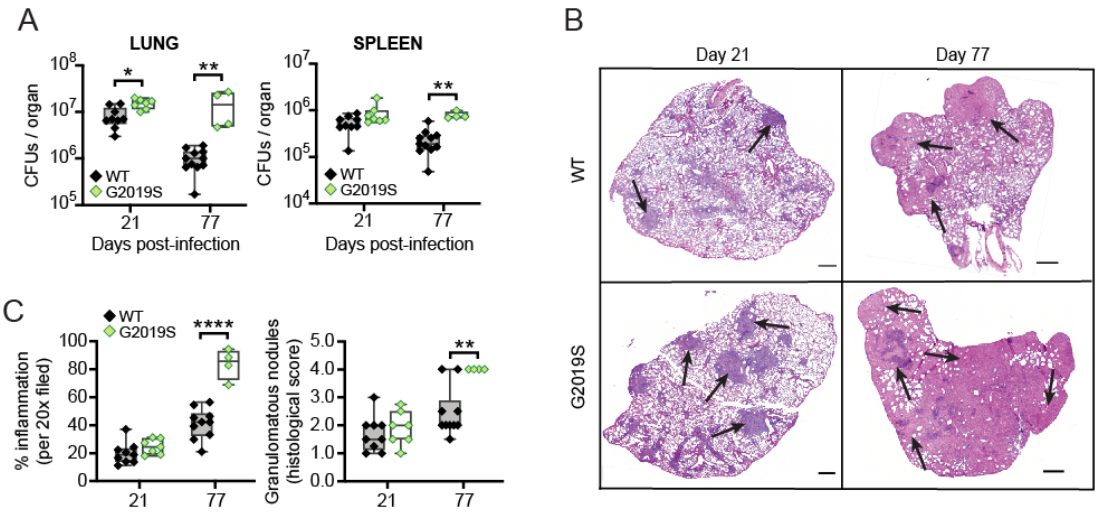


Figure IV-7: *In vivo* Mtb infection of *Lrrk2*$^{G2019S}$ mice (A) CFUs recovered from lungs and spleens of Mtb-infected *Lrrk2*$^{+/+}$ and *Lrrk2*$^{G2019S}$ mice at 21 and 77d post-infection. (B) H&E-stained lung sections from Mtb-infected *Lrrk2*$^{+/+}$ and *Lrrk2*$^{G2019S}$ mice at 21 or 77d post-infection. (C) Semi-quantitative anlysis (by ImageJ pixel density or histology score) of inflammatory nodules shown in (B). *p<0.05, **p<0.01, ***p<0.005, ****p<0.0005

aerosol chamber delivery. Mice were euthanized at 21 and 77d post-infection. We elected not to use a 7d time point for the G2019S mouse infection because we observed no immune cell infiltrates into the lungs at 7d post-infection in controls during our *Lrrk2*$^{-/-}$ mouse experiments. A 126d time point was not possible because by 77d post-infection, the *Lrrk2*$^{G2019S}$ mice were exhibiting weight loss, hunched posture, and reaching the criteria for euthanasia. At experimental end points, lungs and spleens were harvested for CFUs, cytokine expression and histopathology.

*Lrrk2*$^{G2019S}$ mice demonstrated a significant increase in pulmonary bacterial burden at 21d post-infection, and the spleen had a nearly 1.5-fold greater bacterial

burden when compared to *Lrrk2*$^{+/+}$ controls (Figure IV-7A). At 77d post infection, *Lrrk2*$^{G2019S}$ mice had 15-fold higher bacterial burdens in the lungs, and 3.5-fold more in the spleen compared to *Lrrk2*$^{+/+}$ mice (Figure IV-7A). Importantly, when compared to *Lrrk2*$^{+/+}$ controls, although bacterial burdens were higher in the spleens of *Lrrk2*$^{G2019S}$ mice at 21d post-infection, there was no difference in bacterial counts in the lung at this early time point, suggesting that differences in immune readouts cannot be primarily attributed to differences in bacterial burden.

Upon histopathologic evaluation of the organs, I observed significantly more inflammatory infiltrates in the lungs of the *Lrrk2*$^{G2019S}$ mice at both 21 and 77d post-infection (Figure IV-7B). This was particularly evident in the *Lrrk2*$^{G2019S}$ lungs at 77d post-infection, where over 80% of alveolar spaces were occluded by inflammatory infiltrates, compared to less than 50% of the pulmonary parenchyma in *Lrrk2*$^{+/+}$ mice (Figure IV-7C).

I evaluated the inflammatory cell populations in the lungs and observed that at 21d post-infection the majority of the nodules were comprised of lymphocytes, macrophages and neutrophils. ImageJ quantification showed significantly more viable and degenerate neutrophils in the lungs of *Lrrk2*$^{G2019S}$ mice at 21d (Figure IV-8A-B). By 77d post-infection, the number of neutrophils in the lungs was reduced, but persisted to a greater extent in the *Lrrk2*$^{G2019S}$ mice than in the *Lrrk2*$^{+/+}$, and the majority of neutrophils were viable with rare cells undergoing inflammatory cell death (Figure IV-8B). At 77d post-infection, inflammation was characterized by granulomatous and neutrophilic nodular infiltrates with eosinophilic proteinaceous fluid that in the

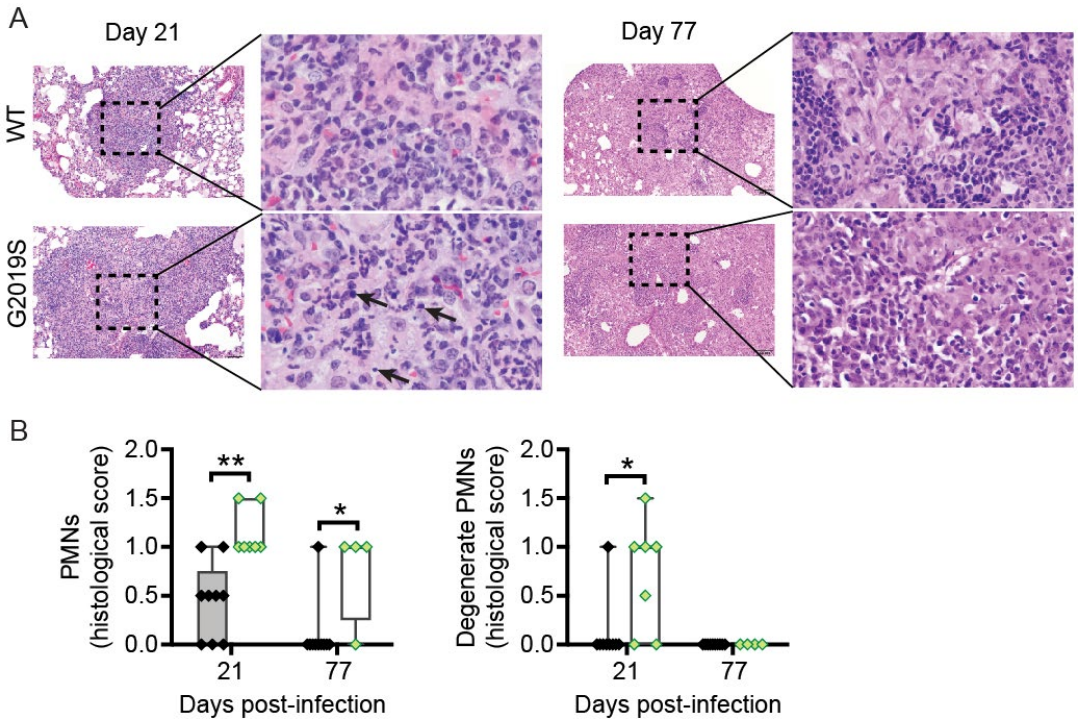


Figure IV-8: *Lrrk2*$^{G2019S}$ mice have more neutrophilic inflammation in their lungs. (A) Representative histology images of lungs of *Lrrk2*$^{+/+}$ and *Lrrk2*$^{G2019S}$ mice at 21 and 77d post Mtb-infection. Arrows indicate nuclear debris. (B) Semiquantitative analysis of neutrophils in lungs shown in (A). *p<0.05, **p<0.01, ***p<0.005,

*Lrrk2*$^{G2019S}$ mice often replaced over 80% of the lung pulmonary parenchyma (Figure IV-8A).

*Brain Immune Cells Are Activated Following Mtb Infection*

Because existing literature indicates a link between chronic inflammation and neurodegenerative disease,[163] and given that LRRK2 has been heavily implicated in neuroinflammation,[149,166] our lab in collaboration with the Srinivasan lab sought to investigate markers of neuroinflammation in the brains of *Lrrk2*$^{-/-}$, *Lrrk2*$^{+/-}$, *Lrrk2*$^{G2019S}$

and *Lrrk2*$^{+/+}$mice following Mtb infection. Brains were harvested from Mtb-infected *Lrrk2*$^{-/-}$ and *Lrrk2*$^{+/-}$ at 7, 21 and 126d post-infection, and from *Lrrk2*$^{G2019S}$ and *Lrrk2*$^{+/+}$ mice at 21 and 77d post-infection. We chose three brain regions relevant to PD to evaluate: the substantia nigra pars compacta (SNc) and the ventral tegmental area (VTA) were chosen because they contain dopaminergic cell bodies. The dorsal lateral striatum (DLS) was chosen because it contains dopaminergic terminals from the SNc and VTA. Dopaminergic axons from the SNc and VTA follow the nigrostriatal dopaminergic pathway rostrally to the DLS. These three regions are relevant because loss of dopaminergic neurons in these regions is a hallmark of PD.

**Microglia become more activated following peripheral Mtb infection**

We initially chose to focus on microglia because they are resident neuroimmune cells similar to macrophages. Forty μm thick coronal sections were immunolabeled with IBA1 and microglial reactivity was measured using endogenous IBA1 fluorescence intensity. This was normalized to neuronal nuclear protein (Neun, a marker for mature neurons) fluorescence in the DLS, or tyrosine hydroxylase (TH, marker for dopaminergic neurons) fluorescence in the SNc or VTA.

At 21 and 126d post-infection, *Lrrk2*$^{+/-}$ mice showed significant increases in microglia reactivity in the DLS compared to age-matched uninfected controls (Figure IV-9A-B). SNc and VTA microglia showed increased reactivity at 126d post-infection, but not at 21d post-infection (Figure IV-9C-D). *Lrrk2*$^{-/-}$ and *Lrrk2*$^{+/-}$ mice had similar levels of microglia reactivity in the DLS in that reactivity increased at 21 and 126d post-infection in comparison with age-matched uninfected controls (Figure IV-9B). Similarly,

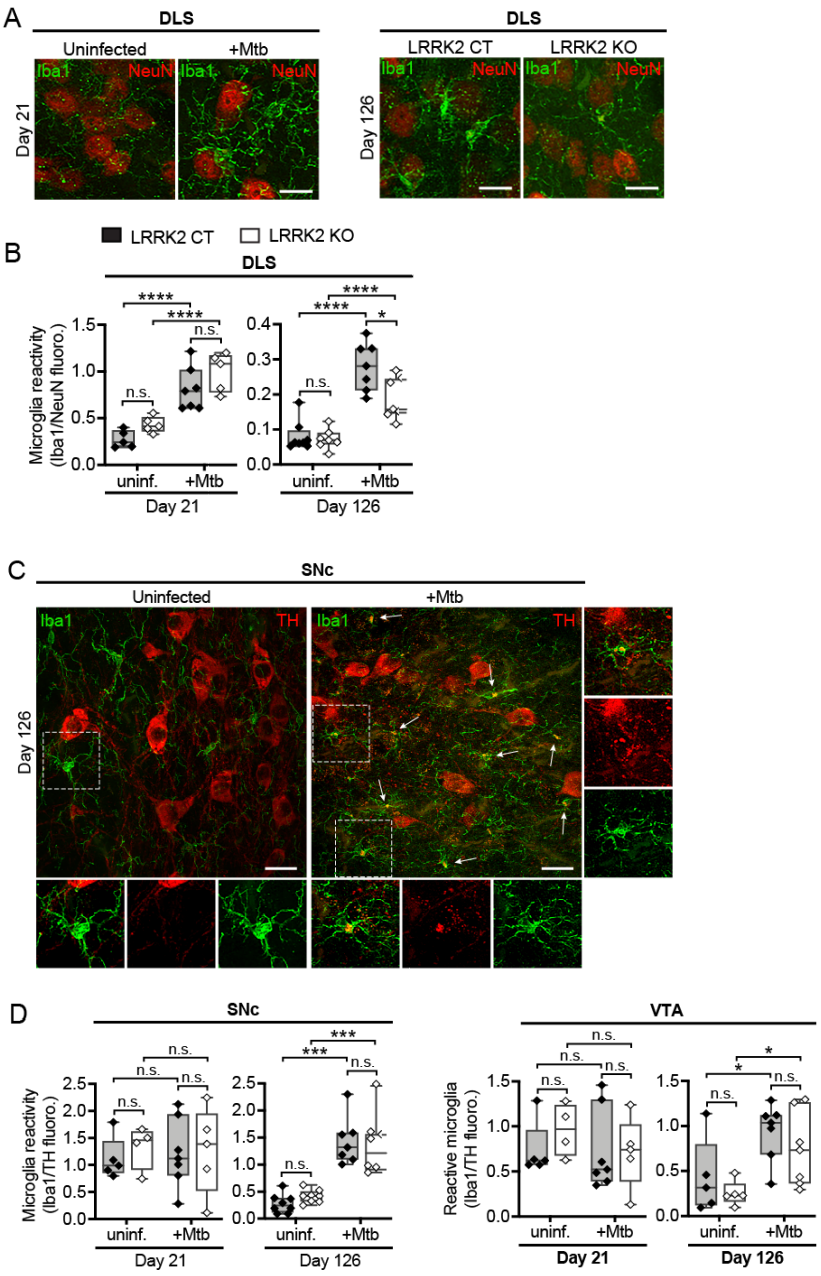


Figure IV-9: *Lrrk2*$^{-/-}$ mice exhibit activation of microglial cells in the brain during Mtb infection. (A) Fluorescence images of reactive microglia in the DLS in Mtb-infected *Lrrk2*$^{-/-}$ vs *Lrrk2*$^{+/-}$ mice. IBA1 (green); NeuN (red). (B) Quantification of DLS microglial reactivity as measured by Iba1 fluorescence relative to NeuN in Mtb-infected or not *Lrrk2*$^{-/-}$ or *Lrrk2*$^{+/-}$ mice at indicated times. (C) As in (A), but in the SNc at 126d post-infection. (D) As in (B) but in the SNc and VTA. Data presented as means ± S.E.M. *p<0.05, **p<0.01, ***p<0.005

SNc and VTA microglia reactivity was unchanged at 21d post-infection, but increased at 126d (Figure IV-9D). Importantly, when controlling for age, infection-induced increases in microglial reactivity was not related to age-related changes in IBA1 expression (Figure IV-9B, D).

Microglia morphology varies depending on the brain region and degree of activation; changes in morphology can be elicited by aging, neurodegeneration and peripheral inflammation.[163] To investigate if Mtb infection results in altered microglial morphology, I used ImageJ to measure the area of microglia soma (cell body) and count the number of microglia processes in the DLS brain region. While uninfected *Lrrk2*$^{-/-}$ and *Lrrk2*$^{+/-}$ microglia had similar numbers of processes, *Lrrk2*$^{-/-}$ microglia developed more processes at 21d post-Mtb infection, compared with *Lrrk2*$^{+/-}$ controls (Figure IV-10A). *Lrrk2*$^{+/-}$ microglia soma became significantly larger at 21d post-infection, consistent with activation,[163] although by 126d post-infection the difference between

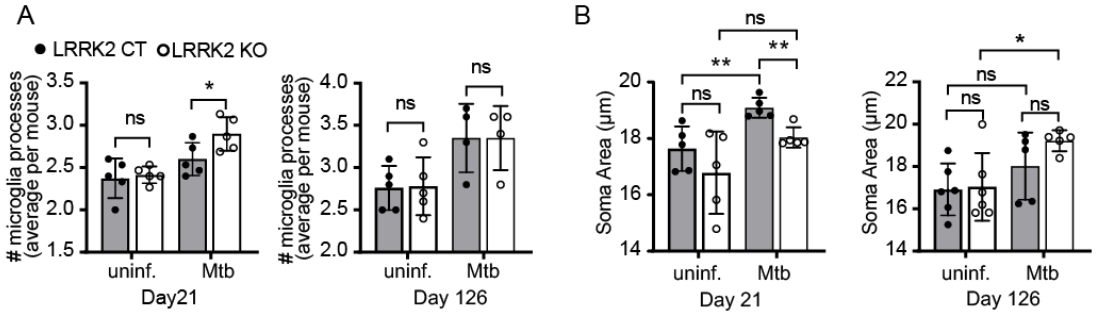


Figure IV-10: DLS microglia morphology is altered during Mtb infection in *Lrrk2*$^{-/-}$ and *Lrrk2*$^{+/-}$mice. (A) Quantification of the average number of processes per microglia. (B) Quantification of microglia soma area. Data presented as means ± SD *p<0.05, **p<0.01.

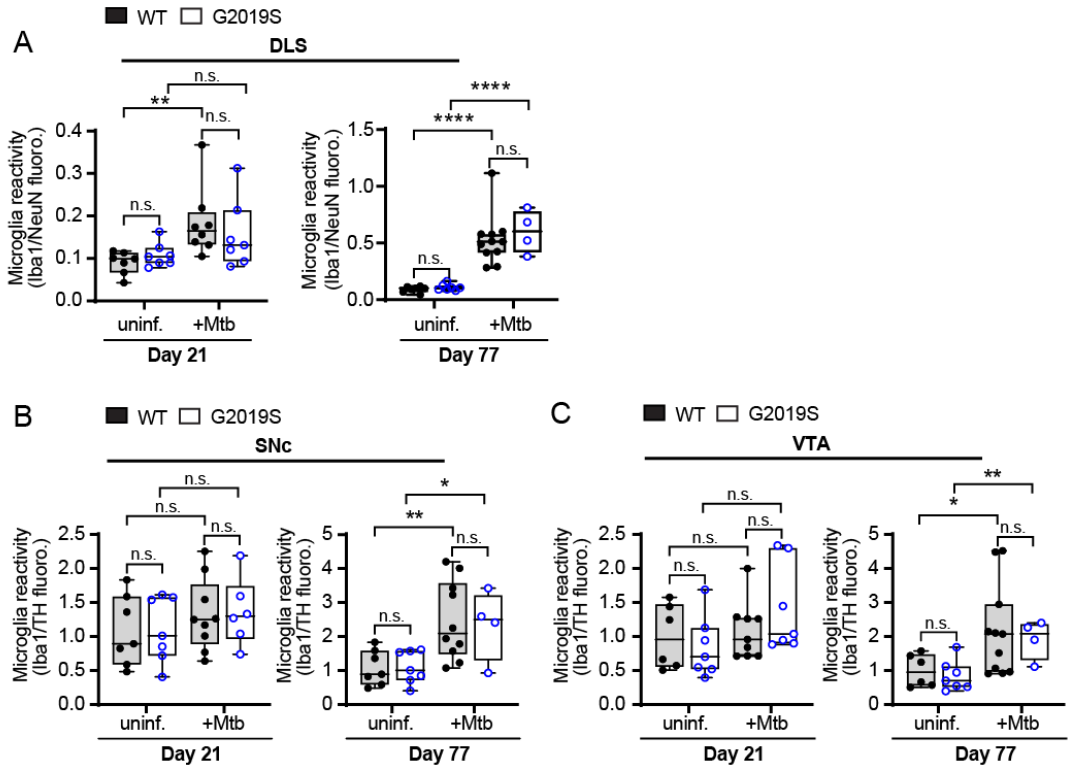


Figure IV-11: *Lrrk2*$^{G2019S}$ mice exhibit activation of microglial cells in the brain during Mtb infection. (A) Quantification of microglial reactivity in the DLS as measured by Iba1 fluorescence relative to Neun fluorescence in Mtb-infected *Lrrk2*$^{G2019S}$ or *Lrrk2*$^{+/+}$mice compared to uninfected age-matched controls. (B) Quantification of microglial reactivity in the SNc as measured by Iba1 fluorescence relative to TH florescence. (C) As in B but in the VTA. Data represented as means ± S.E.M. *p<0.05, **p<0.01, ***p<0.005.

Mtb-infected and uninfected controls was not significant (Figure IV-10B). *Lrrk2*$^{-/-}$ microglia soma trended larger at 21d post-infection, but did not reach statistical significance until 126d post-infection (Figure IV-10B). Genotypic changes were only noted at 21d post-infection, where *Lrrk2*$^{-/-}$ microglia had smaller soma than *Lrrk2*$^{+/-}$ controls (Figure IV-10B).

We next examined microglial reactivity in *Lrrk2*$^{G2019S}$ and *Lrrk2*$^{+/+}$mice. *Lrrk2*$^{+/+}$mice had a significant increase in microglial reactivity in the DLS at both 21 and 77d post-infection when comparing Mtb-infected mice to uninfected, age-matched controls, whereas *Lrrk2*$^{G2019S}$ mice only showed increased microglial reactivity at 77d post-infection (Figure IV-11A). When compared to uninfected controls, microglia in the VTA and SNc from both *Lrrk2*$^{+/+}$ and *Lrrk2*$^{G2019S}$ mice only showed increased reactivity at 77d post-infection (Figure IV-11B-C). At no time point were genotypic differences observed between *Lrrk2*$^{+/+}$ and *Lrrk2*$^{G2019S}$ microglial reactivity in any of the examined brain regions (Figure IV-11A-C).

**Astrocytes become more activated following peripheral infection with Mtb**

We next examined astrocyte reactivity in the same brain regions because astrocytes are another neural cell type with an important role in modulating neural activity. We used GFAP immunofluorescence intensity as a readout for astrocyte reactivity. In the DLS, GFAP fluorescence was normalized to NeuN fluorescence, and in the SNc and VTA regions, GFAP fluorescence was normalized to TH fluorescence.

We began by evaluating brains from *Lrrk2*$^{-/-}$ and *Lrrk2*$^{+/-}$ mice infected or not with Mtb for 21 or 126 d. When compared to uninfected mice, we observed a significant increase in GFAP fluorescence in Mtb-infected *Lrrk2*$^{+/-}$ astrocytes in the DLS at 126d post-infection (Figure IV-12A, C), indicating chronic infection with Mtb increases astrocyte reactivity in the DLS. At 21d post-infection, SNc astrocytes showed 4-fold lower GFAP fluorescence, but curiously at 126d post-infection had 3-fold higher GFAP fluorescence (Figure IV-12B-C). VTA astrocytes from *Lrrk2*$^{+/-}$ mice trended similar to

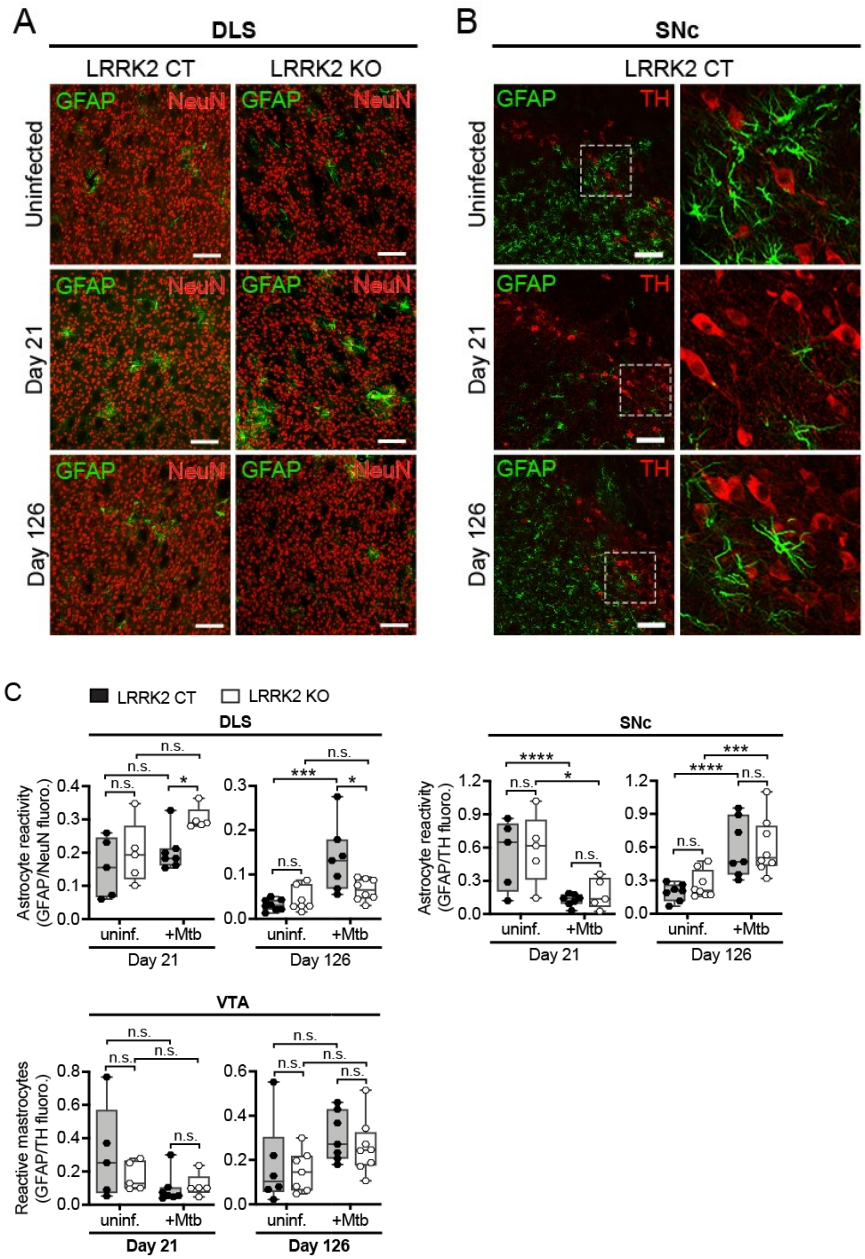


Figure IV-12**:** *Lrrk2*$^{-/-}$ mice exhibit activation of astrocytes in the brain during Mtb infection. (A) Fluorescence images of reactive astrocytes in the DLS in Mtb-infected *Lrrk2*$^{-/-}$ vs *Lrrk2*$^{+/-}$ mice at 21 or 126d. GFAP (green); Neun (red). (B) As in (A) but in the SNc. GFAP (green); TH (red). (C) Quantification of astrocyte reactivity in the DLS, SNc, and VTA as measured by GFAP fluorescence relative to NeuN or TH fluorescence in Mtb-infected *Lrrk2*$^{-/-}$ and *Lrrk2*$^{+/-}$ mice. Data represented as means +/- S.E.M. *p<0.05, **p<0.01, ***p<0.005

the SNc but failed to reach statistical significance (Figure IV-12C).

We observed no difference between Mtb-infected and uninfected *Lrrk2*$^{-/-}$ mice in GFAP expression in the DLS at 21 or 126d post-infection (Figure IV-12C, Figure IV-13). SNc astrocytes from *Lrrk2*$^{-/-}$ and *Lrrk2*$^{+/-}$ mice had significantly lower GFAP expression at 21d post-infection, but higher GFAP by 126d post-infection, and GFAP fluorescence in the VTA was similar at both 21 and 126d post-infection (Figure IV-12C).

Interestingly, when compared to uninfected mice, we observed a 2-fold (*Lrrk2*$^{+/+}$) and 3-fold (*Lrrk2*$^{G2019S}$) increase in GFAP expression in the DLS of Mtb-infected mice at 77d post-infection (Figure IV-13A). In the VTA, an increase in astrocyte reactivity between uninfected and Mtb-infected astrocytes was limited to *Lrrk2*$^{G2019S}$ mutant mice at 77d post-infection. When comparing *Lrrk2*$^{+/+}$ and *Lrrk2*$^{G2019S}$ mice, no genotypic differences were observed in any brain regions, although *Lrrk2*$^{G2019S}$ SNc astrocytes trended toward greater reactivity at 77d post-infection, but failed to reach statistical significance.

Together, these data indicate that astrocytes become more reactive in the DLS and SNc at later stages of Mtb infection, mirroring the progression of neurodegeneration in idiopathic PD. Thus, we concluded that chronic TB infection dramatically alters the reactivity profile of astrocytes in the DLS, SNc and VTA, and that astrocyte reactivity following Mtb infection is dependent on *Lrrk2* expression.

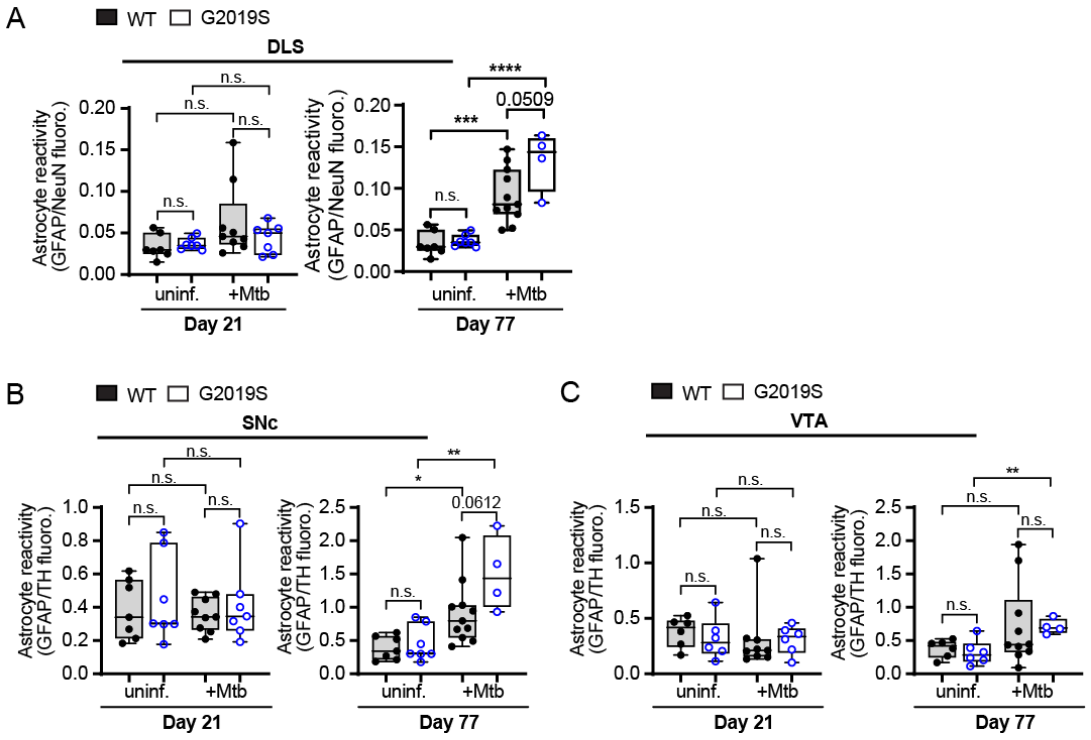


Figure IV-13**:** *Lrrk2*$^{G2019S}$ mice exhibit activation of astrocytes in the brain during Mtb infection. (A) Quantification of microglial reactivity in the DLS as measured by Iba1 fluorescence relative to Neun fluorescence in *Lrrk2*$^{G2019S}$ or *Lrrk2*$^{+/+}$mice infected with Mtb for 21 or 77d compared to uninfected age-matched controls. (B) Quantification of microglial reactivity in the SNc as measured by Iba1 fluorescence relative to TH florescence. (C) As in B but in the VTA. Data represented as means +/- S.E.M. *p<0.05, **p<0.01, ***p<0.005.

### *Mice Overexpressing the Lrrk2*$^{G2019S}$ *Allele Have Reduced Bacterial Dissemination During Infection with L. monocytogenes*

Having previously observed that LRRK2 activity exacerbates chronic Mtb-induced inflammation in the lung and is detrimental to host survival, we hypothesized that a similarly enhanced inflammatory response to an acute infectious disease might be

beneficial to the host. *L. monocytogenes* is an enteric pathogen that can produce acutely fatal outcomes in the absence of a swift and robust immune response. We chose an enteric pathogen because previous studies have shown a link between *LRRK2* mutations and GI inflammatory conditions such as inflammatory bowel disease (IBD), Crohn's disease and ulcerative colitis.[150,152,167] Furthermore, the incidence of PD is reported to be higher in IBD patients.[151] Although *L. monocytogenes* and Mtb are both intracellular, gram-positive bacteria, *L. monocytogenes* escapes its vacuole and resides within the cytosol while Mtb remains within a modified, permeabilized phagosome.

To test the impact of the *Lrrk2*$^{G2019S}$ mutation on *Listeria* enterocolitis, we infected mice overexpressing the *Lrrk2*$^{G2019S}$ allele with *L. monocytogenes* by ingestion of contaminated bread to induce a physiologically relevant model. In the ingestion model of *Listeria* enterocolitis, *L. monocytogenes* primarily colonizes the murine cecum and colon, with dissemination to the liver and spleen. We therefore evaluated the distal small intestine, cecum, colon and spleen at 4d post-infection for bacterial loads. *Lrrk2*$^{G2019S}$ and *Lrrk2*$^{+/+}$ mice harbored similar bacterial burdens in the ileum, colon and cecum following infection with *L. monocytogenes*, however, significantly reduced numbers of bacteria were recovered from the spleens of *Lrrk2*$^{G2019S}$ mutant mice (Figure IV-14), suggesting that while the *Lrrk2*$^{G2019S}$ mutation bears no impact on *L. monocytogenes* colonization, it does reduce bacterial dissemination during enteric infection.

Given the degree of inflammatory cell death observed in the *Lrrk2*$^{G2019S}$ mouse lungs during the early stages of Mtb infection, we postulated that *L. monocytogenes* dissemination might be impaired due to enhanced cell death and shedding of infected

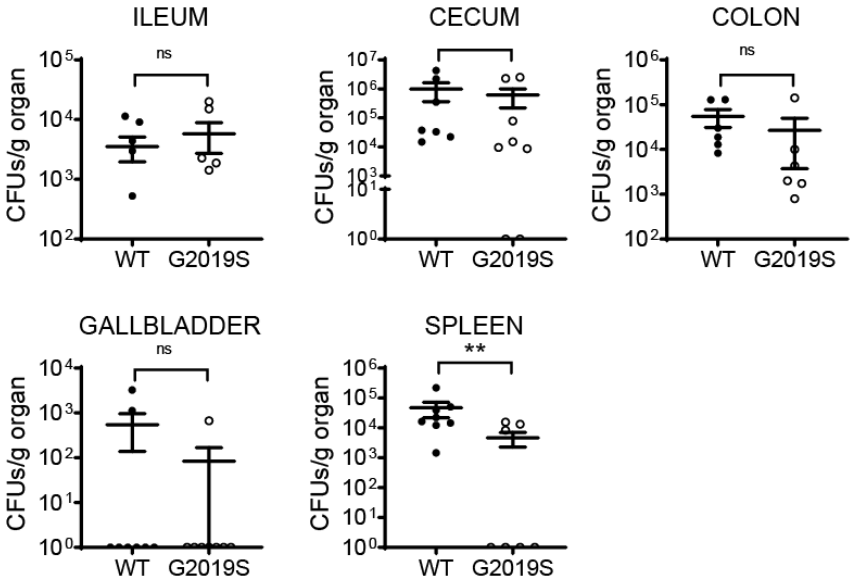


Figure IV-14: Bacterial burden is reduced in the spleens of *Lrrk2*$^{G2019S}$ mice infected with *L. monocytogenes*. CFUs of the ileum, cecum, colon, gallbladder and spleen of mice 4d post-infection with *L. monocytogenes*. Data represented as means ± S.E.M. *p<0.05, **p<0.01, ***p<0.005.

enterocytes. To investigate the impact of the *Lrrk2*$^{G2019S}$ mutation on macrophage survival following infection, we infected BMDMs harvested from mice overexpressing *Lrrk2*$^{G2019S}$ and infected them with *L. monocytogenes*. We used a Lionheart automated microscope with live cell imaging capabilities to follow the cells over 4h, and observed enhanced cell death in *Lrrk2*$^{G2019S}$ macrophages compared to *Lrrk2*$^{+/+}$(Figure IV-15A-B). We also tested bacterial survival *ex vivo* by measuring CFUs in *Lrrk2*$^{G2019S}$ BMDMs but observed no difference in bacterial burdens, suggesting that inflammatory cell death in *Lrrk2*$^{G2019S}$ mutant macrophages is not a result of more permissive bacterial replication (Figure IV-15C).

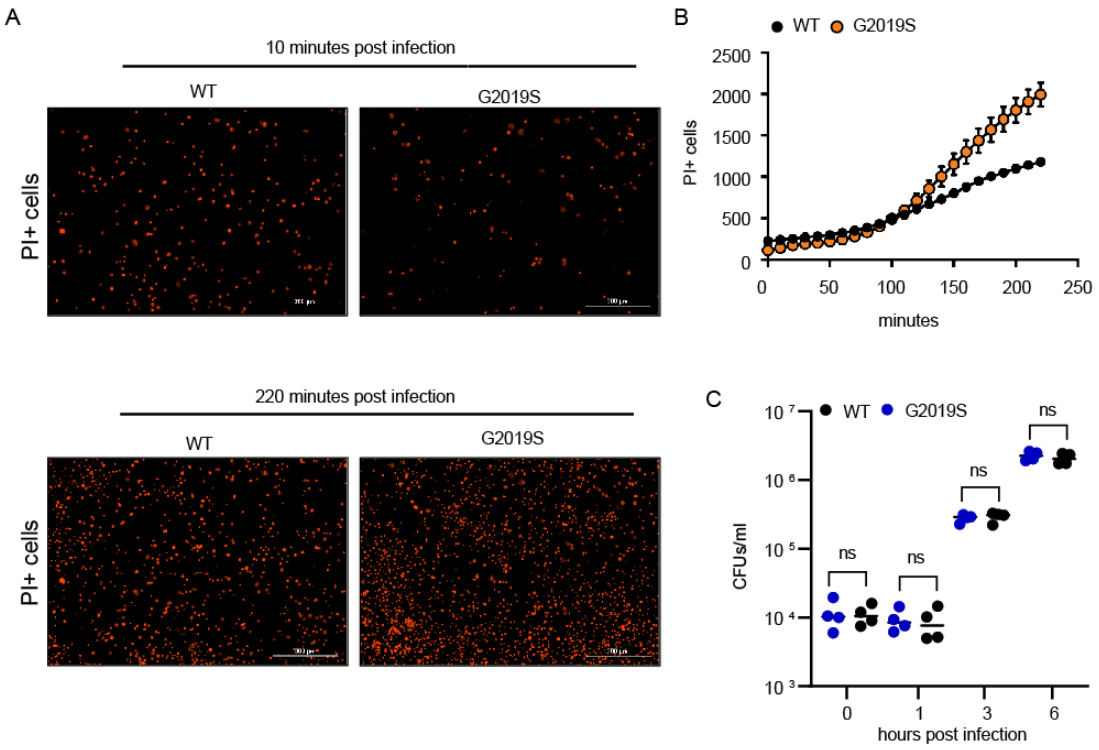


Figure IV-15: *Lrrk2*$^{G2019S}$ macrophages have increased cell death following infection with *L. monocytogenes.* (A) Immunofluorescence images of BMDMs infected with *L. monocytogenes* and stained with propidium iodide (PI) to track cell death at 10 minutes and 220 minutes post-infection. (B) Quantification of PI positive cells over a 4h time course. (C) CFUs from *L. monocytogenes*-infected *Lrrk2*$^{G2019S}$ BMDMs.

## Discussion

Although the genetic risk factors for PD have been studied extensively, numerous studies support a "multiple hit" hypothesis, whereby idiopathic PD is precipitated by extrinsic factors such as infection, gut dysbiosis, or toxin exposure.[101] Additionally, a mounting body of evidence indicate a critical role for LRRK2 in regulating innate immunity. Despite being repeatedly associated with susceptibility to

mycobacterial infection and inflammatory disorders in genome-wide association studies, very little is known about how LRRK2 functions outside of the central nervous system. Here, we provide evidence that loss of *Lrrk2* in macrophages alters type I IFN and ISG expression. Work in our lab has shown that this phenotype is due to elevated levels of cytosolic mtDNA and chronic cGAS activation. During Mtb infection, loss of *Lrrk2* dysregulates type I IFN production and enhances local neutrophil and macrophage infiltration and cell death in the lung. These data help explain why *LRRK2* missense mutations are associated with exacerbated inflammation and poor disease outcomes in leprosy patients.[142]

Mtb is a potent activator of cytosolic DNA sensing,[24,100] and type I IFNs are important biomarkers of Mtb infection associated with poor outcomes in humans and in mouse models of infection.[120] New insights into the requirement of IFNAR signaling for nitric oxide production in macrophages *ex vivo* suggest critical roles for type I IFN induction in cell-intrinsic control of Mtb replication.[168] However, the degree to which these macrophage phenotypes translate to mouse models of infection remains poorly understood. Although we observed a striking type I IFN defect (both higher basal levels and blunted induction) in a number of macrophage primary cells and cell lines, we did not find major differences in infection outcomes in *Lrrk2*$^{-/-}$ vs. *Lrrk2*$^{+/-}$ mice. Our previous experiments demonstrated that while loss of cGAS almost completely abrogates type I IFN expression in macrophages, it has only minor effects *in vivo* (serum IFN-β levels and lung type I IFN/ISG expression levels),[22,23] suggesting that Mtb infection can elicit type I IFN expression in important cGAS-independent ways *in vivo* that we do not yet

fully understand. Another recent publication that investigated the role of *Lrrk2* in controlling Mtb infection does report a significant decrease in CFUs in *Lrrk2*$^{-/-}$ mice at very early infection time points (7 and 14d), which correlates with increased inflammation in the lungs (as we also report).[169] It is likely that minor discrepancies between our data and that reported by others are the consequence of differences in mouse and Mtb strains and the fact that we compared *Lrrk2*$^{-/-}$ and *Lrrk2*$^{+/-}$ littermate controls as opposed to *Lrrk2*$^{+/+}$ controls.

Our *Lrrk2*$^{G2019S}$ mouse Mtb infection has several differences to our *Lrrk2*$^{-/-}$ study. *Lrrk2*$^{G2019S}$ mice demonstrated greater bacterial burden in the lungs and spleen and had massively exacerbated pulmonary inflammation. Together, these findings indicate that mice harboring the *Lrrk2*$^{G2019S}$ allele are incredibly sensitive to Mtb infection, more permissive to bacterial replication, and have exacerbated inflammation and Mtb pathogenesis.

Lastly, we augment our understanding of LRRK2 as a regulator of innate immunity by extending our studies to the food-borne pathogen *L. monocytogenes* and interrogating the outcome of a relatively localized, acute infection in the context of the most common *Lrrk2* mutation, G2019S. It is plausible that an enhanced inflammatory response to an enteric pathogen otherwise capable of producing an acute fatal outcome in the absence of a swift and robust immune response such as *L. monocytogenes* may provide an evolutionary host advantage. Although the *LRRK2*$^{G2019S}$ allele is the most common cause of familial PD, its prevalence is unequally distributed. While 30% of Ashkenazi Jews and over 40% of North African Berber populations with PD bear the

G2019S allele, its prevalence is less than 0.1% in Asian PD patients, suggesting a potential selective pressure in certain populations.[170] It will be crucial moving forward to more directly interrogate the molecular drivers of inflammation and Mtb pathogenesis in *Lrrk2*$^{-/-}$ mice as well as in mouse genotypes associated with human disease susceptibility, such as *Lrrk2*$^{G2019S}$. Because LRRK2 inhibitors are a major area of drug development for the treatment of PD, it is crucial to understand how both loss of and mutations in this protein might impact the ability of patients receiving such therapies to respond to and clear infection.

# CHAPTER V

# CONCLUSIONS AND FUTURE DIRECTIONS

## *Rhodococcus equi*

In conclusion, my work in chapter III reveals several previously unappreciated features of macrophage sensing and response to infection with *R. equi*. First, I demonstrate that macrophage infection with *R. equi* elicits a type I IFN response that is independent of the virulence factor VapA (Figure V-1). Second, I show that this type I IFN response is dependent upon the cGAS/STING/TBK1 axis of the cytosolic DNA sensing pathway. Finally, I show that the cytosolic danger sensors galectin-3, -8, and -9 are recruited to a population of *R. equi*, which suggests that the phagosomal membrane is permeable to the cytosol as early as 4h following infection.

Although these data are exciting, a number of unanswered questions remain. While the recruitment of galectins to *R. equi* provides convincing evidence that the phagosome is permeable to the cytosol, the mechanism by which permeabilization occurs is unclear. Along these lines, the function of the *R. equi* secretions systems is also unknown. Future studies with ESX deletions will be useful for testing their contribution to phagosomal permeabilization. The observation that cGAS is required for type I IFN production during infection strongly suggests that *R. equi* infection results in the liberation of DNA into the cytosol, but it is unclear whether bacterial or host DNA serves as the ligand. A simple way to begin to test whether *R. equi* perturbs the mitochondria to release DNA into the cytosol would be to either infect cells in which

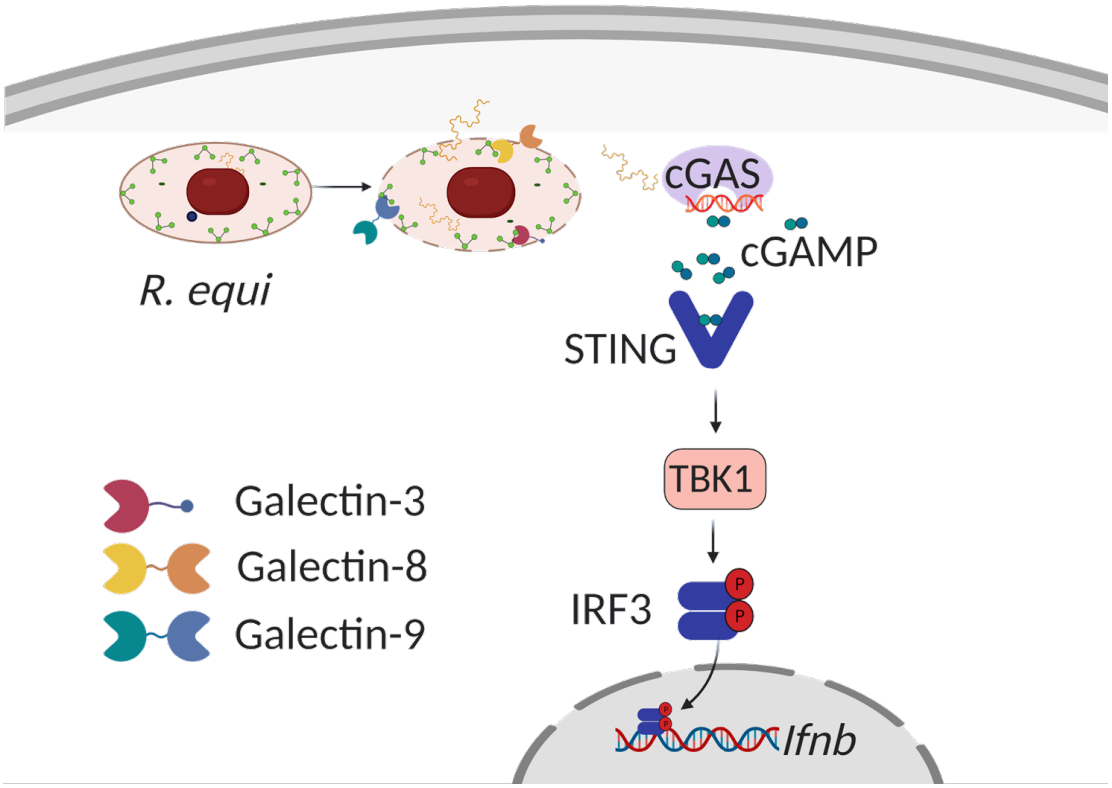


Figure V-1: Model of cytosolic DNA sensing during *R. equi* infection. Created with BioRender.com

mitochondrial DNA has been depleted from the cell and measure type I IFN, or directly measure mitochondrial DNA in the cytosolic fraction following infection. Along these lines, because macrophages lacking STING phenocopy those lacking cGAS, additional studies will be needed to determine what role if any that *R. equi* cyclic dinucleotides play in engaging the cytosolic DNA sensing pathway at the level of STING.

The observations that galectins are recruited to *R. equi* also open up a rich avenue of inquiry. Work by Ferraz and colleagues found that mice lacking galectin-3 were resistant to infection with *R. equi* and had higher levels of pro-inflammatory

cytokines,[171] implying that galectin recruitment could be detrimental for the host. These data contrast with recent work in our lab which shows that Mtb-infected macrophages lacking galectins-3, -8, and -9 are defective in controlling replication.[129] Whether this discrepancy is a result of cell-intrinsic versus host-intrinsic immune responses, bacterial species differences, or differing functions for each of these galectins remains to be seen. Additionally, further studies into the contribution of selective autophagy as a potential anti-microbial mechanism are also warranted.

Lastly, future studies will also be needed to determine the clinical implications of type I IFN during *R. euqi* infection, during both equine and non-equine infection. I hypothesize that type I IFN production would be associated with clinical disease, but given that only one foal in our study became clinically ill, I am unable to draw that conclusion based on our data. However, the teaching hospital provides a rich environment to glean clinical blood samples from naturally infected, sick foals, and mouse models offer an additional opportunity to further investigate this area.

**LRRK2**

Work in Chapter IV centers on an emerging innate immune regulator, LRRK2 (Figure V-2). Our findings show that while macrophages lacking *Lrrk2* have elevated type I IFN at rest, they fail to induce type I IFN upon infection with *M. leprae*. This aberrant innate immune response is manifested as a modest increase in Mtb-induced pulmonary inflammation characterized by enhanced infiltration by neutrophils. Next, we show that mice overexpressing the most common *Lrrk2* mutation, G2019S are exquisitely sensitive to Mtb infection and show an overwhelming exacerbation of Mtb-

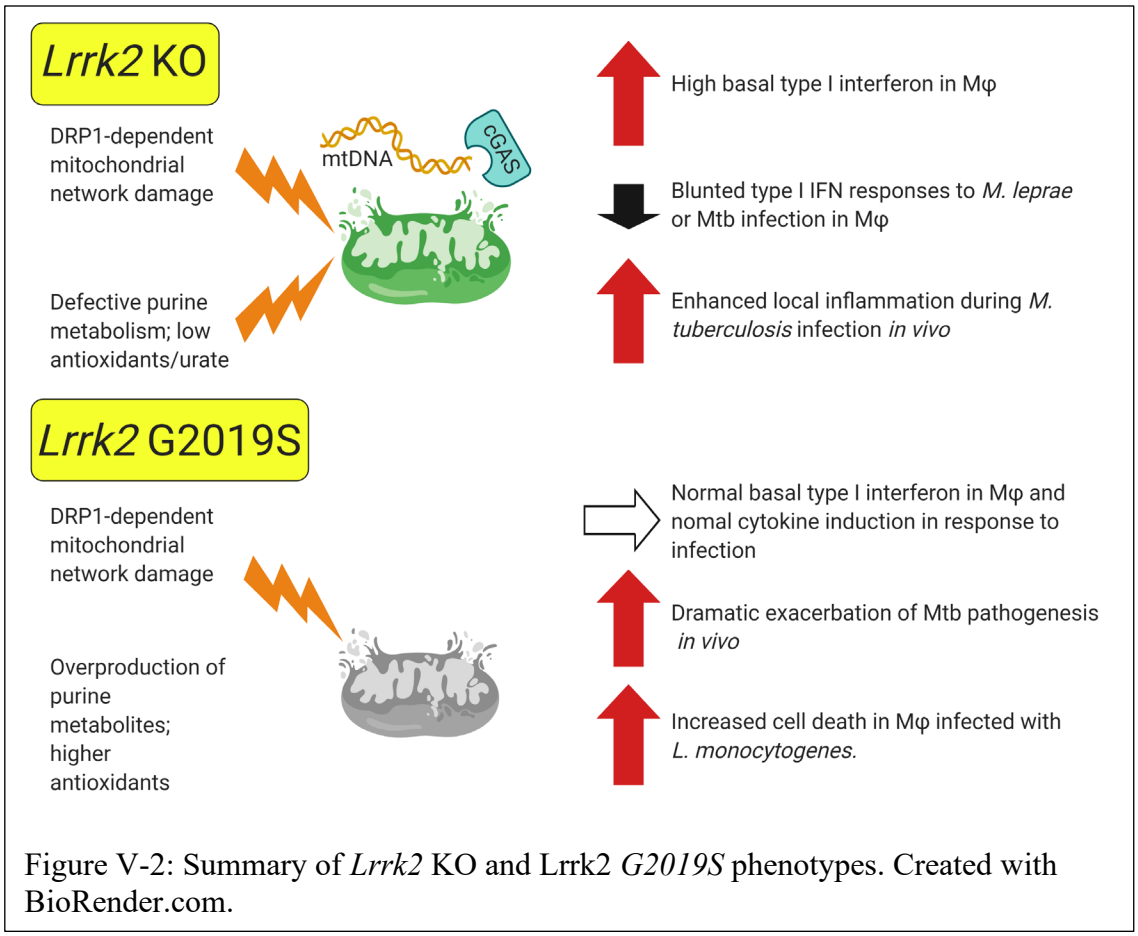


Figure V-2: Summary of *Lrrk2* KO and Lrrk2 *G2019S* phenotypes. Created with BioRender.com.

induced pathogenesis, with near obliteration of functional lung by inflammatory cell infiltrates and significant increases in bacterial burden at later stages of infection. Thirdly, in collaboration with the Srinivasan laboratory, we show that mice infected with Mtb via an aerosol route have increased glial activation in the brain. Lastly, I show that G2019S mice have impaired bacterial dissemination following infection with the enteric pathogen *L. monocytogenes* via oral ingestion. Ongoing work on this project is currently focused on exploring the mechanism behind the cell death phenotype in G2019S

macrophages, particularly the contribution to the pore forming protein gasdermin D and inflammasome activation.

Given the clear role of neutrophils in *Lrrk2*-related mouse phenotypes, additional studies exploring the function of LRRK2 in neutrophils are also be of interest. Along these lines, while we expect that the phenotypes of BMDMs can be extrapolated to alveolar macrophages, experiments specifically looking at this subset of resident macrophages will be key.

While our work on the brain suggests that chronic peripheral inflammation contributes to glial activation, further studies will be needed to evaluate the impact of these activated glial cells on dopaminergic neuron health. Ongoing work in our lab is exploring the cell intrinsic impact of *Lrrk2* on microglial and astrocyte immunity.

Finally, future studies exploring *Lrrk2*-related phenotypes during infection with other enteric pathogens such as *S.* Typhimurium may be informative for determining whether the dissemination defect is limited to oral infection with *L. monocytogenes*. Additionally, since this phenotype seems to occur in the acute stages of infection, absent abundant inflammatory cell infiltration, further work should test whether enterocyte cell death is a contributing factor.

# REFERENCES


1. Abe T, Marutani Y, Shoji I. Cytosolic DNA-sensing immune response and viral infection. Microbiol Immunol. 2019;63(2):51-64. Epub 2019/02/26. doi: 10.1111/1348-0421.12669. PubMed PMID: 30677166.

2. Akira S, Uematsu S, Takeuchi O. Pathogen Recognition and Innate Immunity. Cell. 2006;124(4):783-801. doi: https://doi.org/10.1016/j.cell.2006.02.015.

3. Beutler B. Innate immunity: an overview. Molecular Immunology. 2004;40(12):845-59. doi: https://doi.org/10.1016/j.molimm.2003.10.005.

4. Riera Romo M, Pérez-Martínez D, Castillo Ferrer C. Innate immunity in vertebrates: an overview. Immunology. 2016;148(2):125-39. Epub 2016/04/05. doi: 10.1111/imm.12597. PubMed PMID: 26878338.

5. Hayward JA, Mathur A, Ngo C, Man SM. Cytosolic Recognition of Microbes and Pathogens: Inflammasomes in Action. Microbiol Mol Biol Rev. 2018;82(4):e00015-18. doi: 10.1128/MMBR.00015-18. PubMed PMID: 30209070.

6. Takeda K, Akira S. Toll-like receptors in innate immunity. International Immunology. 2005;17(1):1-14. doi: 10.1093/intimm/dxh186.

7. Tan X, Sun L, Chen J, Chen ZJ. Detection of Microbial Infections Through Innate Immune Sensing of Nucleic Acids. Annual Review of Microbiology. 2018;72(1):447-78. doi: 10.1146/annurev-micro-102215-095605. PubMed PMID: 30200854.

8. Kawai T, Akira S. TLR signaling. Cell Death & Differentiation. 2006;13(5):816-25. doi: 10.1038/sj.cdd.4401850.

9. Kawai T, Akira S. Toll-like Receptors and Their Crosstalk with Other Innate Receptors in Infection and Immunity. Immunity. 2011;34(5):637-50. doi: 10.1016/j.immuni.2011.05.006.

10. Rathinam VAK, Fitzgerald KA. Cytosolic surveillance and antiviral immunity. Curr Opin Virol. 2011;1(6):455-62. Epub 2011/12/04. doi: 10.1016/j.coviro.2011.11.004. PubMed PMID: 22440909.

11. Patrick KL, Bell SL, Watson RO. For Better or Worse: Cytosolic DNA Sensing during Intracellular Bacterial Infection Induces Potent Innate Immune Responses. Molecular Mechanisms of Host-Pathogen Interactions. 2016;428(17):3372-86. doi: http://dx.doi.org/10.1016/j.jmb.2016.04.030.

12. O'Riordan M, Yi CH, Gonzales R, Lee K-D, Portnoy DA. Innate recognition of bacteria by a macrophage cytosolic surveillance pathway. Proc Natl Acad Sci U S A. 2002;99(21):13861-6. Epub 2002/10/01. doi: 10.1073/pnas.202476699. PubMed PMID: 12359878.

13. Sharma D, Kanneganti T-D. The cell biology of inflammasomes: Mechanisms of inflammasome activation and regulation. The Journal of cell biology. 2016;213(6):617-29. doi: 10.1083/jcb.201602089. PubMed PMID: 27325789.

14. Sun L, Wu J, Du F, Chen X, Chen ZJ. Cyclic GMP-AMP Synthase Is a Cytosolic DNA Sensor That Activates the Type I Interferon Pathway. Science. 2013;339(6121):786-91. doi: 10.1126/science.1232458.

15. Wu J, Sun L, Chen X, Du F, Shi H, Chen C, et al. Cyclic GMP-AMP is an endogenous second messenger in innate immune signaling by cytosolic DNA. Science. 2013;339(6121):826-30. Epub 2012/12/20. doi: 10.1126/science.1229963. PubMed PMID: 23258412.

16. Ishikawa H, Ma Z, Barber GN. STING regulates intracellular DNA-mediated, type I interferon-dependent innate immunity. Nature. 2009;461(7265):788-92. doi: 10.1038/nature08476.

17. Woodward JJ, Iavarone AT, Portnoy DA. c-di-AMP secreted by intracellular Listeria monocytogenes activates a host type I interferon response. Science. 2010;328(5986):1703-5. Epub 2010/05/27. doi: 10.1126/science.1189801. PubMed PMID: 20508090.

18. Burdette DL, Monroe KM, Sotelo-Troha K, Iwig JS, Eckert B, Hyodo M, et al. STING is a direct innate immune sensor of cyclic di-GMP. Nature. 2011;478(7370):515-8. doi: 10.1038/nature10429.

19. Zhang C, Shang G, Gui X, Zhang X, Bai X-C, Chen ZJ. Structural basis of STING binding with and phosphorylation by TBK1. Nature. 2019;567(7748):394-8. Epub 2019/03/06. doi: 10.1038/s41586-019-1000-2. PubMed PMID: 30842653.

20. Perry AK, Chow EK, Goodnough JB, Yeh W-C, Cheng G. Differential requirement for TANK-binding kinase-1 in type I interferon responses to toll-like receptor activation and viral infection. J Exp Med. 2004;199(12):1651-8. doi: 10.1084/jem.20040528. PubMed PMID: 15210743.

21. Hemmi H, Takeuchi O, Sato S, Yamamoto M, Kaisho T, Sanjo H, et al. The Roles of Two IκB Kinase-related Kinases in Lipopolysaccharide and Double Stranded

RNA Signaling and Viral Infection. Journal of Experimental Medicine. 2004;199(12):1641-50. doi: 10.1084/jem.20040520.

22. Watson RO, Bell SL, MacDuff DA, Kimmey JM, Diner EJ, Olivas J. The cytosolic sensor cGAS detects Mycobacterium tuberculosis DNA to induce type I interferons and activate autophagy. Cell Host & Microbe. 2015;17:811--9. doi: 10.1016/j.chom.2015.05.004.

23. Collins Angela C, Cai H, Li T, Franco Luis H, Li X-D, Nair Vidhya R, et al. Cyclic GMP-AMP Synthase Is an Innate Immune DNA Sensor for Mycobacterium tuberculosis. Cell Host & Microbe. 2015;17(6):820-8. doi: 10.1016/j.chom.2015.05.005.

24. Manzanillo Paolo S, Shiloh Michael U, Portnoy Daniel A, Cox Jeffery S. Mycobacterium Tuberculosis Activates the DNA-Dependent Cytosolic Surveillance Pathway within Macrophages. Cell Host & Microbe. 2012;11(5):469-80. doi: http://dx.doi.org/10.1016/j.chom.2012.03.007.

25. Storek KM, Gertsvolf NA, Ohlson MB, Monack DM. cGAS and Ifi204 cooperate to produce type I IFNs in response to Francisella infection. Journal of Immunology. 2015;194:3236--45. doi: 10.4049/jimmunol.1402764.

26. Zhang Y, Yeruva L, Marinov A, Prantner D, Wyrick PB, Lupashin V. The DNA sensor, cyclic GMP-AMP synthase, is essential for induction of IFN-β during Chlamydia trachomatis infection. Journal of Immunology. 2014;193:2394--404. doi: 10.4049/jimmunol.1302718.

27. Lazear HM, Schoggins JW, Diamond MS. Shared and Distinct Functions of Type I and Type III Interferons. Immunity. 2019;50(4):907-23. doi: 10.1016/j.immuni.2019.03.025. PubMed PMID: 30995506.

28. Espinosa V, Dutta O, McElrath C, Du P, Chang Y-J, Cicciarelli B, et al. Type III interferon is a critical regulator of innate antifungal immunity. Sci Immunol. 2017;2(16):eaan5357. doi: 10.1126/sciimmunol.aan5357. PubMed PMID: 28986419.

29. Schoggins JW. Interferon-stimulated genes: what do they all do? Annual review of virology. 2019;6:567-84.

30. Michalska A, Blaszczyk K, Wesoly J, Bluyssen HAR. A Positive Feedback Amplifier Circuit That Regulates Interferon (IFN)-Stimulated Gene Expression and Controls Type I and Type II IFN Responses. Frontiers in immunology. 2018;9:1135-. doi: 10.3389/fimmu.2018.01135. PubMed PMID: 29892288.

31. Crosse KM, Monson EA, Beard MR, Helbig KJ. Interferon-stimulated genes as enhancers of antiviral innate immune signaling. J Innate Immun. 2018;10(2):85-93.

32. Hwang SY, Hertzog PJ, Holland KA, Sumarsono SH, Tymms MJ, Hamilton JA, et al. A null mutation in the gene encoding a type I interferon receptor component eliminates antiproliferative and antiviral responses to interferons alpha and beta and alters macrophage responses. Proceedings of the National Academy of Sciences. 1995;92(24):11284-8.

33. Muller U, Steinhoff U, Reis L, Hemmi S, Pavlovic J, Zinkernagel RM, et al. Functional role of type I and type II interferons in antiviral defense. Science. 1994;264(5167):1918-21.

34. Stanley SA, Johndrow JE, Manzanillo P, Cox JS. The Type I IFN response to infection with Mycobacterium tuberculosis requires ESX-1-mediated secretion and contributes to pathogenesis. The Journal of Immunology. 2007;178(5):3143-52.

35. Mayer-Barber KD, Andrade BB, Oland SD, Amaral EP, Barber DL, Gonzales J, et al. Host-directed therapy of tuberculosis based on interleukin-1 and type I interferon crosstalk. Nature. 2014;511(7507):99-103. doi: 10.1038/nature13489.

36. Auerbuch V, Brockstedt DG, Meyer-Morse N, O'Riordan M, Portnoy DA. Mice lacking the type I interferon receptor are resistant to Listeria monocytogenes. J Exp Med. 2004;200(4):527-33. Epub 2004/08/09. doi: 10.1084/jem.20040976. PubMed PMID: 15302899.

37. O'Connell RM, Saha SK, Vaidya SA, Bruhn KW, Miranda GA, Zarnegar B, et al. Type I Interferon Production Enhances Susceptibility to Listeria monocytogenes Infection. J Exp Med. 2004;200(4):437.

38. Manca C, Tsenova L, Bergtold A, Freeman S, Tovey M, Musser JM, et al. Virulence of a Mycobacterium tuberculosis clinical isolate in mice is determined by failure to induce Th1 type immunity and is associated with induction of IFN-α/β. Proceedings of the National Academy of Sciences. 2001;98(10):5752-7. doi: 10.1073/pnas.091096998.

39. Antonelli LR, Rothfuchs AG, Gonçalves R, Roffê E, Cheever AW, Bafica A, et al. Intranasal Poly-IC treatment exacerbates tuberculosis in mice through the pulmonary recruitment of a pathogen-permissive monocyte/macrophage population. J Clin Invest. 2010;120(5):1674-82.

40. Diamond MS, Farzan M. The broad-spectrum antiviral functions of IFIT and IFITM proteins. Nature Reviews Immunology. 2013;13(1):46-57. doi: 10.1038/nri3344.

41. Ghosh S, Marsh ENG. Viperin: An ancient radical SAM enzyme finds its place in modern cellular metabolism and innate immunity. Journal of Biological Chemistry. 2020;295(33):11513-28.

42. Abbas YM, Laudenbach BT, Martínez-Montero S, Cencic R, Habjan M, Pichlmair A, et al. Structure of human IFIT1 with capped RNA reveals adaptable mRNA binding and mechanisms for sensing N1 and N2 ribose 2′-O methylations. Proceedings of the National Academy of Sciences. 2017;114(11):E2106-E15. doi: 10.1073/pnas.1612444114.

43. Yu A, Skorupka KA, Pak AJ, Ganser-Pornillos BK, Pornillos O, Voth GA. TRIM5α self-assembly and compartmentalization of the HIV-1 viral capsid. Nature communications. 2020;11(1):1307-. doi: 10.1038/s41467-020-15106-1. PubMed PMID: 32161265.

44. Verhelst J, Parthoens E, Schepens B, Fiers W, Saelens X. Interferon-Inducible Protein Mx1 Inhibits Influenza Virus by Interfering with Functional Viral Ribonucleoprotein Complex Assembly. Journal of Virology. 2012;86(24):13445-55. doi: 10.1128/jvi.01682-12.

45. Ji DX, Yamashiro LH, Chen KJ, Mukaida N, Kramnik I, Darwin KH, et al. Type I interferon-driven susceptibility to Mycobacterium tuberculosis is mediated by IL-1Ra. Nat Microbiol. 2019;4(12):2128-35. Epub 2019/10/14. doi: 10.1038/s41564-019-0578-3. PubMed PMID: 31611644.

46. John SP, Sun J, Carlson RJ, Cao B, Bradfield CJ, Song J, et al. IFIT1 Exerts Opposing Regulatory Effects on the Inflammatory and Interferon Gene Programs in LPS-Activated Human Macrophages. Cell Rep. 2018;25(1):95-106.e6. doi: https://doi.org/10.1016/j.celrep.2018.09.002.

47. Teles RMB, Graeber TG, Krutzik SR, Montoya D, Schenk M, Lee DJ, et al. Type I Interferon Suppresses Type II Interferon–Triggered Human Anti-Mycobacterial Responses. Science. 2013;339(6126):1448--53. doi: https://dx.doi.org/10.1126/science.1233665.

48. Toledo Pinto TG, Batista-Silva LR, Medeiros RCA, Lara FA, Moraes MO. Type I Interferons, Autophagy and Host Metabolism in Leprosy. Frontiers in immunology. 2018;9:806-. doi: 10.3389/fimmu.2018.00806. PubMed PMID: 29755459.

49. Vázquez-Boland JA, Giguère S, Hapeshi A, MacArthur I, Anastasi E, Valero-Rello A. Rhodococcus equi: The many facets of a pathogenic actinomycete. Veterinary Microbiology. 2013;167(1):9-33. doi: https://doi.org/10.1016/j.vetmic.2013.06.016.

50. Zink MC, Yager JA, Prescott JF, Fernando MA. Electron microscopic investigation of intracellular events after ingestion of Rhodococcus equi by foal alveolar macrophages. Veterinary Microbiology. 1987;14(3):295-305. doi: https://doi.org/10.1016/0378-1135(87)90117-9.

51. Muscatello G. Rhodococcus equi pneumonia in the foal – Part 1: Pathogenesis and epidemiology. The Veterinary Journal. 2012;192(1):20-6. doi: https://doi.org/10.1016/j.tvjl.2011.08.014.

52. Reuss SM, Cohen ND. Update on Bacterial Pneumonia in the Foal and Weanling. Veterinary Clinics of North America: Equine Practice. 2015;31(1):121-35. doi: https://doi.org/10.1016/j.cveq.2014.11.004.

53. Lopez AM, Hines MT, Palmer GH, Alperin DC, Hines SA. Identification of pulmonary T-lymphocyte and serum antibody isotype responses associated with protection against Rhodococcus equi. Clin Diagn Lab Immunol. 2002;9(6):1270-6. doi: 10.1128/cdli.9.6.1270-1276.2002. PubMed PMID: 12414760.

54. Takai S, Imai Y, Fukunaga N, Uchida Y, Kamisawa K, Sasaki Y, et al. Identification of virulence-associated antigens and plasmids in Rhodococcus equi from patients with AIDS. Journal of Infectious Diseases. 1995;172(5):1306-11.

55. Cohen ND, Carter CN, Scott HM, Chaffin MK, Smith JL, Grimm MB, et al. Association of soil concentrations of Rhodococcus equi and incidence of pneumonia attributable to Rhodococcus equi in foals on farms in central Kentucky. American journal of veterinary research. 2008;69(3):385-95.

56. Rocha JN, Cohen ND, Bordin AI, Brake CN, Giguère S, Coleman MC, et al. Oral administration of electron-beam inactivated Rhodococcus equi Failed to protect foals against intrabronchial infection with live, virulent R. equi. PloS one. 2016;11(2):e0148111.

57. Venner M, Reinhold B, Beyerbach M, Feige K. Efficacy of azithromycin in preventing pulmonary abscesses in foals. The Veterinary Journal. 2009;179(2):301-3. doi: https://doi.org/10.1016/j.tvjl.2007.10.002.

58. Cohen ND. Rhodococcus equi Foal Pneumonia. Veterinary Clinics of North America: Equine Practice. 2014;30(3):609-22. doi: https://doi.org/10.1016/j.cveq.2014.08.010.

59. Giguère S, Cohen ND, Keith Chaffin M, Hines SA, Hondalus MK, Prescott JF, et al. Rhodococcus equi: Clinical Manifestations, Virulence, and Immunity. Journal of Veterinary Internal Medicine. 2011;25(6):1221-30. doi: https://doi.org/10.1111/j.1939-1676.2011.00804.x.

60. Hondalus MK. Pathogenesis and virulence of Rhodococcus equi. Veterinary Microbiology. 1997;56(3):257-68. doi: https://doi.org/10.1016/S0378-1135(97)00094-1.

61 Willingham-Lane JM, Berghaus LJ, Giguère S, Hondalus MK. Influence of Plasmid Type on the Replication of Rhodococcus equi in Host Macrophages. mSphere. 2016;1(5):e00186-16. doi: 10.1128/mSphere.00186-16. PubMed PMID: 27747295.

62 Stranahan LW, Plumlee QD, Lawhon SD, Cohen ND, Bryan LK. Rhodococcus equi infections in goats: characterization of virulence plasmids. Veterinary pathology. 2018;55(2):273-6.

63. Davis W, Steficek B, Watson G, Yamini B, Madarame H, Takai S, et al. Disseminated Rhodococcus equi infection in two goats. Veterinary pathology. 1999;36(4):336-9.

64. Bryan L, Clark S, Díaz-Delgado J, Lawhon S, Edwards J. Rhodococcus equi infections in dogs. Veterinary pathology. 2017;54(1):159-63.

65. Takai S, Martens RJ, Julian A, Ribeiro MG, de Farias MR, Sasaki Y, et al. Virulence of Rhodococcus equi isolated from cats and dogs. Journal of Clinical Microbiology. 2003;41(9):4468-70.

66. Farias M, Takai S, Ribeiro MG, Fabris V, Franco S. Cutaneous pyogranuloma in a cat caused by virulent Rhodococcus equi containing an 87 kb type I plasmid. Australian veterinary journal. 2007;85(1-2):29-31.

67. Herath S, Lewis C, Nisbet M. Increasing awareness of Rhodococcus equi pulmonary infection in the immunocompetent adult: a rare infection with poor prognosis. NZ Med J. 2013;126:165-74.

68. Kedlaya I, Ing MB, Wong SS. Rhodococcus equi Infections in Immunocompetent Hosts: Case Report and Review. Clinical Infectious Diseases. 2001;32(3):e39-e46. doi: 10.1086/318520.

69. Lin WV, Kruse RL, Yang K, Musher DM. Diagnosis and management of pulmonary infection due to Rhodococcus equi. Clinical Microbiology and Infection. 2019;25(3):310-5. doi: https://doi.org/10.1016/j.cmi.2018.04.033.

70. von Bargen K, Scraba M, Krämer I, Ketterer M, Nehls C, Krokowski S, et al. Virulence-associated protein A from Rhodococcus equi is an intercompartmental pH-neutralising virulence factor. Cell Microbiol. 2019;21(1):e12958. doi: 10.1111/cmi.12958.

71. Letek M, González P, MacArthur I, Rodríguez H, Freeman TC, Valero-Rello A, et al. The Genome of a Pathogenic Rhodococcus: Cooptive Virulence Underpinned by Key Gene Acquisitions. PLOS Genetics. 2010;6(9):e1001145. doi: 10.1371/journal.pgen.1001145.

72. Jain S, Bloom BR, Hondalus MK. Deletion of vapA encoding Virulence Associated Protein A attenuates the intracellular actinomycete Rhodococcus equi. Mol Microbiol. 2003;50(1):115-28. doi: https://doi.org/10.1046/j.1365-2958.2003.03689.x.

73. Letek M, Ocampo-Sosa AA, Sanders M, Fogarty U, Buckley T, Leadon DP, et al. Evolution of the Rhodococcus equi vap pathogenicity island seen through comparison of host-associated vapA and vapB virulence plasmids. J Bacteriol. 2008;190(17):5797-805. Epub 2008/07/07. doi: 10.1128/JB.00468-08. PubMed PMID: 18606735.

74. Coulson GB, Miranda-CasoLuengo AA, Miranda-CasoLuengo R, Wang X, Oliver J, Willingham-Lane JM, et al. Transcriptome reprogramming by plasmid-encoded transcriptional regulators is required for host niche adaption of a macrophage pathogen. Infect Immun. 2015;83(8):3137-45. Epub 2015/05/26. doi: 10.1128/IAI.00230-15. PubMed PMID: 26015480.

75. Wright LM, Carpinone EM, Bennett TL, Hondalus MK, Starai VJ. VapA of Rhodococcus equi binds phosphatidic acid. Mol Microbiol. 2018;107(3):428-44. Epub 2017/12/22. doi: 10.1111/mmi.13892. PubMed PMID: 29205554.

76. Rofe AP, Davis LJ, Whittingham JL, Latimer-Bowman EC, Wilkinson AJ, Pryor PR. The Rhodococcus equi virulence protein VapA disrupts endolysosome function and stimulates lysosome biogenesis. Microbiologyopen. 2017;6(2):e00416. Epub 2016/10/19. doi: 10.1002/mbo3.416. PubMed PMID: 27762083.

77. Toyooka K, Takai S, Kirikae T. Rhodococcus equi can survive a phagolysosomal environment in macrophages by suppressing acidification of the phagolysosome. Journal of Medical Microbiology. 2005;54(11):1007-15. doi: https://doi.org/10.1099/jmm.0.46086-0.

78. Berghaus LJ, Giguère S, Bordin AI, Cohen ND. Effects of priming with cytokines on intracellular survival and replication of Rhodococcus equi in equine macrophages. Cytokine. 2018;102:7-11. doi: https://doi.org/10.1016/j.cyto.2017.12.011.

79. Kanaly ST, Hines SA, Palmer GH. Cytokine modulation alters pulmonary clearance of Rhodococcus equi and development of granulomatous pneumonia. Infect Immun. 1995;63(8):3037-41. doi: 10.1128/IAI.63.8.3037-3041.1995. PubMed PMID: 7622227.

80. Darrah PA, Hondalus MK, Chen Q, Ischiropoulos H, Mosser DM. Cooperation between Reactive Oxygen and Nitrogen Intermediates in Killing of Rhodococcus equi by Activated Macrophages. Infect Immun. 2000;68(6):3587-93. doi: 10.1128/iai.68.6.3587-3593.2000.

81. Kasuga-Aoki H, Takai S, Sasaki Y, Tsubaki S, Madarame H, Nakane A. Tumour necrosis factor and interferon-gamma are required in host resistance against virulent Rhodococcus equi infection in mice: cytokine production depends on the virulence levels of R. equi. Immunology. 1999;96(1):122-7. doi: 10.1046/j.1365-2567.1999.00657.x. PubMed PMID: 10233686.

82. Nordmann P, Ronco E, Guenounou M. Involvement of Interferon-γ and Tumor Necrosis Factor-α in Host Defense against Rhodococcus equi. The Journal of Infectious Diseases. 1993;167(6):1456-9. doi: 10.1093/infdis/167.6.1456.

83. Jacks S, Giguère S, Crawford PC, Castleman WL. Experimental infection of neonatal foals with Rhodococcus equi triggers adult-like gamma interferon induction. Clin Vaccine Immunol. 2007;14(6):669-77. Epub 2007/04/04. doi: 10.1128/CVI.00042-07. PubMed PMID: 17409222.

84. Liu M, Bordin A, Liu T, Russell K, Cohen N. Gene expression of innate Th1-, Th2-, and Th17-type cytokines during early life of neonatal foals in response to Rhodococcus equi. Cytokine. 2011;56(2):356-64. doi: https://doi.org/10.1016/j.cyto.2011.07.017.

85. Smith CS, Aerts A, Saunderson P, Kawuma J, Kita E, Virmond M. Multidrug therapy for leprosy: a game changer on the path to elimination. The Lancet Infectious Diseases. 2017;17(9):e293-e7. doi: https://doi.org/10.1016/S1473-3099(17)30418-8.

86. White C, Franco-Paredes C. Leprosy in the 21st century. Clin Microbiol Rev. 2015;28(1):80-94. doi: 10.1128/CMR.00079-13. PubMed PMID: 25567223.

87. Fonseca ABdL, Simon MdV, Cazzaniga RA, de Moura TR, de Almeida RP, Duthie MS, et al. The influence of innate and adaptive immune responses on the differential clinical outcomes of leprosy. Infectious Diseases of Poverty. 2017;6. doi: 10.1186/s40249-016-0229-3.

88. Pinheiro RO, Schmitz V, Silva BJdA, Dias AA, de Souza BJ, de Mattos Barbosa MG, et al. Innate Immune Responses in Leprosy. Frontiers in Immunology. 2018;9(518). doi: 10.3389/fimmu.2018.00518.

89. Chavarro-Portillo B, Soto CY, Guerrero MI. Mycobacterium leprae's evolution and environmental adaptation. Acta Tropica. 2019;197:105041. doi: https://doi.org/10.1016/j.actatropica.2019.105041.

90. Gaschignard J, Grant AV, Thuc NV, Orlova M, Cobat A, Huong NT, et al. Pauci- and Multibacillary Leprosy: Two Distinct, Genetically Neglected Diseases. PLOS Neglected Tropical Diseases. 2016;10(5):e0004345. doi: 10.1371/journal.pntd.0004345.

91. Marcinek P, Jha AN, Shinde V, Sundaramoorthy A, Rajkumar R, Suryadevara NC, et al. LRRK2 and RIPK2 Variants in the NOD 2-Mediated Signaling Pathway Are

Associated with Susceptibility to Mycobacterium leprae in Indian Populations. . PLoS ONE 8(8): e73103 doi:101371/journalpone0073103. 2013;8(8):e73103. doi: 10.1371/journal.pone.0073103.

92. de Toledo-Pinto TG, Ferreira ABR, Ribeiro-Alves M, Rodrigues LS, Batista-Silva LR, Silva BJdA, et al. STING-Dependent 2′-5′ Oligoadenylate Synthetase–Like Production Is Required for Intracellular Mycobacterium leprae Survival. The Journal of Infectious Diseases. 2016;214(2):311-20. doi: 10.1093/infdis/jiw144.

93. de Macedo CS, Lara FA, Pinheiro RO, Schmitz V, de Berrêdo-Pinho M, Pereira GM, et al. New insights into the pathogenesis of leprosy: contribution of subversion of host cell metabolism to bacterial persistence, disease progression, and transmission. F1000Res. 2020;9:F1000 Faculty Rev-70. doi: 10.12688/f1000research.21383.1. PubMed PMID: 32051758.

94. WHO. Global Tuberculosis Report 2018. Geneva: World Health Organization, 2018.

95. Amaral EP, Lasunskaia EB, D'Império-Lima MR. Innate immunity in tuberculosis: how the sensing of mycobacteria and tissue damage modulates macrophage death. Microbes and Infection. 2016;18(1):11-20. doi: https://doi.org/10.1016/j.micinf.2015.09.005.

96. Abel L, Fellay J, Haas DW, Schurr E, Srikrishna G, Urbanowski M, et al. Genetics of human susceptibility to active and latent tuberculosis: present knowledge and future perspectives. The Lancet Infectious Diseases. 2018;18(3):e64-e75. doi: https://doi.org/10.1016/S1473-3099(17)30623-0.

97. Perry VH, Cunningham C, Holmes C. Systemic infections and inflammation affect chronic neurodegeneration. Nature Reviews Immunology. 2007;7:161. doi: 10.1038/nri2015.

98. Shen C-H, Chou C-H, Liu F-C, Lin T-Y, Huang W-Y, Wang Y-C, et al. Association Between Tuberculosis and Parkinson Disease: A Nationwide, Population-Based Cohort Study. Medicine (Baltimore). 2016;95(8):e2883-e. doi: 10.1097/MD.0000000000002883. PubMed PMID: 26937925.

99. Newton-Foot M, Warren RM, Sampson SL, van Helden PD, Gey van Pittius NC. The plasmid-mediated evolution of the mycobacterial ESX (Type VII) secretion systems. BMC Evol Biol. 2016;16:62-. doi: 10.1186/s12862-016-0631-2. PubMed PMID: 26979252.

100. Watson RO, Manzanillo PS, Cox JS. Extracellular M. tuberculosis DNA targets bacteria for autophagy by activating the host DNA-sensing pathway. Cell. 2012;150(4):803.

101. Patrick KL, Bell SL, Weindel CG, Watson RO. Exploring the "Multiple-Hit Hypothesis" of Neurodegenerative Disease: Bacterial Infection Comes Up to Bat. Frontiers in Cellular and Infection Microbiology. 2019;9(138). doi: 10.3389/fcimb.2019.00138.

102. Radoshevich L, Cossart P. Listeria monocytogenes: towards a complete picture of its physiology and pathogenesis. Nature Reviews Microbiology. 2018;16(1):32.

103. Ishii KJ, Kawagoe T, Koyama S, Matsui K, Kumar H, Kawai T, et al. TANK-binding kinase-1 delineates innate and adaptive immune responses to DNA vaccines. Nature. 2008;451(7179):725-9.

104. Burton AJ, Giguère S, Berghaus LJ, Hondalus MK, Arnold RD. Efficacy of liposomal gentamicin against Rhodococcus equi in a mouse infection model and colocalization with R. equi in equine alveolar macrophages. Veterinary Microbiology. 2015;176(3):292-300. doi: https://doi.org/10.1016/j.vetmic.2015.01.015.

105. Bordin AI, Suchodolski JS, Markel ME, Weaver KB, Steiner JM, Dowd SE, et al. Effects of Administration of Live or Inactivated Virulent Rhodococccus equi and Age on the Fecal Microbiome of Neonatal Foals. PLOS ONE. 2013;8(6):e66640. doi: 10.1371/journal.pone.0066640.

106. Azevedo MdCS, Ramuno NM, Fachin LRV, Tassa M, Rosa PS, Belone AdFF, et al. qPCR detection of Mycobacterium leprae in biopsies and slit skin smear of different leprosy clinical forms. Brazilian Journal of Infectious Diseases. 2017;21(1):71-8.

107. Martinez AN, Lahiri R, Pittman TL, Scollard D, Truman R, Moraes MO, et al. Molecular Determination of Mycobacterium leprae Viability by Use of Real-Time PCR. Journal of Clinical Microbiology. 2009;47(7):2124-30. doi: 10.1128/JCM.00512-09. PubMed PMID: PMC2708532.

108. Truman RW, Andrews PK, Robbins NY, Adams LB, Krahenbuhl JL, Gillis TP. Enumeration of Mycobacterium leprae Using Real-Time PCR PLoS Neglected Tropical Diseases, 2(11), e328. http://doi.org/10.1371/journal.pntd.0000328. PLoS Neglected Tropical Diseases. 2008;2(11):e328. doi: http://dx.doi.org/10.1371/journal.pntd.0000328.

109. Cywes-Bentley C, Rocha JN, Bordin AI, Vinacur M, Rehman S, Zaidi TS, et al. Antibody to Poly-N-acetyl glucosamine provides protection against intracellular pathogens: Mechanism of action and validation in horse foals challenged with Rhodococcus equi. PLoS pathogens. 2018;14(7):e1007160.

110. Bordin AI, Cohen ND, Giguère S, Bray JM, Berghaus LJ, Scott B, et al. Host-directed therapy in foals can enhance functional innate immunity and reduce severity of Rhodococcus equi pneumonia. Scientific Reports. 2021;11(1):1-13.

111. Schindelin J, Arganda-Carreras I, Frise E, Kaynig V, Longair M, Pietzsch T, et al. Fiji: an open-source platform for biological-image analysis. Nat Methods. 2012;9(7):676-82. doi: 10.1038/nmeth.2019. PubMed PMID: 22743772.

112. Srinivasan R, Henley BM, Henderson BJ, Indersmitten T, Cohen BN, Kim CH, et al. Smoking-Relevant Nicotine Concentration Attenuates the Unfolded Protein Response in Dopaminergic Neurons. J Neurosci. 2016;36(1):65-79. doi: 10.1523/JNEUROSCI.2126-15.2016. PubMed PMID: 26740650.

113. Srinivasan R, Huang BS, Venugopal S, Johnston AD, Chai H, Zeng H, et al. Ca(2+) signaling in astrocytes from Ip3r2(-/-) mice in brain slices and during startle responses in vivo. Nat Neurosci. 2015;18(5):708-17. Epub 2015/04/20. doi: 10.1038/nn.4001. PubMed PMID: 25894291.

114. McQueen CM, Dindot SV, Foster MJ, Cohen ND. Genetic Susceptibility to Rhodococcus equi. Journal of veterinary internal medicine. 2015;29(6):1648-59. Epub 2015/09/04. doi: 10.1111/jvim.13616. PubMed PMID: 26340305.

115. Tripodi M-F, Vigo D, Durante-Mangoni E, Lifschitz A, Corey GR, Stryjewski ME, et al. Rhodococcus equi endocarditis in immunocompetent hosts: report of the first two cases. International Journal of Antimicrobial Agents. 2009;34(5):496-7. doi: https://doi.org/10.1016/j.ijantimicag.2009.06.002.

116. Takai S, Sawada N, Nakayama Y, Ishizuka S, Nakagawa R, Kawashima G, et al. Reinvestigation of the virulence of Rhodococcus equi isolates from patients with and without AIDS. Letters in Applied Microbiology. 2020;71(6):679-83. doi: https://doi.org/10.1111/lam.13386.

117. Yamshchikov AV, Schuetz A, Lyon GM. Rhodococcus equi infection. The Lancet Infectious Diseases. 2010;10(5):350-9. doi: https://doi.org/10.1016/S1473-3099(10)70068-2.

118. Ocampo-Sosa AA, Lewis DA, Navas J, Quigley F, Callejo R, Scortti M, et al. Molecular epidemiology of Rhodococcus equi based on traA, vapA, and vapB virulence plasmid markers. The Journal of infectious diseases. 2007;196(5):763-9.

119. Darrah PA, Monaco MCG, Jain S, Hondalus MK, Golenbock DT, Mosser DM. Innate Immune Responses to Rhodococcus equi. The Journal of Immunology. 2004;173(3):1914-24. doi: 10.4049/jimmunol.173.3.1914.

120. Berry MPR, Graham CM, McNab FW, Xu Z, Bloch SAA, Oni T, et al. An interferon-inducible neutrophil-driven blood transcriptional signature in human tuberculosis. Nature. 2010;466:973. doi: 10.1038/nature09247.

121. Giguère S, Wilkie BN, Prescott JF. Modulation of cytokine response of pneumonic foals by virulent Rhodococcus equi. Infect Immun. 1999;67(10):5041-7. doi: 10.1128/IAI.67.10.5041-5047.1999. PubMed PMID: 10496876.

122. Giguère S, Prescott JF. Cytokine induction in murine macrophages infected with virulent and avirulent Rhodococcus equi. Infect Immun. 1998;66(5):1848-54. doi: 10.1128/IAI.66.5.1848-1854.1998. PubMed PMID: 9573060.

123. Hoffpauir CT, Bell SL, West KO, Jing T, Wagner AR, Torres-Odio S, et al. TRIM14 Is a Key Regulator of the Type I IFN Response during Mycobacterium tuberculosis Infection. J Immunol. 2020;205(1):153-67. Epub 2020/05/13. doi: 10.4049/jimmunol.1901511. PubMed PMID: 32404352.

124. Jefferies CA. Regulating IRFs in IFN Driven Disease. Frontiers in Immunology. 2019;10(325). doi: 10.3389/fimmu.2019.00325.

125. Au W-C, Moore PA, LaFleur DW, Tombal B, Pitha PM. Characterization of the interferon regulatory factor-7 and its potential role in the transcription activation of interferon A genes. Journal of Biological Chemistry. 1998;273(44):29210-7.

126. Bonnard M, Mirtsos C, Suzuki S, Graham K, Huang J, Ng M, et al. Deficiency of T2K leads to apoptotic liver degeneration and impaired NF-kappaB-dependent gene transcription. EMBO J. 2000;19(18):4976-85. doi: 10.1093/emboj/19.18.4976. PubMed PMID: 10990461.

127. Langereis MA, Rabouw HH, Holwerda M, Visser LJ, van Kuppeveld FJM. Knockout of cGAS and STING Rescues Virus Infection of Plasmid DNA-Transfected Cells. Journal of Virology. 2015;89(21):11169-73. doi: 10.1128/jvi.01781-15.

128. Jin L, Hill KK, Filak H, Mogan J, Knowles H, Zhang B, et al. MPYS is required for IFN response factor 3 activation and type I IFN production in the response of cultured phagocytes to bacterial second messengers cyclic-di-AMP and cyclic-di-GMP. J Immunol. 2011;187(5):2595-601. Epub 2011/08/03. doi: 10.4049/jimmunol.1100088. PubMed PMID: 21813776.

129. Bell SL, Lopez KL, Cox JS, Patrick KL, Watson RO. Galectin-8 senses phagosomal damage and recruits selective autophagy adapter TAX1BP1 to control Mycobacterium tuberculosis infection in macrophages. bioRxiv. 2020.

130. Thurston TLM, Wandel MP, von Muhlinen N, Foeglein Á, Randow F. Galectin 8 targets damaged vesicles for autophagy to defend cells against bacterial invasion. Nature. 2012;482(7385):414-8. doi: 10.1038/nature10744.

131. Von Bargen K, Haas A. Molecular and infection biology of the horse pathogen Rhodococcus equi. FEMS Microbiology Reviews. 2009;33(5):870-91. doi: 10.1111/j.1574-6976.2009.00181.x.

132. Quigley J, Hughitt VK, Velikovsky CA, Mariuzza RA, El-Sayed NM, Briken V. The cell wall lipid PDIM contributes to phagosomal escape and host cell exit of Mycobacterium tuberculosis. MBio. 2017;8(2).

133. van der Wel N, Hava D, Houben D, Fluitsma D, van Zon M, Pierson J, et al. M. tuberculosis and M. leprae Translocate from the Phagolysosome to the Cytosol in Myeloid Cells. Cell. 2007;129(7):1287-98. doi: 10.1016/j.cell.2007.05.059.

134. Lienard J, Nobs E, Lovins V, Movert E, Valfridsson C, Carlsson F. The Mycobacterium marinum ESX-1 system mediates phagosomal permeabilization and type I interferon production via separable mechanisms. Proceedings of the National Academy of Sciences. 2020;117(2):1160-6. doi: 10.1073/pnas.1911646117.

135. Wiens KE, Ernst JD. The Mechanism for Type I Interferon Induction by Mycobacterium tuberculosis is Bacterial Strain-Dependent. PLoS pathogens. 2016;12(8):e1005809-e. doi: 10.1371/journal.ppat.1005809. PubMed PMID: 27500737.

136. Sauer J-D, Sotelo-Troha K, von Moltke J, Monroe KM, Rae CS, Brubaker SW, et al. The N Ethyl N Nitrosourea-Induced Goldenticket Mouse Mutant Reveals an Essential Function of Sting in the In Vivo Interferon Response to Listeria monocytogenes and Cyclic Dinucleotides. Infect Immun. 2011;79(2):688-94. doi: 10.1128/iai.00999-10.

137. Dey B, Dey RJ, Cheung LS, Pokkali S, Guo H, Lee J-H, et al. A bacterial cyclic dinucleotide activates the cytosolic surveillance pathway and mediates innate resistance to tuberculosis. Nature Medicine. 2015;21(4):401-6. doi: 10.1038/nm.3813.

138. Barker JR, Koestler BJ, Carpenter VK, Burdette DL, Waters CM, Vance RE, et al. STING-Dependent Recognition of Cyclic di-AMP Mediates Type I Interferon Responses during Chlamydia trachomatis Infection. mBio. 2013;4(3):e00018-13. doi: 10.1128/mBio.00018-13.

139. Thurston TL, Ryzhakov G, Bloor S, Von Muhlinen N, Randow F. The TBK1 adaptor and autophagy receptor NDP52 restricts the proliferation of ubiquitin-coated bacteria. Nat Immunol. 2009;10(11):1215.

140. Kim YS, Silwal P, Kim SY, Yoshimori T, Jo E-K. Autophagy-activating strategies to promote innate defense against mycobacteria. Experimental & Molecular Medicine. 2019;51(12):1-10. doi: 10.1038/s12276-019-0290-7.

141. Zhang G, Deweerd NA, Stifter SA, Liu L, Zhou B, Wang W, et al. A proline deletion in IFNAR1 impairs IFN-signaling and underlies increased resistance to tuberculosis in humans. Nature communications. 2018;9(1):1-9.

142. Fava VM, Manry J, Cobat A, Orlova M, Thuc NV, Ba NN, et al. A Missense LRRK2 Variant Is a Risk Factor for Excessive Inflammatory Responses in Leprosy. PLoS Neglected Tropical Diseases. 2016;10(2):e0004412. doi: http://doi.org/10.1371/journal.pntd.0004412.

143. Wang D, Xu L, Lv L, Su L, Fan Y, Zhang DF, et al. Association of the LRRK2 genetic polymorphisms with leprosyin Han Chinese from Southwest China. Genes and Immunity. 2015;16(2):112--9.

144. Zhang F-R, Huang W, Chen S-M, Sun L-D, Liu H, Li Y, et al. Genomewide Association Study of Leprosy. N Engl J Med. 2009;361(27):2609-18. doi: 10.1056/NEJMoa0903753; 09

145. Bae JR, Lee BD. Function and dysfunction of leucine-rich repeat kinase 2 (LRRK2): Parkinson's disease and beyond. BMB Rep. 2015;48(5):243-8. doi: 10.5483/bmbrep.2015.48.5.032. PubMed PMID: 25703537.

146. Wallings R, Manzoni C, Bandopadhyay R. Cellular processes associated with LRRK2 function and dysfunction. FEBS J. 2015;282(15):2806-26. Epub 2015/05/09. doi: 10.1111/febs.13305. PubMed PMID: 25899482.

147. Rui Q, Ni H, Li D, Gao R, Chen G. The Role of LRRK2 in Neurodegeneration of Parkinson Disease. Curr Neuropharmacol. 2018;16(9):1348-57. Epub 2018/11/. doi: 10.2174/1570159X16666180222165418. PubMed PMID: 29473513.

148. Cookson MR. The role of leucine-rich repeat kinase 2 (LRRK2) in Parkinson's disease. Nat Rev Neurosci. 2010;11(12):791-7. Epub 2010/11/19. doi: 10.1038/nrn2935. PubMed PMID: 21088684.

149. Lee H, James WS, Cowley SA. LRRK2 in peripheral and central nervous system innate immunity: its link to Parkinson's disease. Biochem Soc Trans. 2017;45(1):131-9. Epub 2017/02/15. doi: 10.1042/BST20160262. PubMed PMID: 28202666.

150. Liu Z, Lenardo MJ. The role of LRRK2 in inflammatory bowel disease. Cell Res. 2012;22(7):1092-4. Epub 2012/03/20. doi: 10.1038/cr.2012.42. PubMed PMID: 22430149.

151. Zhu F, Li C, Gong J, Zhu W, Gu L, Li N. The risk of Parkinson's disease in inflammatory bowel disease: A systematic review and meta-analysis. Digestive and Liver Disease. 2019;51(1):38-42. doi: https://doi.org/10.1016/j.dld.2018.09.017.

152. Barrett JC, Hansoul S, Nicolae DL, Cho JH, Duerr RH, Rioux JD, et al. Genome-wide association defines more than 30 distinct susceptibility loci for Crohn's disease. Nat Genet. 2008;40(8):955-62. Epub 2008/06/29. doi: 10.1038/ng.175. PubMed PMID: 18587394.

153. Moehle MS, Daher JPL, Hull TD, Boddu R, Abdelmotilib HA, Mobley J, et al. The G2019S LRRK2 mutation increases myeloid cell chemotactic responses and enhances LRRK2 binding to actin-regulatory proteins. Human molecular genetics. 2015;24(15):4250-67. Epub 2015/04/29. doi: 10.1093/hmg/ddv157. PubMed PMID: 25926623.

154. Herbst S, Gutierrez MG. LRRK2 in Infection: Friend or Foe? ACS Infectious Diseases. 2019. doi: 10.1021/acsinfecdis.9b00051.

155. Gardet A, Benita Y, Li C, Sands BE, Ballester I, Stevens C, et al. LRRK2 is involved in the IFN-gamma response and host response to pathogens. The Journal of Immunology. 2010;185(9):5577.

156. Liu W, Liu Xn, Li Y, Zhao J, Liu Z, Hu Z, et al. LRRK2 promotes the activation of NLRC4 inflammasome during Salmonella Typhimurium infection. J Exp Med. 2017;214(10):3051-66. Epub 2017/08/18. doi: 10.1084/jem.20170014. PubMed PMID: 28821568.

157. Klein RS, Hunter CA. Protective and Pathological Immunity during Central Nervous System Infections. Immunity. 2017;46(6):891-909. doi: https://doi.org/10.1016/j.immuni.2017.06.012.

158. Blank T, Prinz M. Type I interferon pathway in CNS homeostasis and neurological disorders. Glia. 2017;65(9):1397-406. doi: 10.1002/glia.23154.

159. Fuzzati-Armentero MT, Cerri S, Blandini F. Peripheral-Central Neuroimmune Crosstalk in Parkinson's Disease: What Do Patients and Animal Models Tell Us? Frontiers in Neurology. 2019;10(232). doi: 10.3389/fneur.2019.00232.

160. Li J-Q, Tan L, Yu J-T. The role of the LRRK2 gene in Parkinsonism. Molecular Neurodegeneration. 2014;9(1):47. doi: 10.1186/1750-1326-9-47.

161. Lampron A, ElAli A, Rivest S. Innate Immunity in the CNS: Redefining the Relationship between the CNS and Its Environment. Neuron. 2013;78(2):214-32. doi: https://doi.org/10.1016/j.neuron.2013.04.005.

162. Ransohoff RM, Brown MA. Innate immunity in the central nervous system. J Clin Invest. 2012;122(4):1164-71. Epub 2012/04/02. doi: 10.1172/JCI58644. PubMed PMID: 22466658.

163. Andreasson KI, Bachstetter AD, Colonna M, Ginhoux F, Holmes C, Lamb B, et al. Targeting innate immunity for neurodegenerative disorders of the central nervous system. J Neurochem. 2016;138(5):653-93. doi: 10.1111/jnc.13667. PubMed PMID: 27248001.

164. Colombo E, Farina C. Astrocytes: Key Regulators of Neuroinflammation. Trends in Immunology. 2016;37(9):608-20. doi: https://doi.org/10.1016/j.it.2016.06.006.

165. Weindel CG, Bell SL, Vail KJ, West KO, Patrick KLA-Ohoo, Watson RO. LRRK2 maintains mitochondrial homeostasis and regulates innate immune responses to Mycobacterium tuberculosis. LID - 10.7554/eLife.51071 [doi] LID - e51071 [pii]. Elife. 2020;9(2050-084X (Electronic)):e51071. doi: 10.7554/eLife.51071.

166. Russo I, Kaganovich A, Ding J, Landeck N, Mamais A, Varanita T, et al. Transcriptase analysis of LRRK2 knock-out microglia cells reveals alterations of inflammatory- and oxidative stress-related pathways upon treatment with α-synuclein fibrils. Neurobiology of Disease. 2019. doi: https://doi.org/10.1016/j.nbd.2019.05.012.

167. Hui KY, Fernandez-Hernandez H, Hu J, Schaffner A, Pankratz N, Hsu N-Y, et al. Functional variants in the LRRK2 gene confer shared effects on risk for Crohn's disease and Parkinson's disease. Sci Transl Med. 2018;10(423):eaai7795. doi: 10.1126/scitranslmed.aai7795. PubMed PMID: 29321258.

168. Banks DA, Ahlbrand SE, Hughitt VK, Shah S, Mayer-Barber KD, Vogel SN, et al. Mycobacterium tuberculosis Inhibits Autocrine Type I IFN Signaling to Increase Intracellular Survival. The Journal of Immunology. 2019;202(8):2348-59. doi: 10.4049/jimmunol.1801303.

169. Härtlova A, Herbst S, Peltier J, Rodgers A, Bilkei-Gorzo O, Fearns A, et al. LRRK2 is a negative regulator of Mycobacterium tuberculosis phagosome maturation in macrophages. EMBO J. 2018;37(12):e98694. doi: https://doi.org/10.15252/embj.201798694.

170. West AP. Mitochondrial dysfunction as a trigger of innate immune responses and inflammation. Toxicology. 2017;391:54-63. doi: https://doi.org/10.1016/j.tox.2017.07.016.

171. Ferraz LC, Bernardes ES, Oliveira AF, Ruas LP, Fermino ML, Soares SG, et al. Lack of galectin-3 alters the balance of innate immune cytokines and confers resistance to Rhodococcus equi infection. European Journal of Immunology. 2008;38(10):2762-75. doi: https://doi.org/10.1002/eji.200737986.

APPENDIX

SUPPLEMENTAL FIGURES

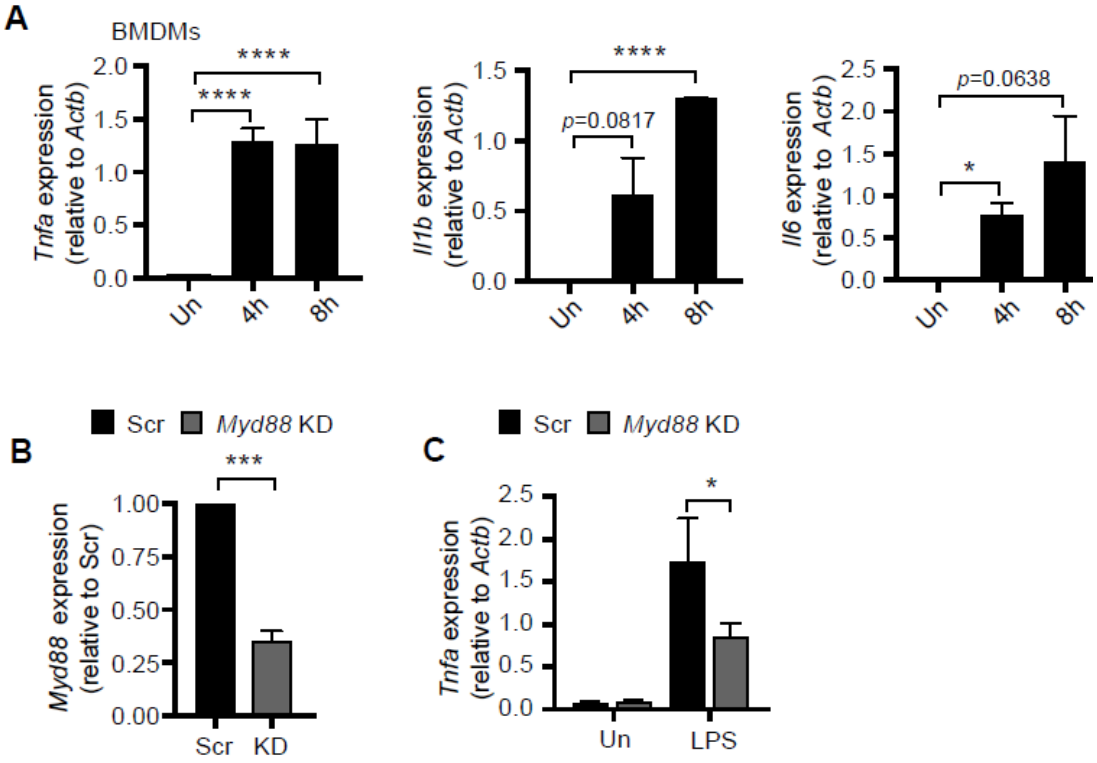


A.1: (A) qRT-PCR of *Tnfa*, *Il1b* and *Il6* in BMDMs at 4 and 8 hours post infection with *R. equi*. (B) qRT-PCR of *Myd88* in RAW 264.7 macrophages with Scr control. (C) qRT-PCR of *Tnfa* in MyD88 KD and Scr macrophages treated with LPS for 4 hours. RT-qPCR represent 3 biological replicates ± SD, n=3. For all experiments in this study, statistical significance was determined using Students' t-test. *p < 0.05, **p < 0.01, ***p < 0.001, ****p < 0.0001, n.s. = not significant.

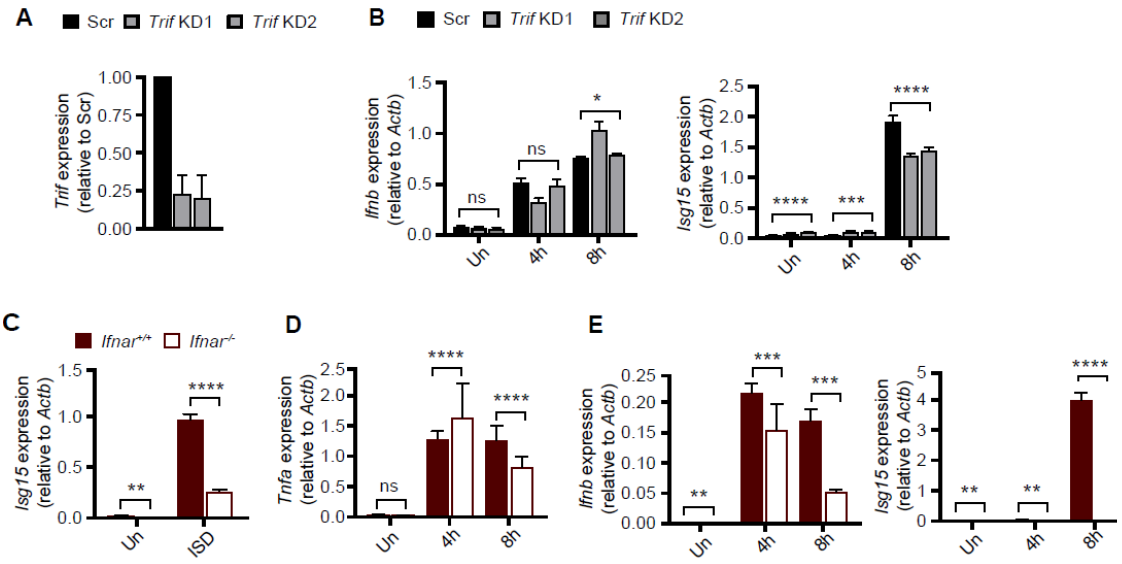


A.2: (A) qRT-PCR of *Trif* in RAW 264.7 KD cells relative to Scr control. (B) qRT-PCR of *Ifnb* and Isg15 in Trif KD and Scr RAW 264.7 macrophages. (C) qRT-PCR of *Isg15* in IFNAR$^{+/+}$ (WT) and IFNAR$^{-/-}$ (KO) BMDMs treated or not with ISD for 4 hours. (D) RT-qPCR of *Tnfa* in IFNAR BMDMs infected with *R. equi* for the indicated times. (E) As in D but *Ifnb* and *Isg15*. RT-qPCR represent 3 biological replicates ± SD, n=3. For all experiments in this study, statistical significance was determined using Students' t-test. *p < 0.05, **p < 0.01, ***p < 0.001, ****p < 0.0001, n.s. = not significant.

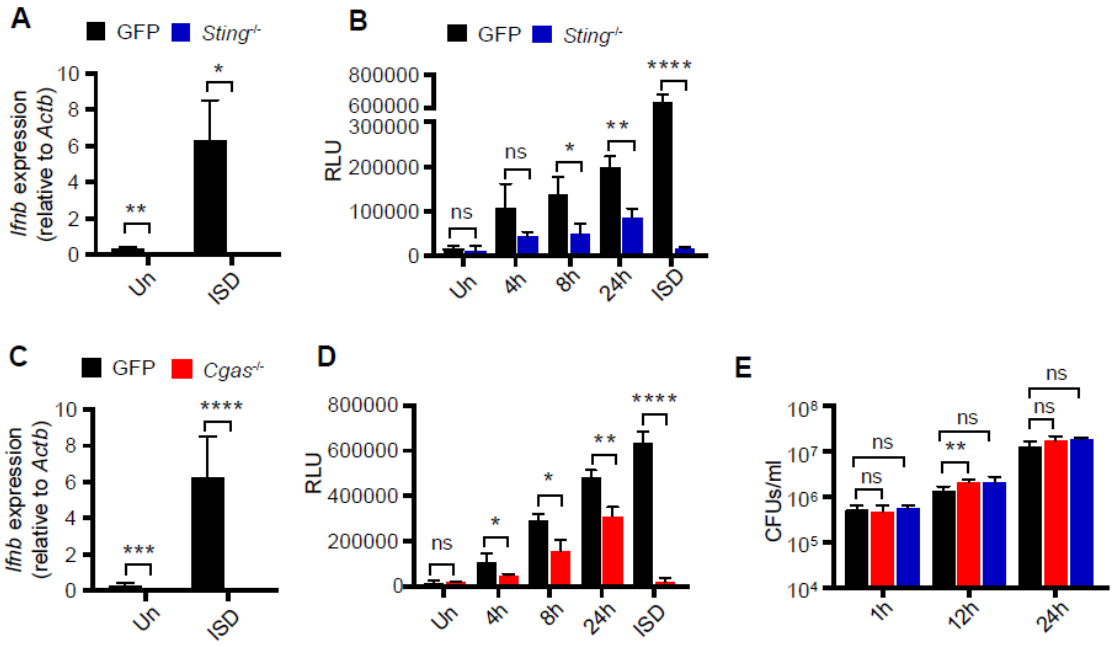


A.3: (A) RT-qPCR of *Ifnb* in GFP control and STING KO RAW 264.7 macrophages treated or not with ISD for 4 hours. (B) ISRE reporter assay measuring relative luminescence units as a readout for type I IFN protein levels secreted into supernatants from GFP control or STING KO RAW 264.7 macrophages infected or not with *R. equi* for the indicated times or treated with ISD for 4 hours. (C) As in F but in GFP control and cGAS KO RAW 264.7 macrophages. (D) As in G but in GFP control and cGAS KO RAW 264.7 macrophages. (E) CFUs of GFP control, cGAS KO and STING KO RAW 264.7 macrophages infected with *R. equi* for the indicated times. RT-qPCR represent 3 biological replicates ± SD, n=3. For all experiments in this study, statistical significance was determined using Students' t-test. *p < 0.05, **p < 0.01, ***p < 0.001, ****p < 0.0001, n.s. = not significant.